NATIONAL AERONAUTICS AND SPACE ADMINISTRATION

Space Programs Summary No. 37-36, Volume III

for the period September 1, 1965 to October 31, 1965

The Deep Space Network

JET PROPULSION LABORATORY
CALIFORNIA INSTITUTE OF TECHNOLOGY
PASADENA, CALIFORNIA

November 30, 1965

NATIONAL AERONAUTICS AND SPACE ADMINISTRATION

Space Programs Summary No. 37-36, Volume III

for the period September 1, 1965 to October 31, 1965

The Deep Space Network

JET PROPULSION LABORATORY
CALIFORNIA INSTITUTE OF TECHNOLOGY
PASADENA, CALIFORNIA

November 30, 1965

Preface

The *Space Programs Summary* is a six-volume, bimonthly publication that documents the current project activities and supporting research and advanced development efforts conducted or managed by JPL for the NASA space exploration programs. The titles of all volumes of the *Space Programs Summary* are:

Vol. I. The Lunar Program (Confidential)

Vol. II. The Planetary–Interplanetary Program (Confidential)

Vol. III. The Deep Space Network (Unclassified)

Vol. IV. Supporting Research and Advanced Development (Unclassified)

Vol. V. Supporting Research and Advanced Development (Confidential)

Vol. VI. Space Exploration Programs and Space Sciences (Unclassified)

The *Space Programs Summary,* Vol. VI consists of an unclassified digest of appropriate material from Vols. I, II, and III; an original presentation of technical supporting activities, including engineering development of environmental-test facilities, and quality assurance and reliability; and a reprint of the space science instrumentation studies of Vols. I and II.

W. H. Pickering, *Director*
Jet Propulsion Laboratory

Space Programs Summary No. 37-36, Volume III

Prepared under Contract No. NAS 7-100, National Aeronautics & Space Administration

Contents

I. Introduction

1. General

The Deep Space Network (DSN) is a precision communication system which is designed to communicate with, and permit control of, spacecraft designed for deep space exploration. The DSN consists of the Deep Space Instrumentation Facility (DSIF), the Space Flight Operations Facility (SFOF), and the DSN Ground Communication System (GCS).

The DSN is a NASA facility, managed by JPL through a contract between NASA and the California Institute of Technology. The Office of Tracking and Data Acquisition is the cognizant NASA office.

It is the policy of the DSN to continuously conduct research and development of new components and systems and to engineer them into the DSN to maintain a state-of-the-art capability.

The DSN has facilities for simultaneously controlling a newly launched spacecraft and a second one already in flight. Within a few months, it will be able to control simultaneously either two newly launched spacecraft plus two in flight or the operations of four spacecraft in flight at the same time. The DSIF is equipped with 85-ft antennas having gains of 53 db at 2300 Mc and a system temperature of 55°K, making it possible to receive significant data rates at distances as far as the planet Mars. To improve the data rate and distance capability, a 210-ft antenna is under construction at the Goldstone Mars station and two additional antennas of this size are planned for installation at overseas stations.

The DSIF utilizes large antennas, low-noise phase-lock receiving systems, and high-power transmitters located at stations positioned around the Earth to track, command, and receive data from deep space probes. Overseas stations are generally operated by personnel of the respective countries. The DSIF stations are:

I.D. No.	Name	Location
11	Goldstone, Pioneer	Goldstone, California
12	Goldstone, Echo	Goldstone, California
13	Goldstone, Venus (R&D)	Goldstone, California
14	Goldstone, Mars (under construction)	Goldstone, California
41	Woomera	Island Lagoon, Australia
42	Tidbinbilla	Canberra, Australia
51	Johannesburg	Johannesburg, South Africa
61	Madrid	Madrid, Spain
71	Spacecraft Monitoring	Cape Kennedy, Florida
72	Spacecraft Guidance and Command (under construction)	Ascension Island

The SFOF is located in a three-story building at the Jet Propulsion Laboratory in Pasadena, California, and utilizes operations control consoles, status and operations displays, computers, data processing equipment for analysis of spacecraft performance and space science experiments, and communication facilities to control space flight operations. This control is accomplished by generating trajectories and orbits, and command and control data, from tracking and telemetry data received from the DSIF in near real-time. The SFOF also reduces the telemetry, tracking, command and station performance data recorded by the DSIF into engineering and scientific information for analysis and use by the scientific experimenters and spacecraft engineers.

The DSN Ground Communication System consists of voice, normal and high data rate teletype circuits provided by the NASA World-Wide Communications Network between each overseas station and the SFOF; teletype and voice circuits between the SFOF, Goldstone Stations, and Cape Kennedy; and a microwave link between the SFOF and Goldstone, provided by the DSN.

II. DSN Technical Systems Design

A new group has been formed to provide an overall DSN Systems Design discipline, including the development of interface control, DSN monitoring and data validation, design control, and data systems, and the anticipation of future requirements. Typical projects that will periodically be reported in future SPS publications are as follows:

(1) Direct command system

(2) DSN monitoring and monitoring area design

(3) DSN simulation

(4) DSN/DSIF monitor and control, Phase I

(5) SFOF systems design

(6) Ground communications systems design

(7) DSIF systems design

A. DSN Monitoring System

Introduction. This article introduces the DSN Monitoring System, which is to be designed, developed, and installed in the DSN. This system is to provide monitoring at points along the data flow path within the DSN — namely, throughout the Deep Space Instrumentation Facility (DSIF) station, the Ground Communications System (GCS), and the Space Flight Operations Facility (SFOF) to obtain a measure of the performance of the DSN in real-time or near real-time.

DSN monitoring system objectives. The objectives of the DSN Monitoring System are to provide:

(1) Performance and failure data to appropriate personnel in real or near real-time for information purposes and to aid in the taking of remedial action.

(2) A data-monitoring function.

(3) The above performance and data-monitoring functions to aid in validation of the output data.

(4) A permanent record of performance and data monitoring.

DSN monitoring system status. Efforts to date have established the functional specifications for the DSN Monitoring System. These functional specifications are now being reviewed and updated. A "DSN Monitor and Control System — Phase 1" project has been established by the DSN and the project organization and assignments have been announced.

Future developments. The immediate task is to complete the design, development, installation, and checkout of the DSN Monitoring System for support of the *Surveyor* and *Lunar Orbiter* flight projects. This is scheduled for completion in the Spring of 1967.

B. DSN Monitor Area

Introduction. A new project has been initiated by the DSN to provide a DSN Monitor Area within the SFOF. The DSN Monitor Area (Fig. 1), which functionally is a part of the overall DSN Monitoring System described on p. 3, is the primary using subsystem of the monitoring information sensed, processed, and provided by the DSN Monitoring System. As such, it is a mission-independent, highly reliable, on-line facility located in the SFOF where selected outputs from the DSN Monitoring System, and from SFOF subsystems, will be displayed to aid in the validation of the DSN output data. The monitor area will house two DSN Monitor and Analysis teams with certain input/output and display equipment.

Subsystem Objectives. As the primary user of data output by the DSN Monitoring System, the Monitor Area

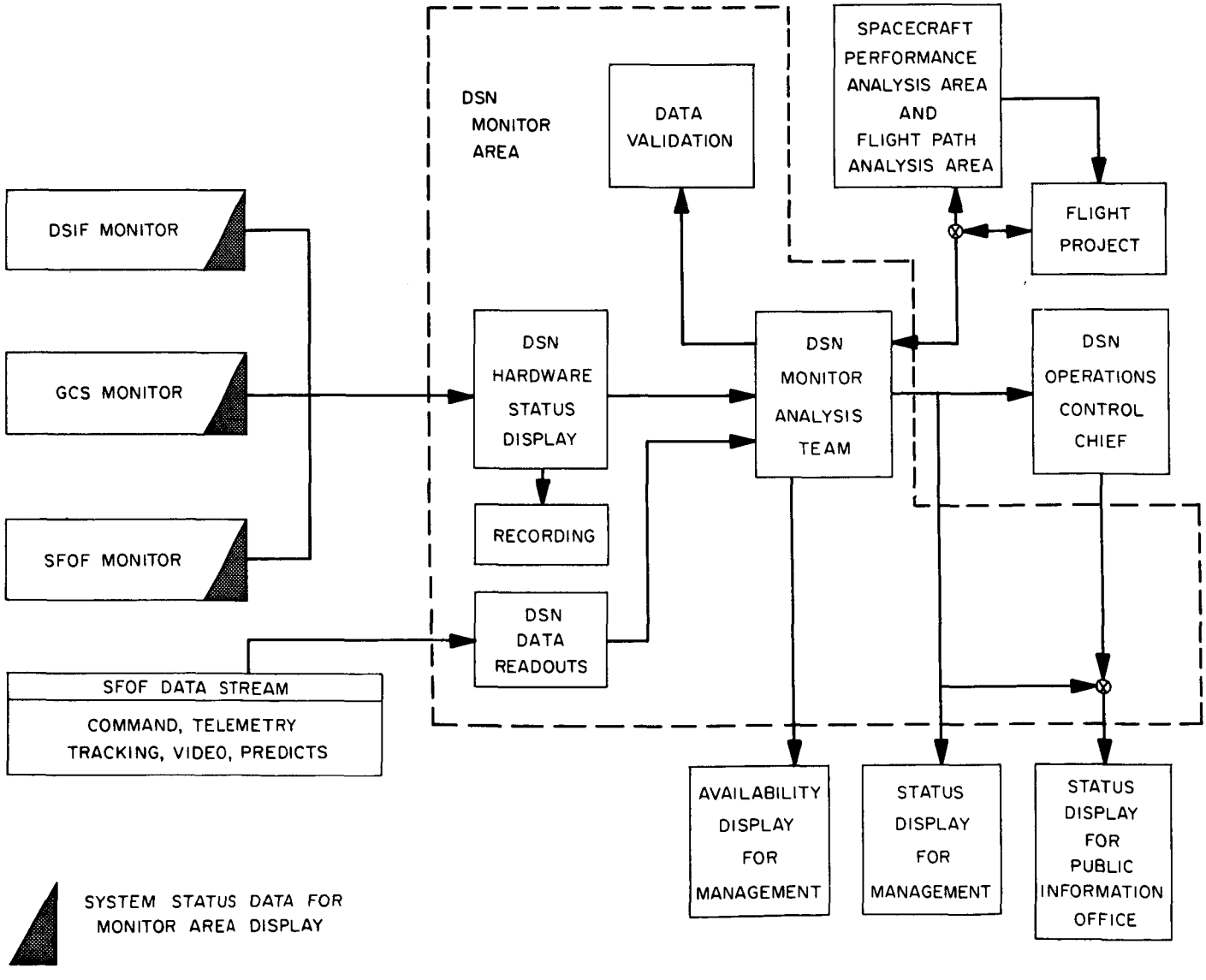

Fig. 1. DSN Monitor Area information flow and control element interfaces

must directly contribute to the objectives specified for the DSN Monitoring System. These contributions are realized by providing:

(1) Recommendations for action to the DSN Operations Control Chief and the flight project resulting from analysis of nonstandard DSN performance.

(2) Validation of DSN data in real-time or near real-time.

(3) DSN management with visibility into the status of the DSN elements and available alternatives.

(4) Displays of DSN and project status for Public Information Office purposes (as a by-product).

(5) A permanent record of system performance measurements for future system analysis.

Subsystem Design. The DSN Monitor Arca, in order to support the mission-independent Monitor and Analysis team, will provide the following:

(1) A display of DSN hardware system performance and status for monitoring.

(2) A display of selected data system outputs for data validation and monitoring.

(3) Displays of DSN systems performance and status for management and PIO.

(4) Special and general-purpose hardware to drive these displays.

(5) Reliable and timely status and performance information from the DSIF, GCS, and SFOF Monitoring Systems, processed by the SFOF DPS to provide the information for the displays specified above.

(6) A backup mode of operation for continuing to monitor DSN operations while the SFOF DPS is down.

(7) The Monitor and Analysis team.

Subsystem Capacity. The subsystem will have sufficient capacity to support simultaneously two missions, with two stations per mission. It is scheduled for implementation by January 1967.

Subsystem Status. The Requirements and Objectives Document, DSN R&O 65-100, is now under review, and a functional specification for the SFOF displays and display buffer is being prepared. A team to produce an operational design leading toward a functional specification for the DSN Monitor Area has been formed.

C. Communications Theory Model of the DSN Ground Communications System

The DSN Ground Communications System is a large, complex serial-parallel array of equipment which is intended to perform many functions. Because of the cost of the system and the cost of preparing the input upon which it acts, it is desirable to understand its functions, and to maintain its performance within specifiable limits. A model of the system should enable the model user to approximate functional relationships within a system, so that the relationships between input-output transformations and system parameters can be predicted and manipulated.

In general terms, the DSN ground communications system is a set of data-transmission links which transfer information from the DSIF receivers to the users in the mission control/operations/analysis areas. This definition provides the basis for a "communications theory" model of the DSN, the functions and limitations of which should become clear in the course of its development. There are terms in the definition which can be defined at present only in an intuitive sense. For example, a "data-transmission link," in its widest sense, portrays a single, contiguous circuit of the electronic equipment, its operators, the physical phenomena (or a phenomenological representation of them) which affect the behavior of the equipment, etc., at some point or interval of time. Data will not be limited at the outset, but can be thought of as any of several electrical outputs of the receivers at the DSIF. It is necessary to specify data only in the modeling of specific problems.

The source to the system is one or more spacecraft, or a simulation of spacecraft. However, for the purpose of the ground communications system, it is often more convenient to view the DSIF receiver system as the source. It is assumed that the experimenter, or other user, is already aware of the spacecraft information limitations; it is the purpose of a ground communications model to provide an understanding and evaluation of the data transfer capabilities of the ground system. Therefore, one

of the useful results of such a model will be the relation of the effect of the system upon data to the final processed accuracy of the data.

The development of the model has proceeded along the following lines. It is assumed that the system can be represented as series-parallel network of functional elements (a block diagram). Then, there will be a general functional block, which is a set, acting upon input to give output, whose elements are:

(1) A transformation or transfer function, which transforms the input function to the output function.

(2) A further "noise" transformation, which often possesses special properties, such as being additive to (1), and having a specified, stationary distribution, etc.

(3) Storage capacity, service times, and waiting times (communication network, or "queue" parameters).

(4) Information rates, or throughput capacity.

These elements are not necessarily independent, but allow sufficient versatility that all blocks in the representation can be replaced by a general block. Such a representation permits modular modification of any particular model.

The system models constructed from communication blocks should allow the study of: (1) system adequacy and capability with respect to any set of specifications on information rate, information accuracy, two-way capabilities, etc., (2) cost versus capability and effectiveness tradeoffs; i.e., operational analysis, (3) planning and establishing communication parameter boundaries on design requirements for future support requirements.

The model should allow the user to appraise, in a quantitative manner, the bounds on accuracy of data which is transferred through a particular system. It should also provide a basis for the design of codes which will optimally combat the system noise within operational constraints.

As a part of the DSN GCS model development, a general error model for errors in digital data is being developed, which can be used in conjunction with the system model, or separately from it, to simulate the effect of a system which introduces error into the digital data. This model is general enough to be representative of systems which exhibit correlated noise, and can be used to study the effectiveness of particular coding schemes.

D. DSN Administrative System Design: DSIF Chart Room

Introduction. Management of the multitudinous tasks of engineering and operation for the vast DSIF network-wide activities requires the generation and use of many diverse kinds of information. One of the tools used for accomplishing a systematic integration of the total data reservoir is the DSIF chart room. It was activated in May 1965. This report describes the background, objective, and current functions of this chart room. In addition, some graphic methodology for presentation of planning and scheduling data is briefly describted.

Background. The planning and scheduling formats for the DSIF were previously prepared solely by manual efforts. Large vellum sheets were used to depict the information. With the rapid expansion of DSIF activities, this manual method of graphic presentation became cumbersome, costly, and time-consuming. It precluded a maximum informational transmittal in the minimum time to the widely dispersed activities of the DSIF. The previous facilities of the DSIF project information center were very inadequate to serve as a chart room where displays of information could have been made available for study.

Objectives. The establishment of the new DSIF chart room dictated that an improved management information system be implemented. This system would be based upon four principal objectives:

(1) To implement and establish a control center, as a focal point for coordination of all engineering and operation information of all DSIF stations.

(2) To develop effective means and methods of data programming for planning and scheduling of the DSIF activities.

(3) To develop communications to provide timely status on all DSIF stations and a system for quick response to problem action items of scheduling for the network.

(4) To implement and establish a focal point for transmitting expeditiously scheduling data when performance, planning or other requirements have been changed.

Graphic presentation is accomplished by paste-up strips of data produced by a photo-composing machine. This machine sets copy on photosensitive 35-mm film or opaque

paper, and delivers finished prints in about 90 sec. Photographs are made of the finished wall displays for quick reproduction.

The criteria for evaluation of the above graphic presentation models were based upon these factors:

(1) The types of formats that have facilitated the comprehension of scheduling data by all users.

(2) The type of formats that have assisted in a more penetrating analysis of the information displayed.

(3) The type of format that has provided added interest in the information and thereby has been readily used by the recipients.

Current functions. Updating procedures have been promulgated for the acquisition of information on a systematic level of managerial discrimination of the data. The chart room functions primarily as a working area in which this information is received from various levels; it is reviewed, analyzed, and posted on either of two wall types of displays. A large display panel, 5 × 8 ft, depicts the initial implementation phase of a DSIF station. Other smaller panels, 30 × 40 in., indicate the overseas activities of DSIF stations. Fig. 2 depicts the present layout. The large wall-size panel, 5 × 8 ft, can be seen on the right side of the picture. The smaller plexiglass displays are shown on the left side. The room also serves as a managerial conference area for planning and scheduling discussions.

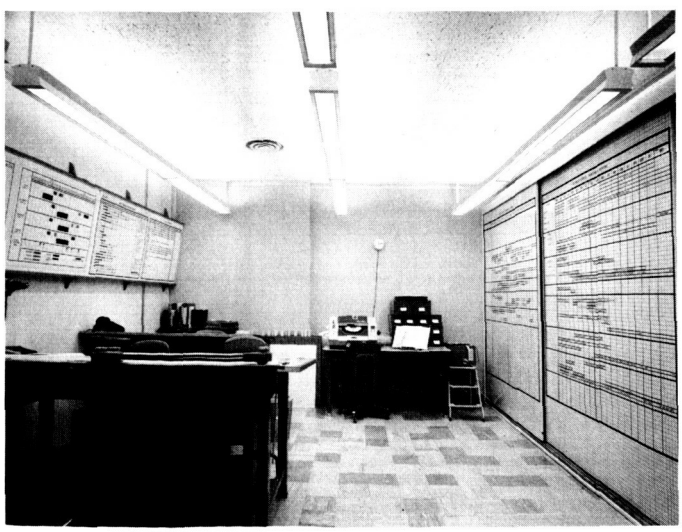

Fig. 2. DSIF chart room

E. DSN Utilization Scheduling, Administrative Systems Design

Administrative systems designs have been completed for three complimentary utilization scheduling systems. These systems provide the vehicle for coordinating the various flight projects and internal DSN requests for use of DSN facilities and the means for disseminating the integrated plan to all concerned.

1. 10-Day Scheduling System

A new concept for scheduling the immediate activities of the DSN was developed which could replace the present 10-day DSN schedule. It produces a master display for real-time operation and rescheduling during any portion of the 10-day period, printed copies of the schedule for distribution and semiautomatic teletype transmission to distant stations.

The schedule is composed of specially formatted request cards arranged chronologically in special holders to form a complete schedule. Separate holders are provided for the SFOF, GCS, and each DSIF station. When mounted side by side, a complete DSN-wide schedule results.

The schedule cards display the key data along the upper edge with indications of the items and time required. The time is indicated numerically for high resolution and pictorially for quick visual analysis.

This system was developed for manual operation with conversion to an equivalent computer-operated system, being a simple transition with minimal changes in the request cards and principles of operation.

2. Detailed 12-wk Scheduling System

A new system has been developed for 12-wk scheduling which will allow detailed analysis of the various users requirements. It considers each individual activity separately, rather than just the weekly total for each project. A complete schedule is produced which indicates, by project grouping, each individual test or operational activity, its duration and the items required. Project subtotals are indicated as are the weekly totals. A comparison is made with the specified operational times of each item and open time as well as the excessive requirements are calculated.

The system is based upon machine processing of the individual request and automatic calculation of the various arithmetic operations. The system is also designed in such a manner that initial operation may be implemented on a manual basis, with gradual transition to computer operation.

3. 16-mo Scheduling System

A 16-mo scheduling system has been developed for long-range utilization scheduling. This system, which is ready for immediate implementation, is patterned after the current 12-wk scheduling system. It is based upon total project requirements per calendar month, and covers only the major items of the SFOF and DSIF stations.

The schedule is based on daily periods per month, except in the case of the SFOF data-processing system, which uses total hours per month. The schedule covers the 16 mo beyond the time interval covered by the 12-wk schedule and is in four 4-mo sections. It is revised and reissued on an 8-wk cycle.

III. Tracking Stations Engineering and Operations

A. Goldstone Operations

The *Mariner IV* mission termination was recorded by the Echo Station at 23:05:07 GMT, October 1, 1965, as a result of a command transmitted by the Venus Station's 100-kw transmitter at 22:30:17 GMT on the same day. A month earlier, the Pioneer Station left the *Mariner* mission to prepare for the *Surveyor* Project. With the termination of the *Mariner* program, the Echo Station began preparing for the *Pioneer* space probe and the *Lunar Orbiter* Project.

1. Mariner IV Project

a. Echo Station. The second turn-on of the *Mariner IV* TV equipment (*SPS 37-35*, Vol. III, p. 14) was accomplished using the Echo Station 10-kw transmitter. From that point until the mission termination, the tracking was relatively routine. Several experiments were conducted, using the spacecraft received signals as a reference. A signal-to-noise estimator series of tests was conducted until the termination. Also, a diversity receiver test was performed using the coordinated facilities of the Echo, Pioneer, and Venus Stations.

During the final portion of the *Mariner* tracking only minor equipment troubles were encountered. Because of a malfunction in the Echo Station maser cryogenic assembly and the resulting necessary maser cooldown time, the Venus Station operated in the receive mode with the Echo Station recording the telemetry for one day during the final month.

b. Venus Station. Command transmission to the spacecraft remained the prime function of the Venus Station until termination of the *Mariner IV* mission. During the final two weeks, the Echo Station 10-kw transmitter was able to establish two-way lock with the spacecraft, but had insufficient power to lock up the command loop. At a distance of 192 million miles from the Earth, the full capabilities of the Venus Station 100-kw transmitter to command the spacecraft were used. At the time the final command was transmitted, the round-trip time for a signal to reach the spacecraft and return to Earth was 35 min.

2. Pioneer Project

Installation and testing of the *Pioneer* Project mission-dependent equipment began in April 1965 (*SPS 37-33*,

Vol. III, pp. 7–9; *SPS 37-34*, Vol. III, p. 5; *SPS 37-35*, Vol. III, p. 15). During the final weeks of the *Mariner IV* tracking at Echo, interface and operational testing was performed between the end of the station posttracking calibrations and the start of the next day's tracking countdown. These tests included a series of spacecraft orientations between the Echo Station ground equipment and a *Pioneer* Project spacecraft test model. The *Pioneer* Project test model is mounted on the end of an 8-ft boom, to the north of the Echo Station collimation tower reflector antenna (Fig. 1). The boom is mounted on an intervalometer sequencer having a minimum stepping of 1 deg, allowing for simulated postlaunch orientation of the spacecraft for ground control determination.

Ames NASA personnel were on hand at the termination of the *Mariner* mission to assist the station personnel in preparing the S-band system final interfaces with the *Pioneer* Project mission-dependent equipment; final interface and integration testing began immediately following the posttracking calibrations. *Mariner* mission-dependent equipment, including the ground command *read-write-verify,* was removed and shipped, and the Echo Station was readied for a full *Pioneer* Project configuration and final tests. These tests included subsystem tests, daily and Type II orientation tests, and Type II orientation emergency mode tests.

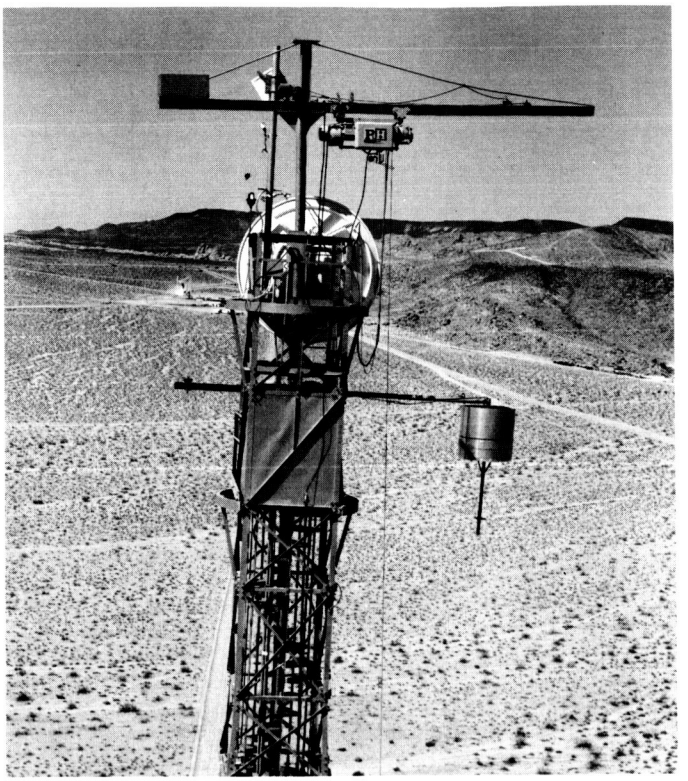

Fig. 1. *Pioneer* spacecraft test model mounted on Echo collimation tower

3. *Surveyor* Project

Testing with the *Surveyor* T-21 test model was completed on October 8, and the spacecraft was removed from Goldstone on October 12. The tests were continuations of the earlier tests (*SPS 37-35*, Vol. III, p. 15) and included crew training, system compatibility, and major subsystem tests.

Tests of the spacecraft horizontal camera were performed and good 200-line pictures were recorded by the ground equipment at the Pioneer Station. With the departure of the T-21 test model, Hughes Aircraft Co. and Pioneer Station personnel continued interface and subsystem tests. Preparations for later scheduled DSIF-SFOF net integration tests are in progress.

4. *Lunar Orbiter*

Boeing operations personnel arrived at the Echo Station in September and began preparations for the arrival of the *Lunar Orbiter* equipment. The two rooms formerly used for the *Ranger* ground equipment were modified to include humidity control and an access to the new S-band wing basement for equipment interfacing with the DSIF S-band system. Two former offices were rebuilt into three separate dark rooms, complete with an extensive drainage system (Fig. 2). *Lunar Orbiter* mission film will be processed here prior to leaving the station.

The major racks of the *Lunar Orbiter* ground equipment arrived at Goldstone on October 11 and were delivered to the Echo Station control building. Installation of the equipment was started and is currently in progress (Figs. 3 and 4). Concurrent with equipment installation, *Lunar Orbiter* computer programs are receiving preliminary operational tests using the S-band digital instrumentation subsystem.

5. *Pioneer* Station Testing

While preparing for the *Surveyor* mission, the Pioneer Station continued to be the overseas staging center for initial testing of S-band equipment and systems. The Ascension Island equipment was shipped to the island in mid-September. Supplementing the regular complement at Ascension Island, experienced subsystem personnel

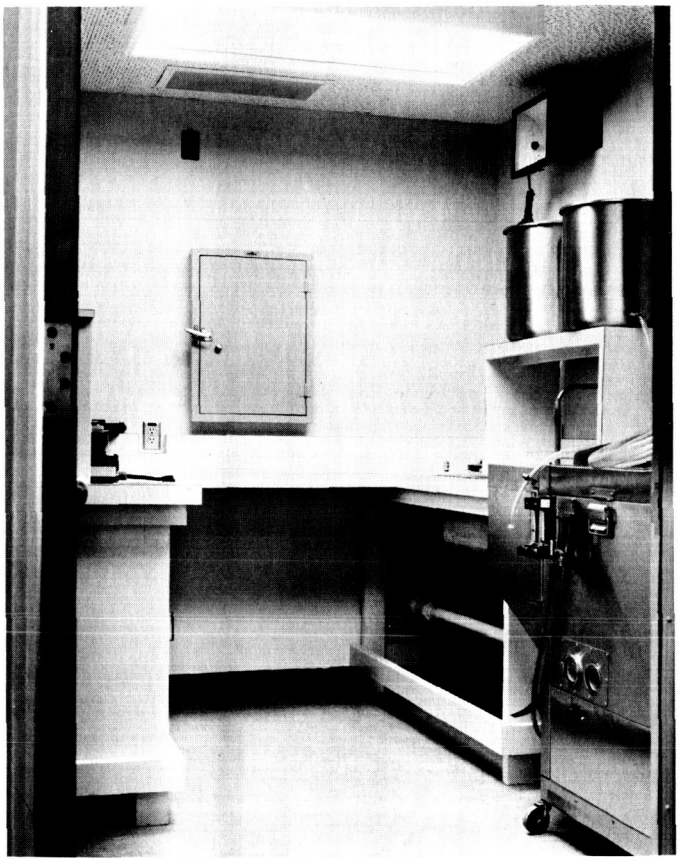

Fig. 2. *Lunar Orbiter* dark room

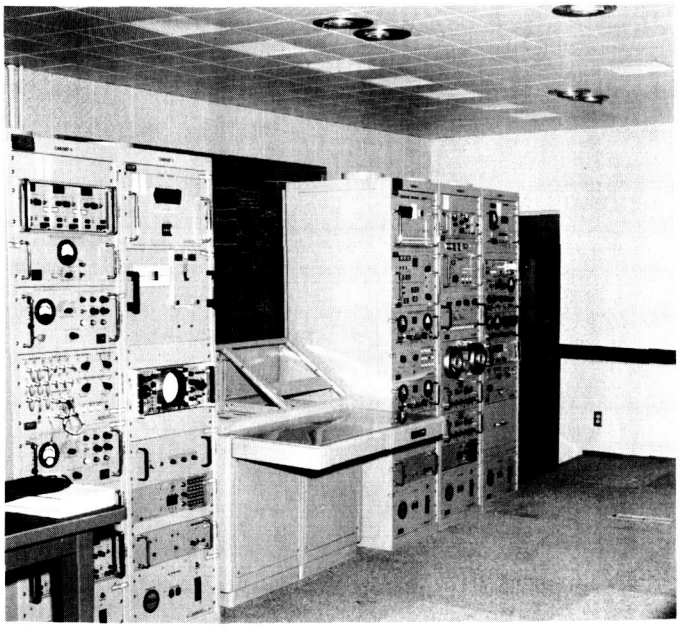

Fig. 3. *Lunar Orbiter* video-associated equipment and command and telemetry electronics

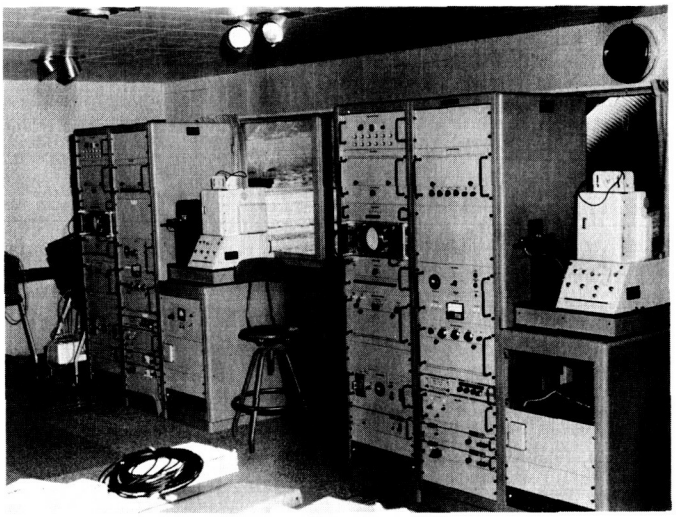

Fig. 4. *Lunar Orbiter* video ground reconstruction electronics

from Goldstone arrived at Ascension Island in October to assist in the installation and operational testing.

Equipment for the Madrid DSIF-62 Station and the MSFN backup system are currently being assembled. Located in the MSFN Annex building, the major portions of the DSIF-62 analog instrumentation subsystem have arrived and are being placed for testing. The digital instrumentation subsystem for the MSFN backup system has arrived and is being installed in the west wing of the control building.

6. DSIF-14 Mars Station

The subsystem components of the S-band system continue to arrive and are being stored at the Echo Station, awaiting installation at the Mars Station. The digital instrumentation subsystem, however, has already been installed at the Mars Station and installation operational testing is in progress. The station control and monitor console and the frequency timing subsystems have also been installed. However, testing of these subsystems is scheduled for a later date.

Station operations personnel are continuing the Rohr-sponsored classes on the operation and maintenance of the antenna servohydraulics drive subsystem. Spare equipment and spare parts are being ordered and are catalogued for storage as they arrive at Goldstone. Assistance is being given to assembly and testing of the master equatorial drive system.

Two 14 × 36-ft extensions are being added to the Generator building (Fig. 5). The new extensions will be used to provide accommodations for additional power equipment to be installed in the 210-ft antenna. Fig. 6 shows the 210-ft antenna in the near completion stage.

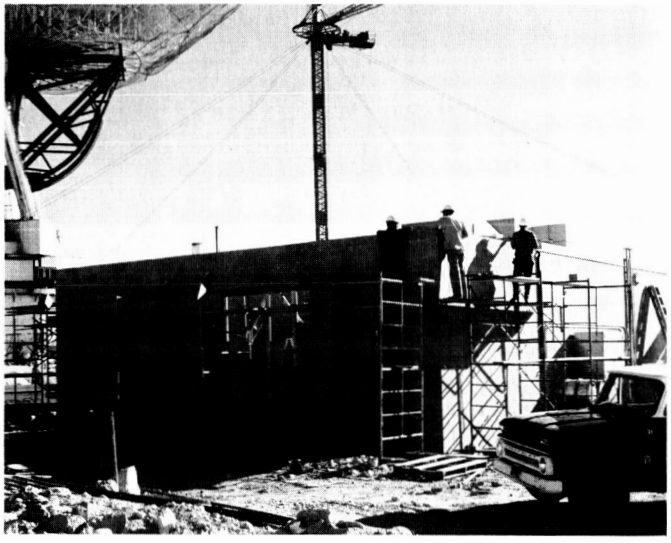

Fig. 5. Mars generator building extensions

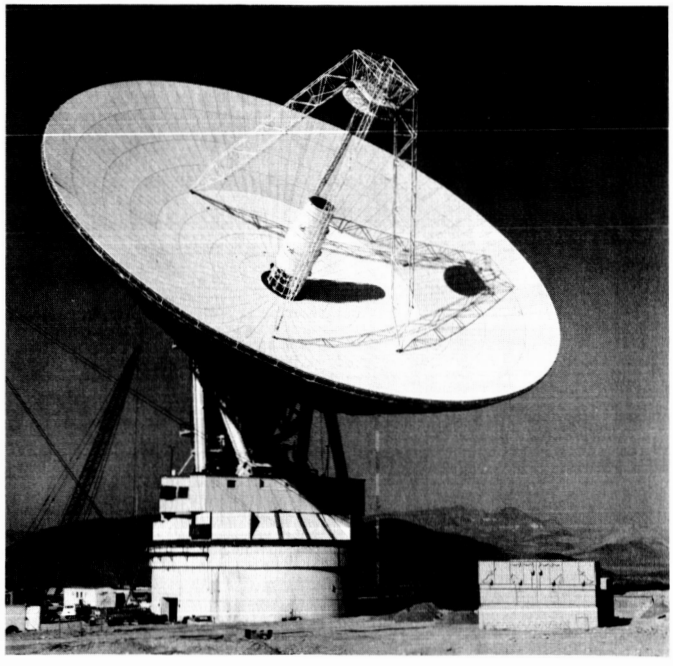

Fig. 6. 210-ft antenna in near completion stage

B. Real-Time Computation, Plotting, and Transmission of *Mariner IV* Occultation Data

As a part of the *Mariner IV* Project, three computer programs were written for computing, plotting, and transmitting data related to occultation of the *Mariner IV* spacecraft. Two of these computer programs were written for the Digital Instrumentation Subsystem (DIS) (Fig. 7) at the Pioneer Station of the Deep Space Instrumentation Facility (DSIF), and one was written for the SDS 930 computer at the Echo Station.

The programs written for the Pioneer Station provided for real-time computation of doppler residuals and integrated doppler phase change, from 15 min before to 15 min after occultation of the *Mariner IV* spacecraft. The program written for the Echo Station was used by the SDS 930 computer for reading the TTY information and plotting the data on the Benson-Lehner Plotter, for display via closed-circuit TV at JPL.

The programs written for the Pioneer Station also provided for data conversion and teletype transmittal at 100 wpm to the Systems Data Analysis (SDS) Group at the DSIF Station and to the JPL Space Flight Operations Facility (SFOF) at JPL, for real-time plotting and analysis. The three programs may also be used for other spacecraft mission operations.

The following equipment was used in occultation computations and resultant data processing:

(1) Digital instrumentation subsystem (Fig. 7), consisting of the following: SDS 910/920 digital computer, two magnetic tape units, communication buffer, line printer, Moseley plotter, and card reader.

(2) Teletype, 100 wpm communication equipment, to transmit data to SFOF.

(3) SDS 930 digital computer and Benson-Lehner Plotter located at the DSIF Echo Station.

(4) IBM 7044 digital computer and plotter located at the SFOF.

The purpose of the first program at the Pioneer Station is to read incoming teletype doppler predictions generated at JPL by the orbit determination (OD) group, to interpolate these data to 1-sec doppler predictions, and to write the data so obtained on magnetic tape. The purpose

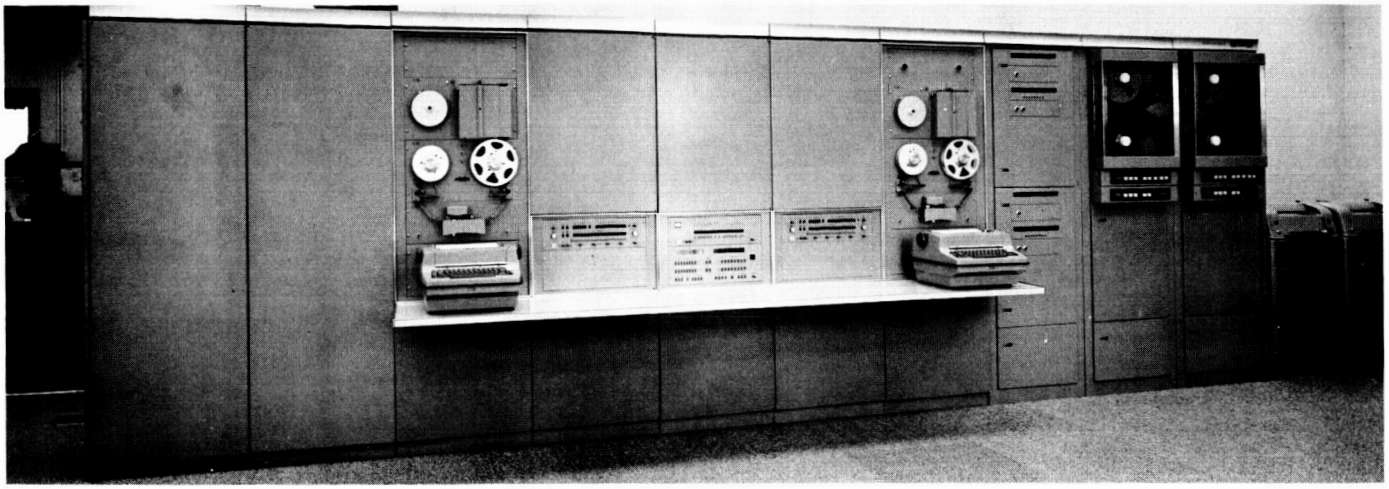

Fig. 7. Digital instrumentation system (DIS), Pioneer Station

of the second program is to gather raw doppler data from the tracking data handling (TDH) subsystem of the Pioneer Station and compare this data with the doppler predicts. The required outputs are then computed for output to the line printer, Moseley plotter, and teletype lines (TTY). The computer program written for the Echo Station enables the SDS 930 computer to read the TTY information and plot the data on the Benson-Lehner Plotter. This plotted information is, in turn, displayed via closed-circuit TV at JPL.

The first program to be executed by the DIS during an occultation experiment is the Doppler Predictions Interpolation (Fig. 8). This program takes the 5-min doppler predictions directly from the TTY tape, interpolates them to 1-sec doppler predictions, and writes the predictions on magnetic tape. Modification of the SDS 920 paper tape reader was required to enable the computer to read the teletype tape. Two safety features are incorporated into the subroutine to save time in reclaiming bad teletype images. One of these features is the added capability to type in any combination of the first five teletype images, the number required for properly initiating the interpolation program. This feature provides a breakpoint setting, allowing the operator to type in the correct image if a teletype image is bad. Another safety is a negative time check. If the time is interpreted as negative for some reason, the program ignores the time and passes control to the typewriter for entering the correct time value.

The control statements for the Predict Interpolation Program (Figs. 8, 9, and 10) are entered on the typewriter (start-time of predicts, end-time of predicts, predict-time interval, desired predict interval, number N of points for

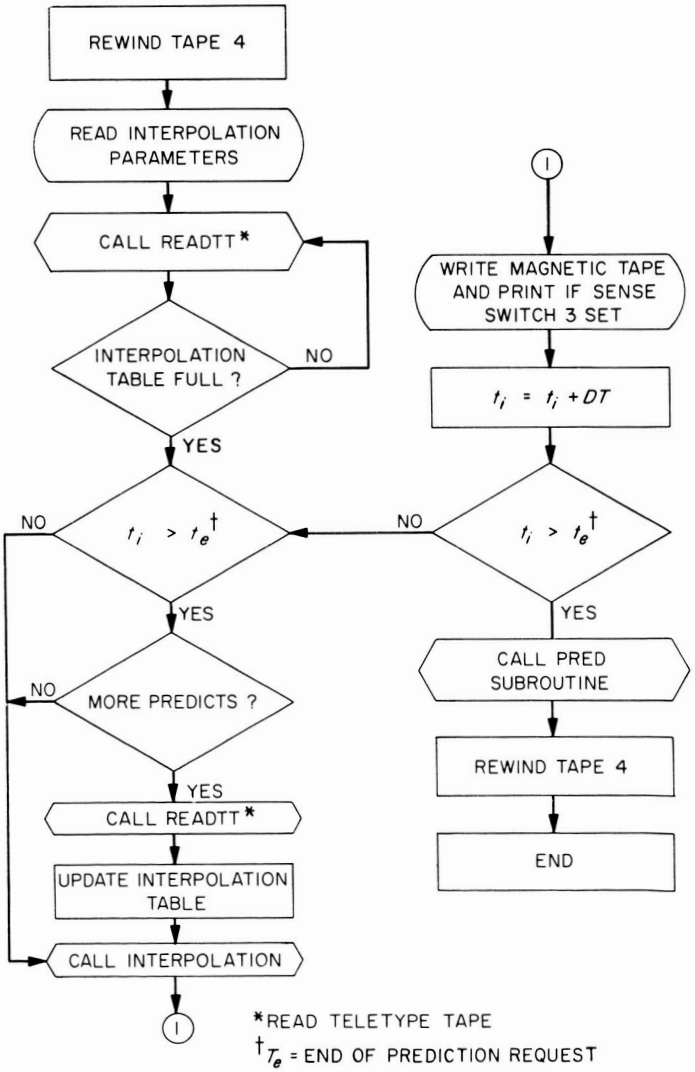

Fig. 8. Prediction interpolation program flow chart

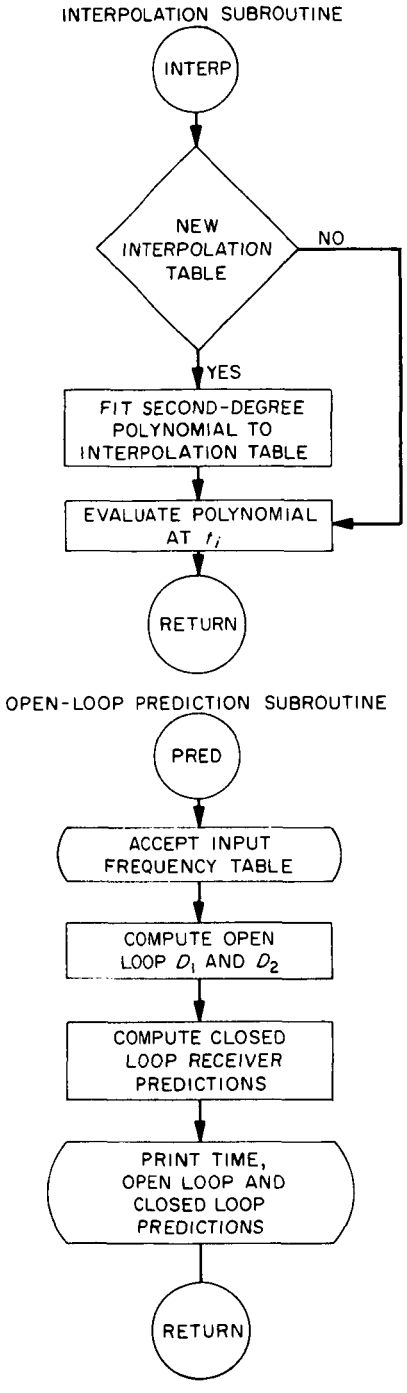

Fig. 9. Interpolation subroutine flow chart

interval, degree of polynomial). The first N points are read in from the paper tape reader. The program does its interpolation as close to the center of the polynomial fit as possible. The desired 1-sec predictions are written in binary on magnetic tape with the following format

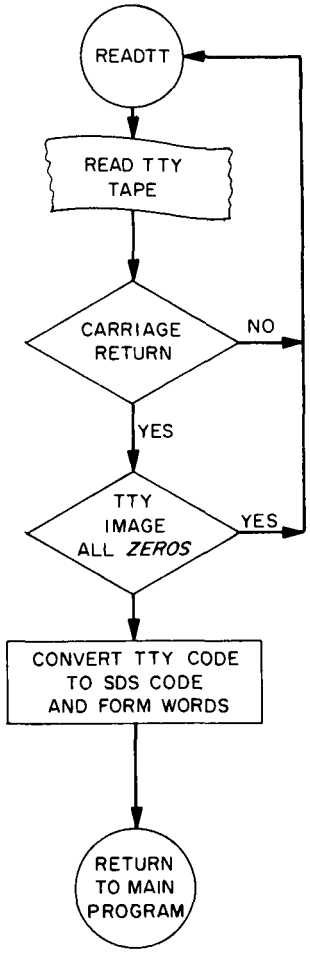

Fig. 10. Teletype tape-read subroutine flow chart

(time in seconds, one-way doppler, two-way doppler). Another feature of the program is its capability to calculate and list predicted receiver frequencies to be used by the RF Techniques Group for the open loop receivers at Pioneer and Echo Stations.

The standard DSIF predictions generated in the SFOF were converted to open-loop one-way and two-way (F_1 and F_2) receiver frequencies per the following equations:

$$F_1 = \frac{10^6 - D_1 - (50 \times 10^6)}{96} + F_R \frac{240}{221} + 125.0$$

$$F_2 = \frac{10^6 - D_2 - (50 \times 10^6)}{96} + F_T \frac{240}{221} + 125.0$$

where

D_1 = the predicted one-way biased doppler for the closed-loop receiver

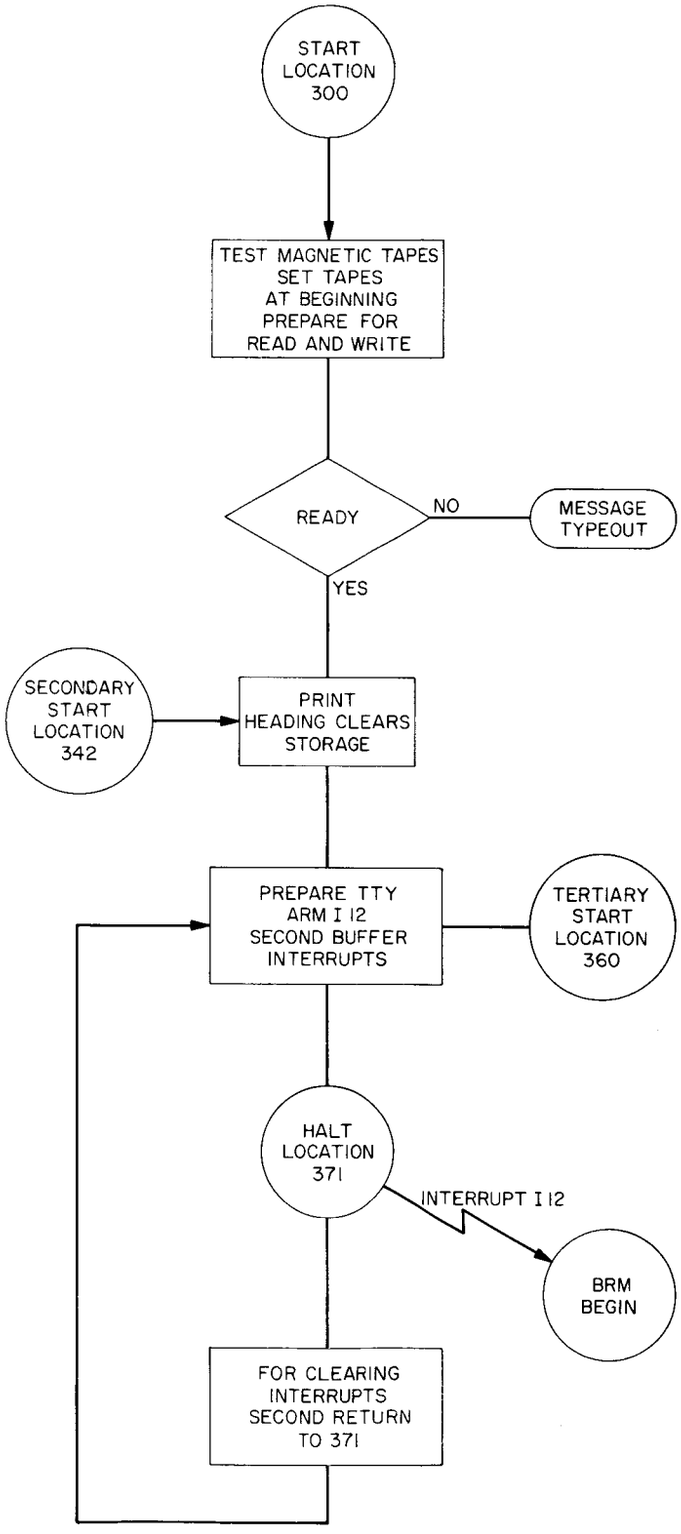
START LOCATION 300
TEST MAGNETIC TAPES SET TAPES AT BEGINNING PREPARE FOR READ AND WRITE
READY
NO
MESSAGE TYPEOUT
YES
SECONDARY START LOCATION 342
PRINT HEADING CLEARS STORAGE
PREPARE TTY ARM I 12 SECOND BUFFER INTERRUPTS
TERTIARY START LOCATION 360
HALT LOCATION 371
INTERRUPT I 12
BRM BEGIN
FOR CLEARING INTERRUPTS SECOND RETURN TO 371

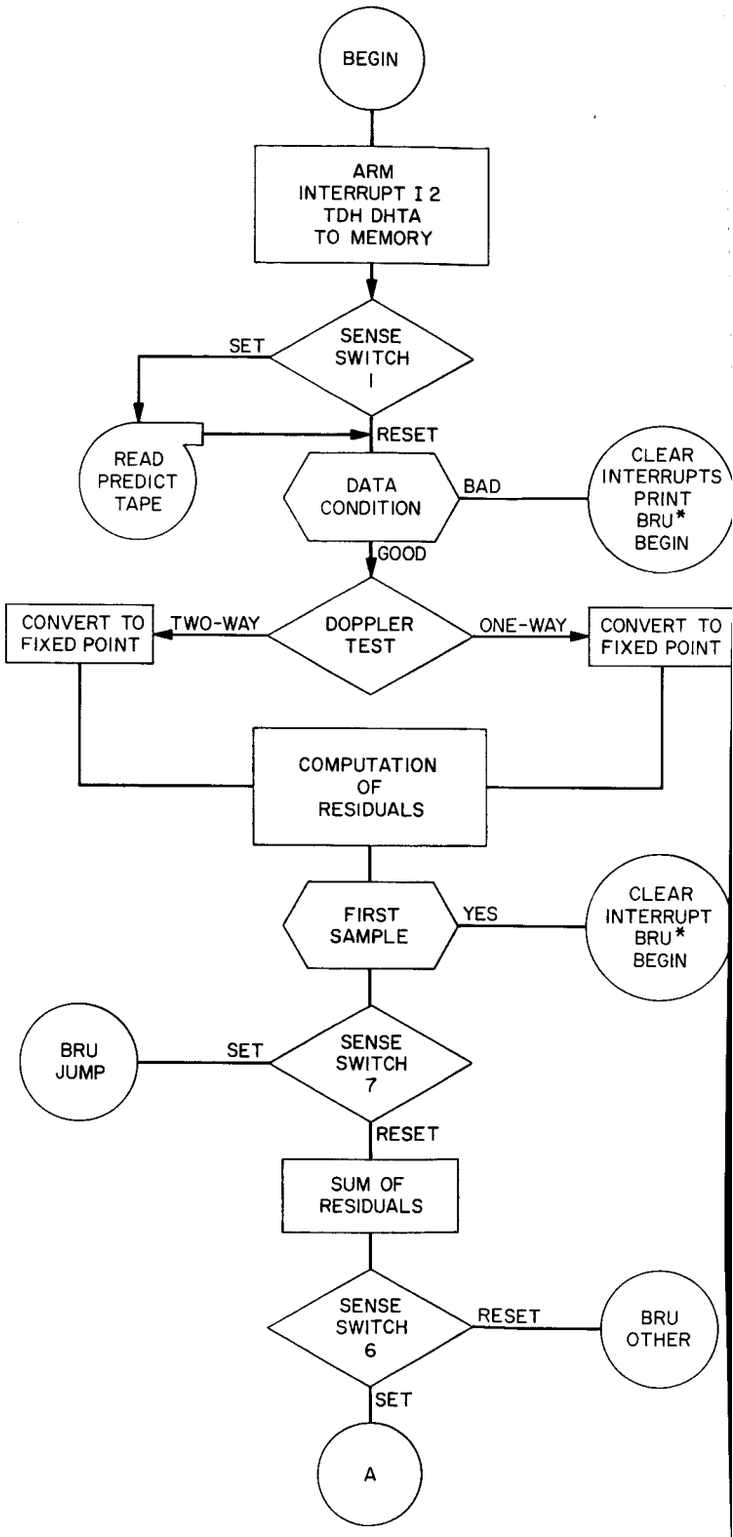
BEGIN
ARM INTERRUPT I 2 TDH DHTA TO MEMORY
SET
SENSE SWITCH 1
RESET
READ PREDICT TAPE
DATA CONDITION
BAD
CLEAR INTERRUPTS PRINT BRU* BEGIN
GOOD
CONVERT TO FIXED POINT
TWO-WAY
DOPPLER TEST
ONE-WAY
CONVERT TO FIXED POINT
COMPUTATION OF RESIDUALS
FIRST SAMPLE
YES
CLEAR INTERRUPT BRU* BEGIN
BRU JUMP
SET
SENSE SWITCH 7
RESET
SUM OF RESIDUALS
SENSE SWITCH 6
RESET
BRU OTHER
SET
A

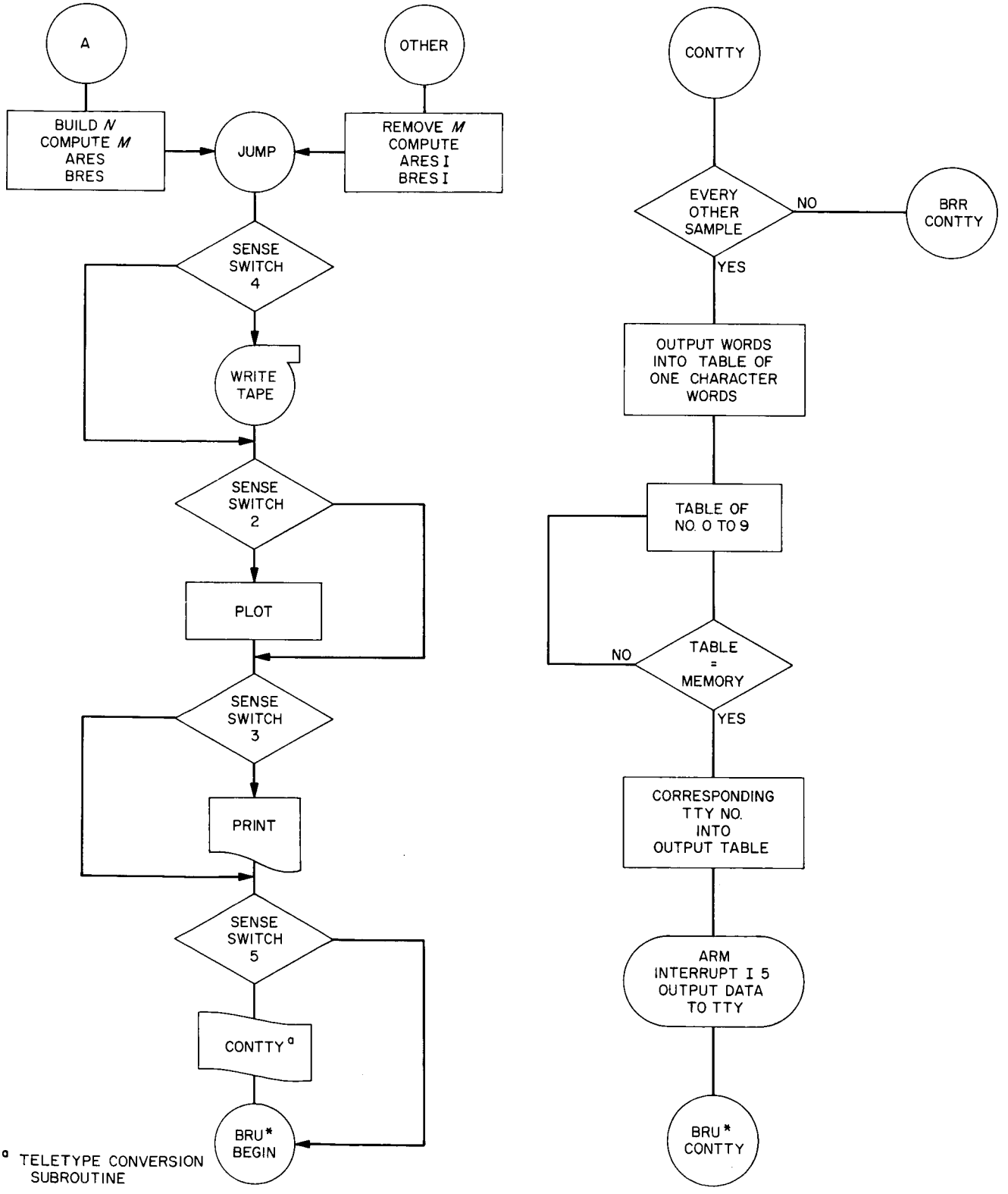

Fig. 11. Real-time occultation program flow chart

D_2 = the predicted two-way biased doppler for the closed-loop receiver

F_R = the closed-loop receiver reference frequency used for the one-way closed-loop predictions

F_T = the predicted transmitter frequency for two-way closed-loop doppler

10^6 = the 1-Mc doppler bias

50×10^6 = the 50-Mc IF

125.0 = an empirically determined constant for the open-loop receiver

The closed-loop doppler occultation predictions were then interpolated to 1-sec intervals as follows:

$$D_{ij} = A_{oj} + A_{1j}\, t_i + A_{2j}\, t_i^2$$

Where t_i is the interpolation time and A_{oj}, A_{1j}, and A_{2j} are coefficients determined by a second-degree, least square curve fit to five predicted doppler samples centered about t_i. D_{ij} is the interpolated doppler at time t_i($j = 1$ for one-way doppler, $j = 2$ for two-way doppler).

The occultation program (Fig. 11) is a real-time interrupt-dependent program; or, in other words the program depends upon interrupts for its execution. The TDH data is gathered by the program and compared with the doppler predictions. The program searches the magnetic tape for current predictions, compares the observed doppler (converted to cycles per second) with the predicted, writes the residuals on magnetic tape, transmits the residuals to the line printer, plots the residuals on the Moseley Plotter. Time (GMT) and scaled doppler residuals are then transmitted over high-speed teletype lines. All functions and computations of the program require 1.8 sec of time. All eight sense switches are used to control output subroutines and certain internal computations.

The real-time occultation program (Fig. 11) makes use of quite a number of specially written subroutines and SDS programmed operators. Programmed operators permit the calling of subroutines with a single instruction of the same form as machine instructions. The computer uses Locations 100 to 177 to uniquely transfer to the subroutines. The computer records the return address at location zero so that program continuity is maintained. The SDS programmed operators used are the double precision fixed point arithmetic package (XDPA), the binary-to-decimal double-precision fixed-point package (BDD), the binary-to-decimal single-precision fixed-point package (BID), and decimal-to-binary single-precision fixed package (DIB). Three special subroutines (Fig. 11) are the four-bit decimal word to the six-bit decimal word, the six-bit decimal word to the five-bit decimal teletype word, and the four-bit decimal word to binary. The sense switches are utilized by the program in such a manner that all the peripheral equipment and some of the computations can be called manually while the program is in the operating mode.

The desired 1-sec sample rate presents a problem of timing. The computer is fully able to perform all functions required within the interval of 1 sec, but the high-speed teletype lines require 1.8 sec to transmit each set of required data for plotting. (Fig. 12 illustrates the TTY paper tape output and predict formats.) In order to transmit as much information as possible, only every other data sample result is sent on the teletype line during real-time. The raw data and the analysis for each data sample are stored on magnetic tape and printed on the line printer (Fig. 13). After the real-time run, all or any portion of the analysis can be sent over the high-speed communications system to expand any desired part of the real-time plotted data.

The program at real-time is dependent on interrupts for its execution. One magnetic tape contains the predicted 1-sec doppler. If the interrupt system delivers good data, as determined from the data condition code, from the TDH subsystem the program computes both the doppler residual and integrated doppler. The program does its computations as follows:

$$\text{Observed doppler (DOPPL)} = \frac{\text{Present doppler count (DOPP)} - \text{Last doppler count (DOP1)}}{\text{(Doppler multiplier) (time interval)}}$$

The predicted doppler (PREDO) is read from magnetic tape. If bad data condition is observed, the program automatically reinitializes and waits for the next interrupt. Good data condition code allows the program to continue. Under this condition:

$$\text{DOPPL} - \text{PREDO} = \text{Residual (RESID)}$$

With Sense Switches 6 and 7 set, the program computes the following:

$$\text{ARES} = (\text{RESID} + \text{BIAS}_1)\,(\text{SCALE}_1)$$

$$\text{BRES} = \left(\sum_1^N \text{RESID} + \text{BIAS}_2\right)(\text{SCALE}_2).$$

ARES and BRES are teletype outputs (Figs. 8, 9, and 10). BIAS_1, BIAS_2, SCALE_1, and SCALE_2 are scale fac-

(a) PUNCHED TELETYPE TAPE, OUTPUT FORMAT

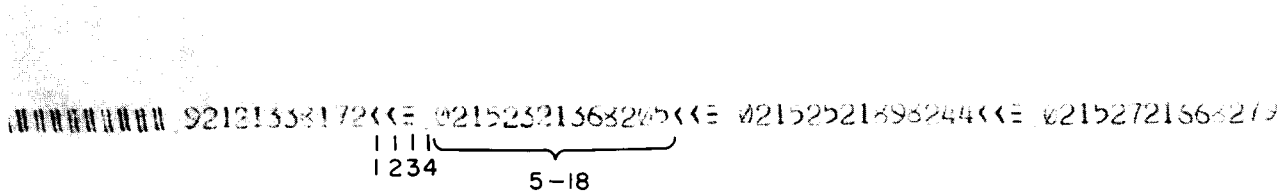

1. CARRIAGE RETURN
2. CARRIAGE RETURN
3. LINE FEED
4. FIGURES
5. TENS OF HOURS
6. UNITS OF HOURS
7. TENS OF MINUTES
8. UNITS OF MINUTES
9. TENS OF SECONDS
10. UNITS OF SECONDS
11. THOUSANDS OF RESIDUAL (ARES)
12. HUNDREDS OF RESIDUAL
13. TENS OF RESIDUAL
14. UNITS OF RESIDUAL
15. THOUSANDS OF RESIDUAL (BRES)
16. HUNDREDS OF RESIDUAL
17. TENS RESIDUAL
18. UNITS OF RESIDUAL

(b) PUNCHED TELETYPE TAPE, PREDICT FORMAT

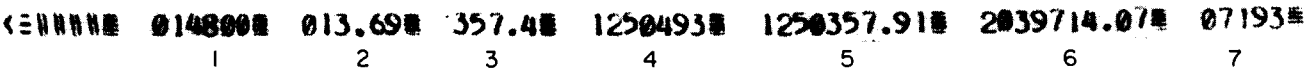

1. GMT (hr, min, sec)
2. LOCAL HOUR ANGLE
3. DECLINATION ANGLE
4. ONE-WAY DOPPLER
5. TWO-WAY DOPPLER
6. RANGE
7. PREDICTION IDENTIFIER AND DAY OF YEAR

Fig. 12. Tape punching, output and predict formats

tors for plotting, and N (the number of residuals) is stored for computing:

$$\text{MEAN}\,(M) = \frac{1}{N}\sum_{1}^{N}\text{RESID, where } N = 1, 2, 3, \cdots$$

When Sense Switch 6 is reset, the mean is removed from the residuals, to provide

$$C = \text{RESID} - M$$

$$D = \sum_{1}^{N} C$$

$$\text{ARES} = (C - \text{BIAS}_1)\,(\text{SCALE}_1)$$

$$\text{BRES} = (D - \text{BIAS}_2)\,(\text{SCALE}_2).$$

This program also has the capability of storing each residual sample in memory in such a manner that all the computations can be done in a reverse-time sequence, if desired. This capability is particularly needed for post-occultation. The program results are written on magnetic tape and printed on the line printer (Fig. 13). The plot subroutine uses the Moseley Plotter to plot the residuals at the DSIF station, as illustrated in Fig. 14.

The program is physically contained on punched green Mylar tape. This program tape is read into the memory of the SDS 920 by the standard fill procedure. Once the program is in memory, it can be initialized by three modes, primary, secondary, and tertiary. The primary mode clears particular storage areas, tests for the proper configuration and rewinds the Alpha and Beta magnetic tapes, prints the headings and arms the interrupt. The secondary mode prints the heading, clears storage areas,

MARINER MARS OCCULTATION EXPERIMENT JULY 14,1965

DAY	TIME	CONDITION	COUNT	OBS. DOPPLER	PREDICT DOPPLER	RESIDUALS
0196	221412	8040	0466437466	237047.5330078	237049.1552734	-1.5722656
0196	221418	8040	0477815037	237049.3955078	237050.9980469	-1.6025391
0196	221424	8040	0489194296	237051.2705078	237052.8408203	-1.5703125
0196	221430	8040	0500572848	237053.1230469	237054.6855469	-1.5625000
0196	221436	8040	0511951486	237054.9580078	237056.5292969	-1.5712891
0196	221442	8040	0523330212	237056.7910156	237058.3730469	-1.5820313
0196	221448	8040	0534709028	237058.6660156	237060.2207031	-1.5546875
0196	221454	8040	0546087932	237060.5000000	237062.0673828	-1.5673828
0196	221500	8040	0557466924	237062.3330078	237063.9150391	-1.5820313
0196	221506	8040	0568846006	237064.2080078	237065.7626953	-1.5546875
0196	221512	8040	0580225175	237066.0205078	237067.8173828	-1.5917969
0196	221518	8040	0591604432	237067.8535156	237069.4619141	-1.6083984
0196	221524	8040	0602983761	237069.7705078	237071.3110234	-1.5410156
0196	221530	8040	0614363216	237071.5625000	237073.1630859	-1.6005859
0196	221536	8040	0625742742	237073.4580078	237075.0146484	-1.5566406
0196	221542	8040	0637122355	237075.2910156	237076.8662109	-1.5751953
0196	221548	8040	0648502061	237077.1875000	237078.7197266	-1.5322266
0196	221554	8040	0659881854	237079.0205078	237080.5732422	-1.5527344
0196	221600	8040	0671261735	237080.8535156	237082.4277344	-1.5742188
0196	221606	8040	0682641706	237082.7285156	237084.2832031	-1.5546875
0196	221612	8040	0694021766	237084.5630078	237086.1386719	-1.5756641
0196	221618	8040	0705401915	237086.4375000	237087.9951172	-1.5576172
0196	221624	8040	0716782153	237088.2910156	237089.8525391	-1.5615234
0196	221630	8040	0728162462	237090.1875000	237091.7109375	-1.5234375
0196	221636	8040	0739542898	237092.0000000	237093.5693359	-1.5693359
0196	221642	8040	0750923403	237093.8955078	237095.4287109	-1.5332031
0196	221648	8040	0762303999	237095.7080078	237097.2890625	-1.5810547
0196	221654	8040	0773684683	237097.5830078	237099.1503906	-1.5673828
0196	221700	8040	0785065459	237099.5000000	237101.0117187	-1.5117187
0196	221706	8040	0796446325	237101.3330078	237102.8740234	-1.5410156
0196	221712	8040	0807827270	237103.1875000	237104.7373047	-1.5498047
0196	221718	8040	0819208315	237105.0410156	237106.6005859	-1.5595703
0196	221724	8040	0830589450	237106.9160156	237108.4648437	-1.5488281
0196	221730	8040	0841970672	237108.7910156	237110.3300781	-1.5390625
0196	221736	8040	0853351984	237110.6660156	237112.1962890	-1.5302734
0196	221742	8040	0864733385	237112.5205078	237114.0625000	-1.5419922
0196	221748	8040	0876114877	237114.4160156	237115.9296875	-1.5136719
0196	221754	8040	0887496458	237116.2705078	237117.7978515	-1.5273437
0196	221800	8040	0898877128	237118.1250000	237119.6660156	-1.5410156
0196	221806	8040	0910259869	237120.0205078	237121.5351562	-1.5146484

Fig. 13. Raw data and data analysis sample printout

and arms the interrupts. The tertiary mode arms the interrupts. These three initializing modes are for purposes of either determining a new mean, subtracting a previously determined mean, or for not rewinding the predict tape.

The interrupt system brings the day number, time, data condition code, and raw doppler count to the computer via TDH and sends the time (GMT), residuals, and integrated doppler to the high-speed teletype lines (Fig. 12). The I12 interrupt controlled by the TDH subsystem delivers the raw data. The I5 interrupt controls the teletype output from the computer. The program may also sample analog data up to 100 times/sec with the I6 interrupt.

The computations are made only when good data condition has been received. The data condition code is a four-character numeric word. The characters must indicate the following conditions:

(1) Doppler average time as nondestructive

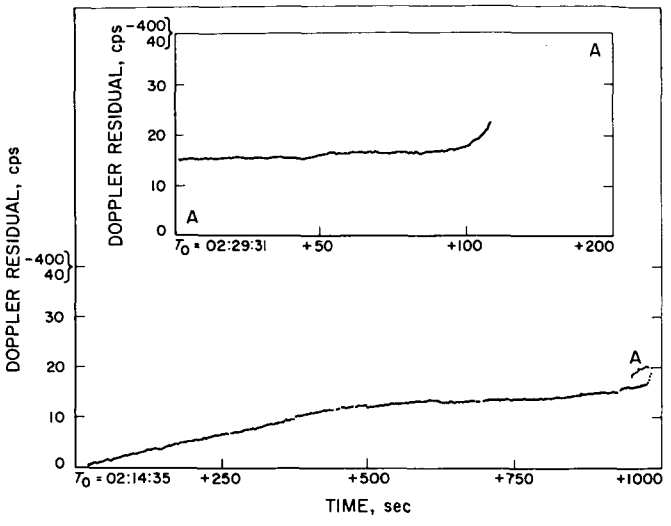

Fig. 14. Plot of residuals at DSIF station

(2) Receiver and servo data condition as good doppler and angle data or as good doppler and bad angle data

(3) Doppler mode as one-way (C_1) or two-way (C_2) or two-way, two-station noncoherent (C_3)

(4) Atomic frequency standard in lock.

The program during the occultation period can be readied for the playback of selected 1-sec samples by setting a sense switch. The program then halts until the experimenter is ready for the requested playback. The playback occurs during occultation. After the generation of post-occultation predicts, the computer memory is cleared. The program is loaded again and started; bad condition code is received until the moment of receiver lockup (emersion). The residuals are stored in memory, beginning with the moment of emersion. After about 15 min the program may be stopped by setting a sense switch, and the computer readied for working the computations in the reverse time sequence or, in other words, computing backward to occultation exit.

The purpose of the 930 Occultation Plot Program is to plot doppler residuals on the Benson-Lehner Point Plotter located at the Echo Station computer facility, as shown in Fig. 15. This plot is then displayed via closed-circuit TV in the SFOF for rapid interpretation of the results.

The equipment required to perform this operation includes the following:

(1) SDS 930 digital computer

(2) Benson-Lehner Model K point plotter

(3) Closed circuit TV equipment

(4) 100-wpm TTY page printer and reperforator

(5) TTY to SDS 930 interface electronics

The computer program generated to perform this function is fairly simple and straightforward. Since the input data (Fig. 12) is already scaled from 0 to 9999, the program merely has to convert from Baudot Code to formatted BCD for output to the plotter (Fig. 14). The x value is scaled from GMT values with the first GMT being set as x_0. Successive GMT's are differenced with x_0 and multiplied by an appropriate scale factor. The basic flow chart for this program is illustrated in Fig. 15.

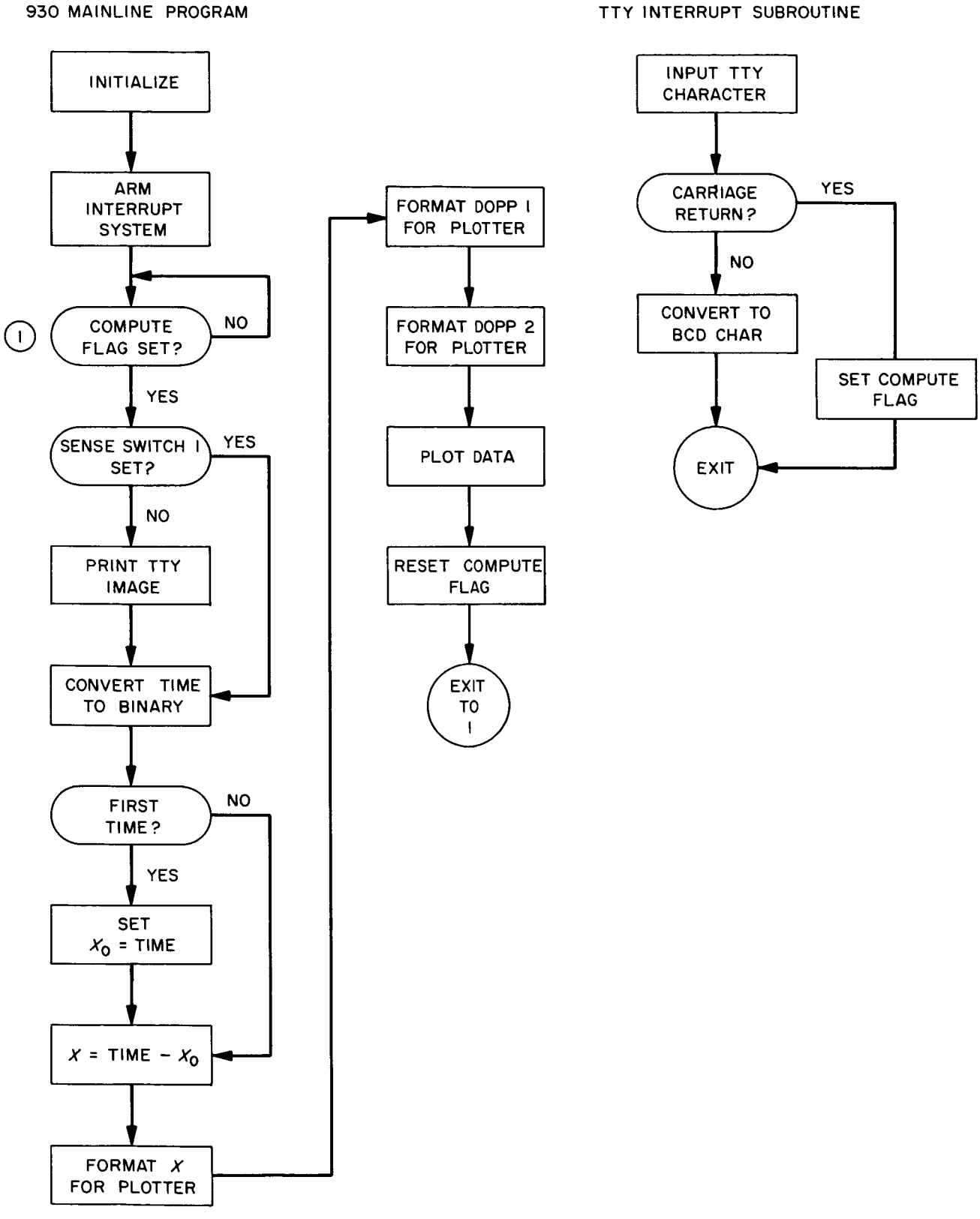

Fig. 15. 930 Mainline program and TTY interrupt subroutine flow chart

IV. Communications Engineering Development

A. S-Band Implementation for DSIF

1. DSIF Microwave Switch Control Assembly

Six microwave switch control assemblies for the DSIF S-band system have been installed and are presently fully operational. They are located at DSIF Stations 11, 12, 41, 42, 51, and 61. Two more assemblies have been delivered and are awaiting installation at DSIF 14 and 62. The design of the assembly is discussed in *SPS 37-25*, Vol. III, pp. 53–57. Some of the operating stations were used as prime and the others as backup for the *Mariner IV* mission. No microwave switch-control assembly failures have been reported. Operation during *Mariner IV* tracking indicated no performance deficiencies.

All documentation is now complete with the exception of the *Operating and Maintenance Manual* and the *Test Procedure*. These documents have been released for final publication and are due for distribution by December 1, 1965. All spares were delivered before April 1965. These spares are complete operating modules and include for each station: one switching and interlock logic, one rack control panel, four switch controllers, one mode control panel, and one interface connection panel.

2. Acquisition Aid for the Ascension Island Station (DSIF 72)

a. Performance. The acquisition aid monopulse antenna (Fig. 1) has been completed and tested at the JPL

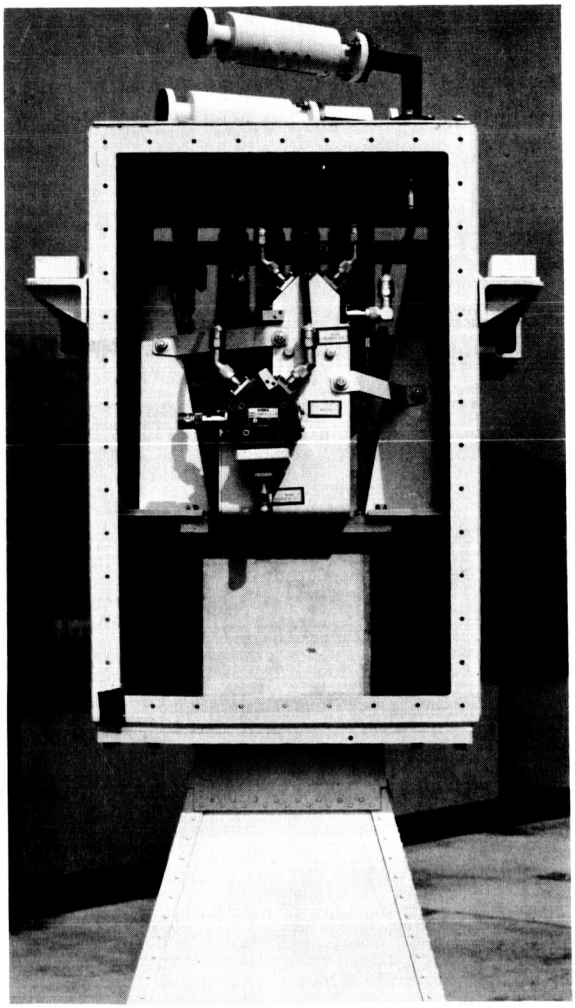

Fig. 1. Acquisition aid monopulse antenna

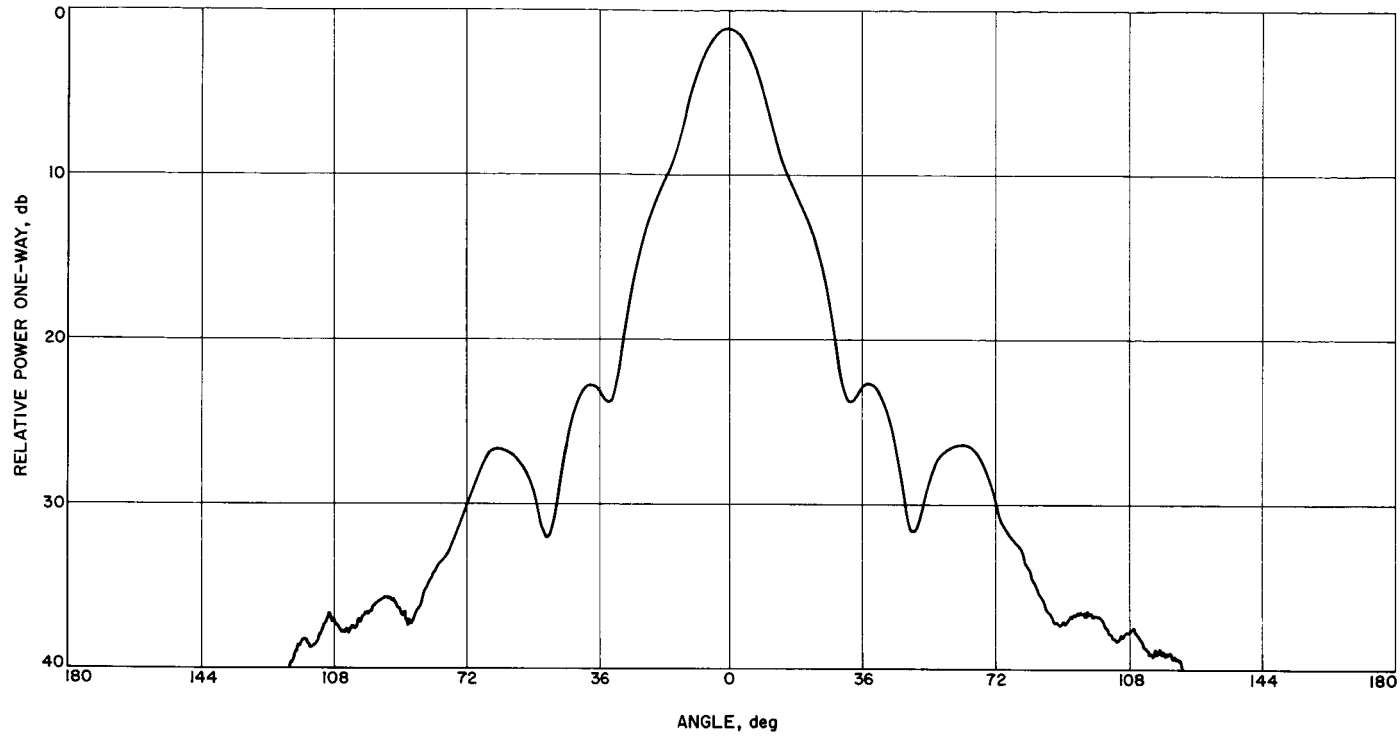

Fig. 2. RCP sum channel pattern

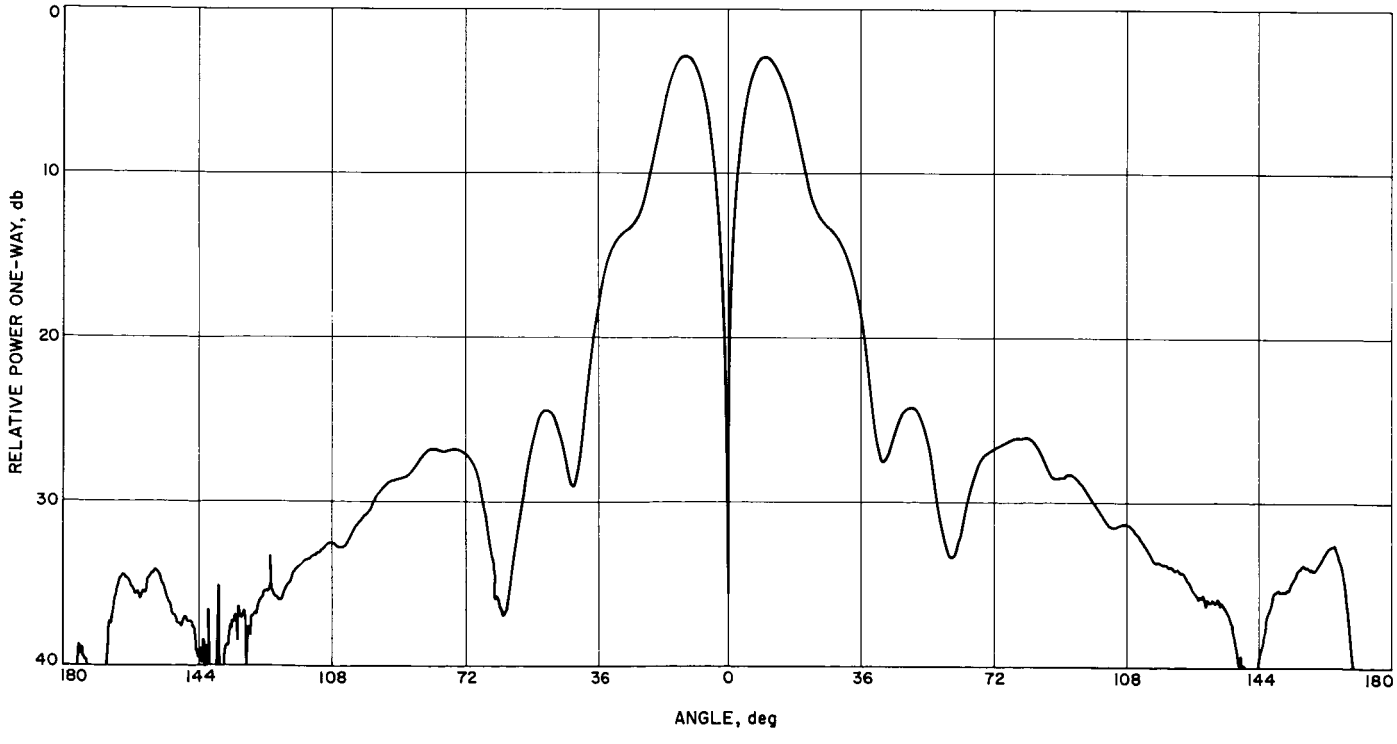

Fig. 3. RCP azimuth pattern

Mesa Antenna Range facility. Sum and error channel patterns are shown in Figs. 2 through 4. The right-hand circular polarization (RCP) sum channel beamwidth is 16.5 deg at the half-power points. Ellipticity is less than 0.4 db on axis at 2295 Mc and less than 1.8 db from 2270 to 2320 Mc. Linear Polarization (LP) patterns made over the band from 2270 to 2320 Mc show that good performance in both the sum and error channels (Figs. 5 and 6) is achieved. If the requirement arose, improved performance for the 2270 to 2300 Mc band could be easily obtained by redesigning the polarizer section for 2285-Mc center frequency instead of the 2295 ±5 Mc band now used. The bridge and remaining coaxial system is, to a large extent, frequency-insensitive.

The RCP error channel peaks are separated approximately 22½ deg with typical null depths greater than 38 db. The boresight null depth and null position vary with plane of polarization for an incident linear polarization, due to mechanical nonsymmetry in the polarizer and coaxial bridge; however, this boresight shift is less than ±0.12 deg from a nominal boresight zero. In addition, the error peak position changes with plane of polarization, due to the different gains of the modes generated in the multimode error channel phasing section. Maximum spread is from 18 to 23 deg, which is not expected to cause a significant servo-tracking problem.

Final measurements made on the polarizer section (SN 1) indicate a maximum VSWR of 1:07:1 and typical isolation greater than 30 db between RCP and LCP outputs (*SPS 37-33*, Vol. III, p. 29). VSWR of the bridge measured at the ⅞ and 1⅝ in. coaxial line outputs are typically those of the hybrid junction ports used; coaxial tuners are used in each channel at the 30-ft antenna apex to match the outputs.

Isolation between azimuth and elevation error channels is 27 db, and isolation between the error channel and sum channel is greater than 40 db. The maximum VSWR measured on any RCP bridge output from 2270 to 2320 Mc was 1.4:1. No attempt was made to match at other than the center frequency of 2295 Mc. The monopulse antenna is presently en route to Ascension Island.

The transmitter antenna (Fig. 7) was installed in the Pioneer Station 30-ft antenna for mechanical fit and then shipped to Ascension Island. Ellipticity is less than 0.4 db, and VSWR less than 1.07:1 with any combination of horn sections.

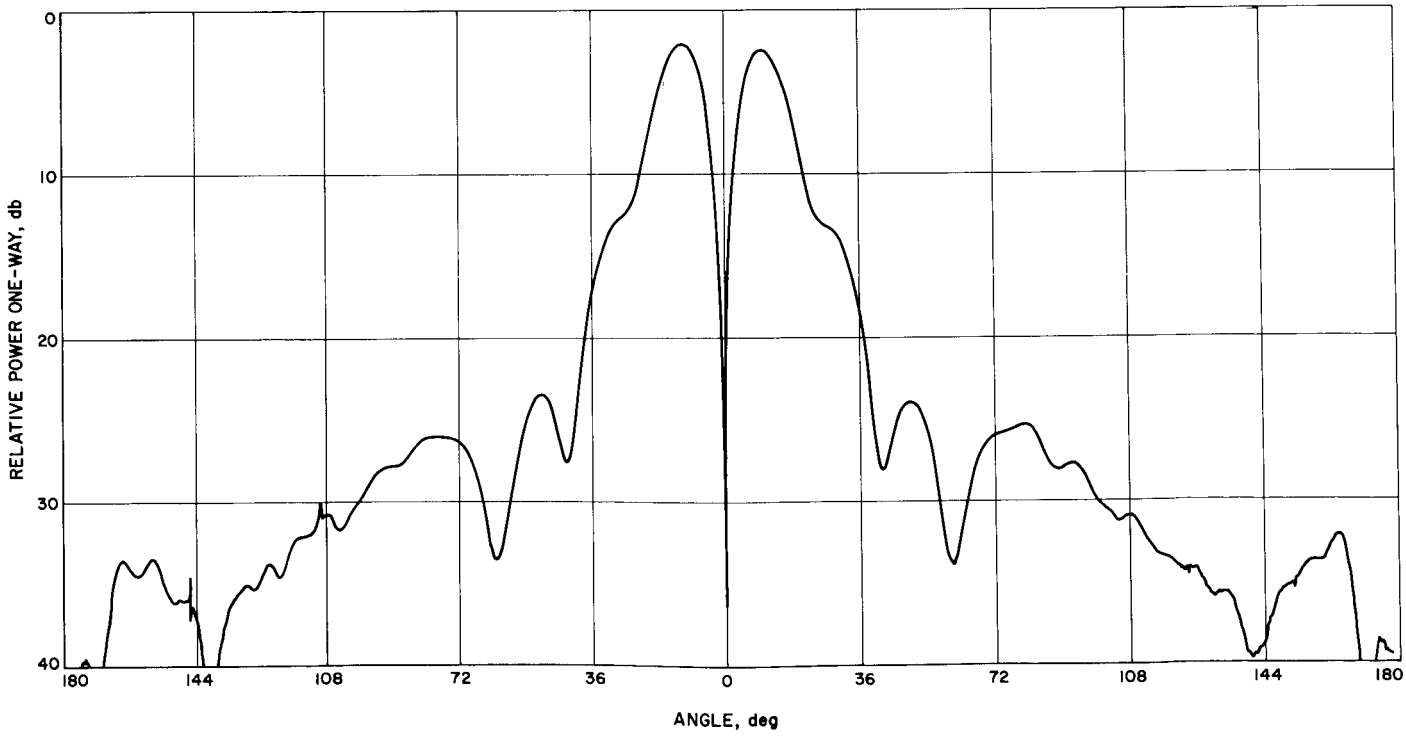

Fig. 4. RCP elevation pattern

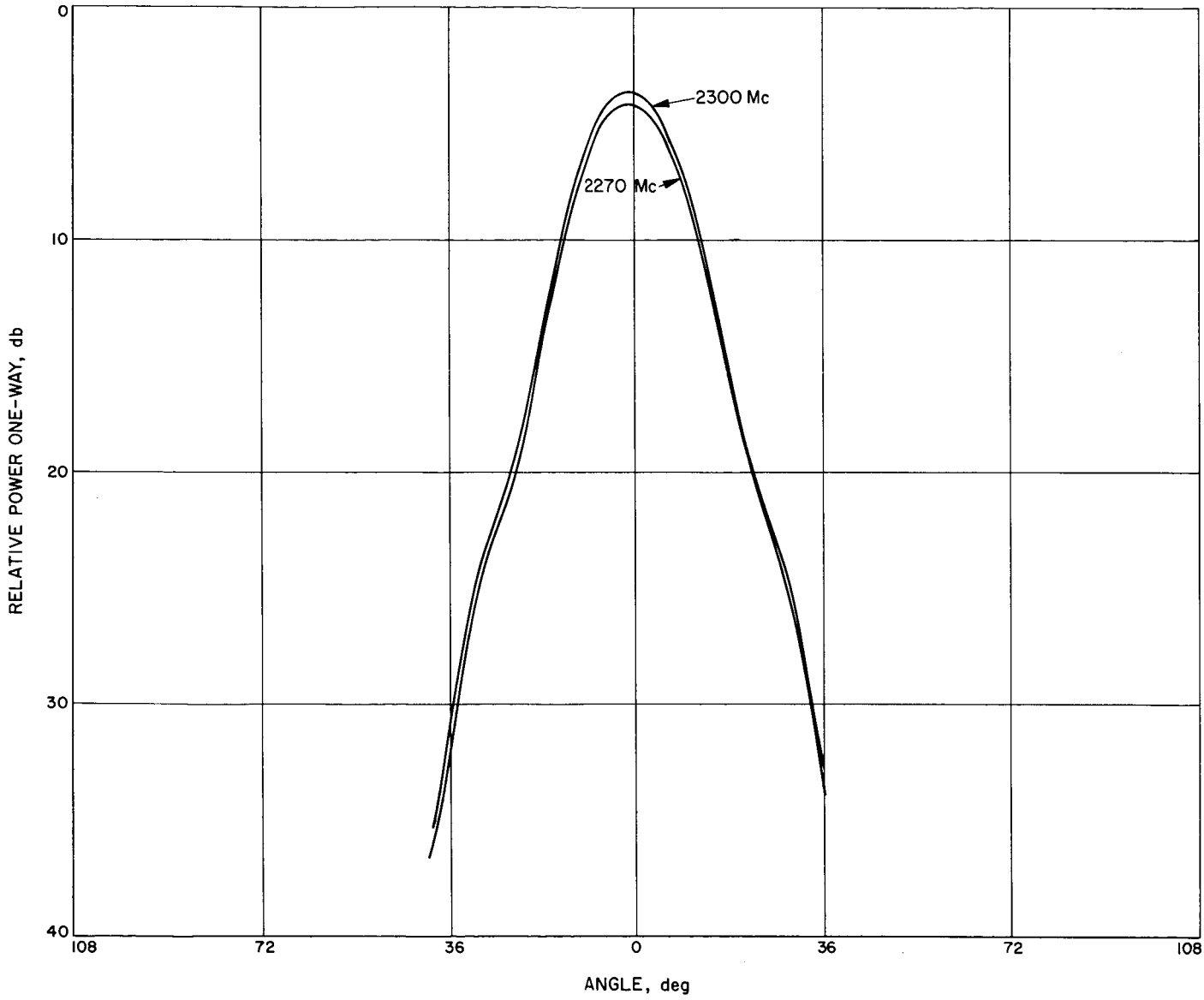

Fig. 5. LP sum channel pattern at 2270, 2295, and 2320 Mc

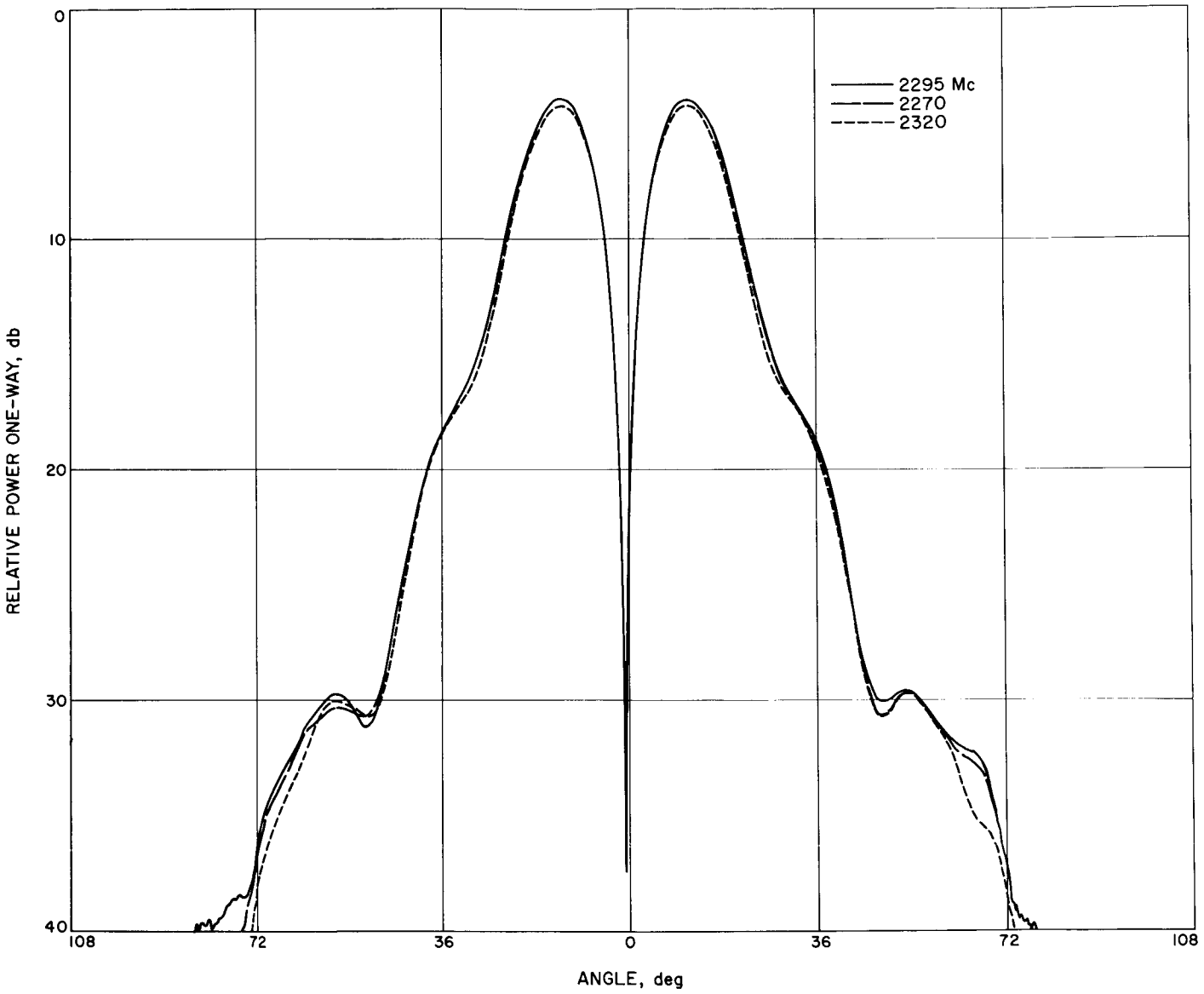

Fig. 6. LP azimuth channel pattern at 2270, 2295, and 2320 Mc

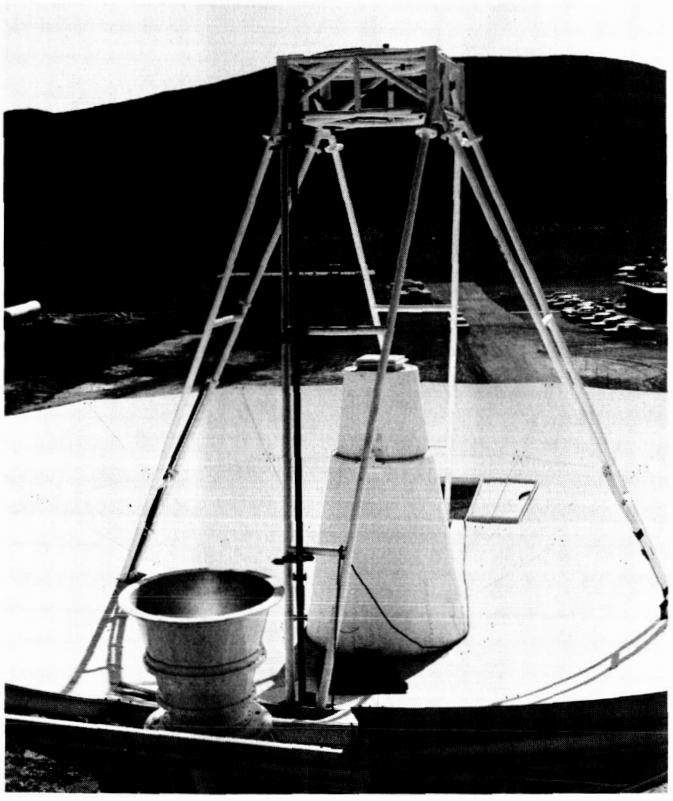

Fig. 7. Transmitter horn

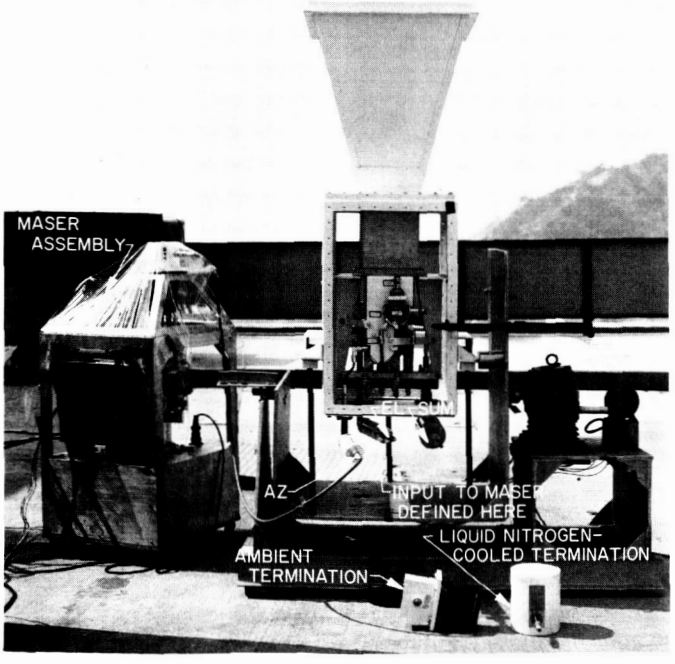

Fig. 8. Antenna noise temperature calibration setup (antenna pointing at zenith)

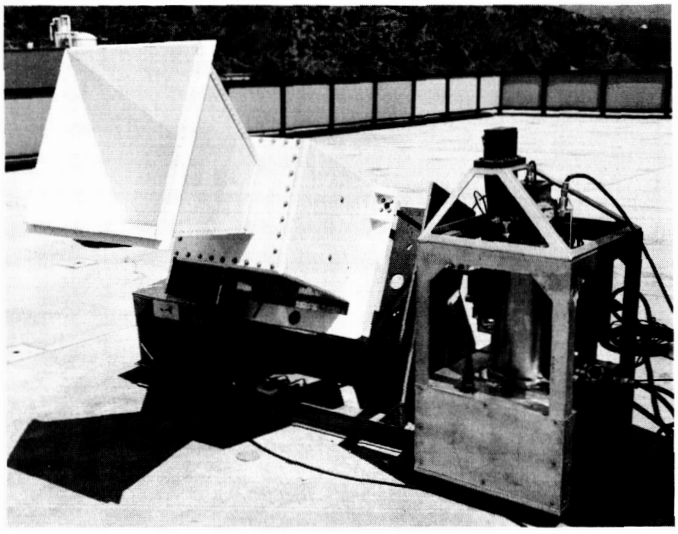

Fig. 9. Acquisition aid antenna at a lower than zenith elevation angle

b. Noise Temperature Calibrations: Measurement Procedure and Results. Measurements of antenna noise temperature were made with the antenna pointing at the sky at various elevation angles. Photographs of the test setup and the antenna in the zenith and lower elevation angle positions may be seen in Figs. 8 and 9. The noise temperature instrumentation consisted of a 2295-Mc radiometric traveling wave maser (TWM) and receiver system. Two noise temperature reference standards, a nitrogen-cooled termination and an ambient termination, were used to calibrate the radiometer recorder scale.

The measurement procedure was to switch the maser input manually between the antenna monopulse channels and the reference terminations with the antenna positioned at various elevation angles. For ease of calibration, transitions to Type N connector size were used to enable use of a flexible RG9 cable and Type N connector for quick connect and disconnect to the reference noise temperature standards (Fig. 8). The maser input is defined as the input to the RG9 cable. An example of the noise temperature recording of the elevation channel may be seen in Fig. 10. Fig. 11 shows a noise temperature recording of the sum, elevation, and azimuth channels at zenith (90 deg elevation angle).

The effective antenna noise temperatures of the various antenna channels as determined from reduced data are plotted in Fig. 12. The effective temperatures at the zenith position for the sum, azimuth, and elevation channels are 62.2, 51.4, and 52.8°K, respectively. The

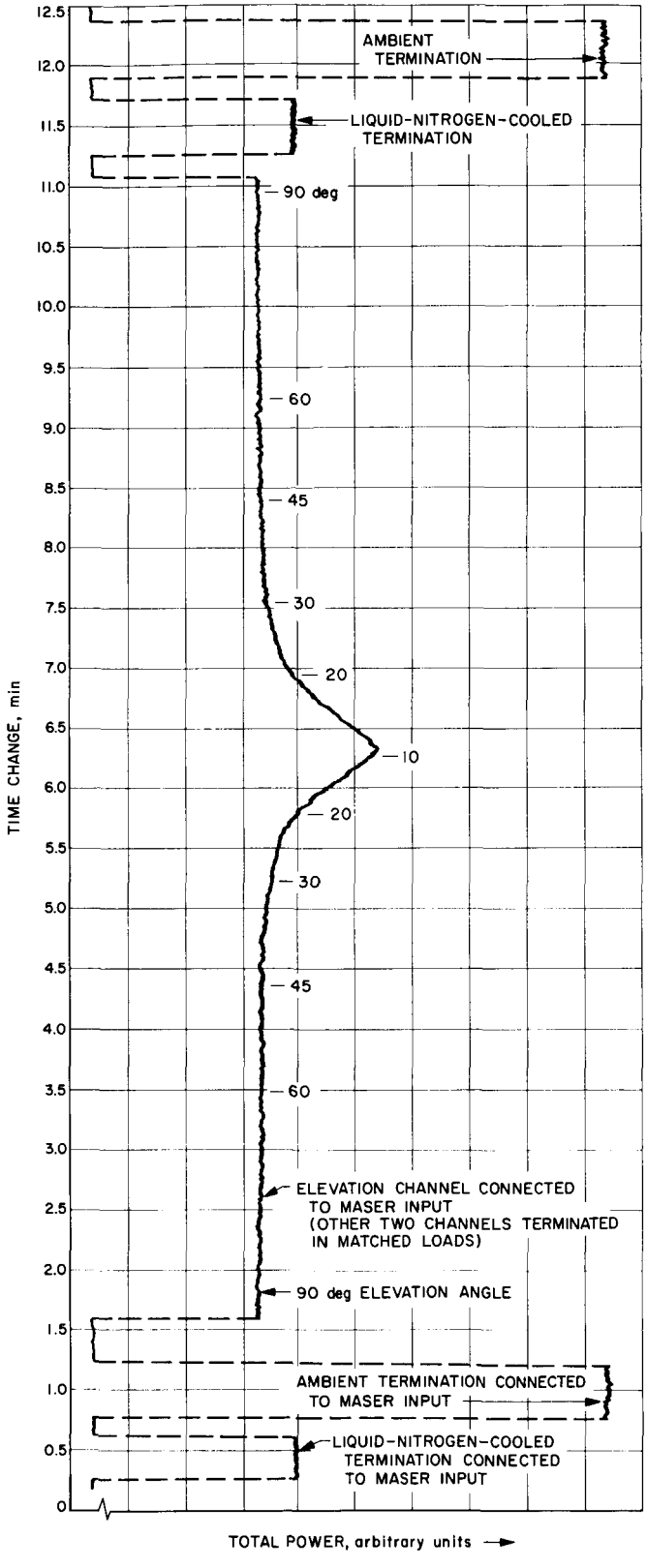

Fig. 10. Noise temperature recording for elevation channel

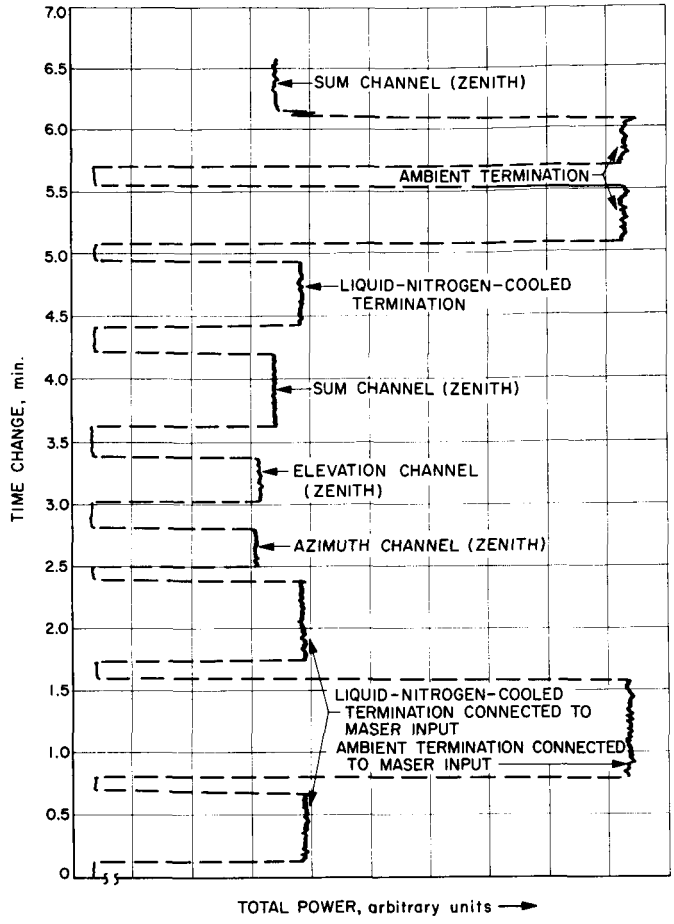

Fig. 11. Noise temperature recording (antenna at zenith position)

losses of the transitions used in the measurements were evaluated, and their temperature contributions have been accounted for in determining the effective temperatures of the various antenna channels. The effective temperatures shown in Fig. 12 are defined at the 1⅝-in. (EIA) output flange for the sum channel and the ⅞-in. (EIA) output flanges for the azimuth and elevation channels. The best estimate of the measured probable error (p.e.) of the effective antenna temperatures shown is $\pm 1.5°K$.[1]

At low elevation angles, the effective antenna temperatures of the elevation channel is higher than those of either sum and azimuth channels (Fig. 12). The higher

[1] The measured probable error does not include deviations which would occur if antenna temperatures had been measured in a flat desert ground environment. It should be noted that the effective antenna temperature given in this report was measured in the antenna test environment as seen from the roof of Bldg. 238 at JPL. The effects of a non-uniform horizon for this test environment have not been evaluated in this reporting.

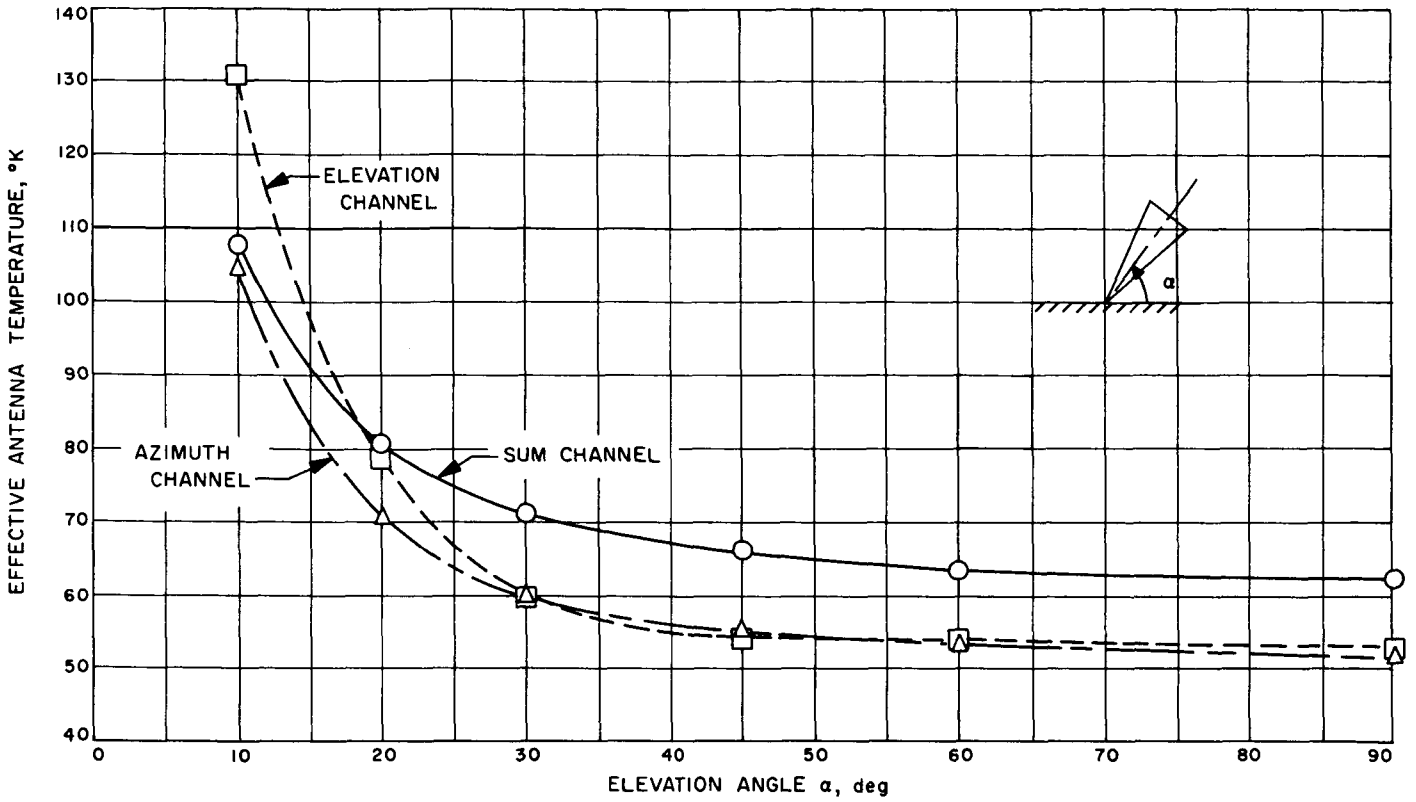

Fig. 12. Acquisition aid antenna effective noise temperatures

value could be explained by the fact that as the antenna is being scanned towards the lower elevation angles, one of the main antenna beams for the elevation channel will intercept the ground environment sooner than either the main beams of the azimuth channel or the sum channel.

Another parameter of interest for the acquisition aid antenna is the line loss of each of the monopulse channels. An attempt was made to make a direct measurement of line loss using standard insertion loss measurement techniques, but difficulties were encountered due to the lack of proper transitional equipment. An alternate method of determining antenna line loss is to use the measured values of effective antenna temperature, the measured ambient temperature, and estimated values of antenna temperature for the lossless transmission line case. This method will be explained further in the following discussion.

The expression for the effective antenna temperature is given as

$$T'_A = (1 - L^{-1})\, T_0 + L^{-1} T_A \qquad (1)$$

where

L = line loss ratio of the transmission line between the horn mouth and the reference plane where T'_A is defined (Fig. 13).

T_0 = physical transmission line temperature, °K

T_A = antenna temperature for the lossless transmission line case defined at the horn mouth, °K

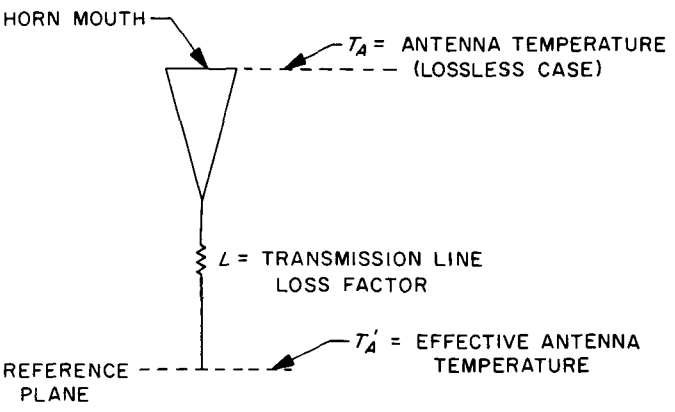

Fig. 13. Effective antenna temperature and transmission line loss

Solving Eq. (1) for the line loss ratio, we obtain

$$L = \left[\frac{T_0 - T_A}{T_0 - T'_A}\right] \tag{2}$$

The values of T'_A are the experimentally determined effective noise temperatures given in Fig. 12. The physical transmission line temperature was measured during the experiment to be 291.6 ±0.2°K p.e.

For determination of T_A, assume that the antenna pattern in a spherical coordinate system (ρ, ξ, Ψ, where ξ and Ψ are the azimuthal and polar angles, respectively) has a circular symmetry with respect to ξ. (Refer to Fig. 31 of Ref. 1 for coordinate system.) If the antenna environment is subdivided into N annular solid angle subregions starting from $\Psi = 0°$ to $\Psi = 180°$, then the value of antenna temperature for the lossless case may be obtained from the approximate formula,

$$T_A \simeq \sum_{k=1}^{N} T_k(\eta_B)_k \tag{3}$$

where

T_k = average brightness temperature of the kth subregion in degrees Kelvin.

η_k = fractional power contained in the kth annular solid angle subregion. It may also be defined as the contribution of the kth subregion to beam efficiency.

The RCP antenna patterns for the acquisition aid antenna illuminated in RCP and LCP and a computer program were used to determine values of $(\eta_B)_k$ for each antenna channel. A discussion of antenna patterns to fractional power contained in an antenna beam is given in Ref. 1.

The values of T_k used in Eq. (3) for the subregion between zenith ($\psi = 0$ deg) and the horizon ($\psi = 90$ deg), were obtained from sky brightness temperature curves published by Hogg in Ref. 2. A zenith sky brightness temperature of 2.45°K was used for computations for antenna temperature at 2295 Mc. For simplification, an average constant value of 240°K was assumed for T_k in the antenna back lobe region (90 deg $\leq \psi \leq$ 180 deg).

The accuracy of the approximate formula given by Eq. (3) improves as N increases. For calculation of antenna temperatures for the acquisition aid antenna, a value of 45 was used for N. A summary of the calculated antenna temperatures and line losses as determined from Eq. (2) and (3), respectively, are given in Table 1.

The probable errors for T_A shown in Table 1 include probable antenna pattern errors and the probable error due to uncertainty of the values used for sky and ground brightness temperatures. For calculations of the latter probable error, the sky and ground temperature values T_k, used to calculate T_A in Eq. (3), were estimated to have a maximum error of ±10%.

The total probable error in determining L is a function of the individual probable errors of the variables in Eq. (2). As shown in Ref. 3, the total probable error of the insertion loss factor L may be expressed as

$$(PE_L)^2 = \left(\frac{\partial L}{\partial T_0}\right)^2 PE^2_{T_0} + \left(\frac{\partial L}{\partial T_A}\right)^2 PE^2_{T_A} + \left(\frac{\partial L}{\partial T'_A}\right)^2 PE^2_{T'_A} \tag{4}$$

Then

$$PE_L = \frac{1}{(T_0 - T'_A)^2}\sqrt{[(T'_A - T_A)\,PE_{T_0}]^2 + [(T_0 - T'_A)\,PE_{T_A}]^2 + [(T_0 - T_A)PE_{T'_A}]^2} \tag{5}$$

Table 1. Measured and calculated temperatures and line losses for the acquisition aid antenna

Antenna channel	Measured zenith T'_A, °K	Measured T_0, °K	Calculated zenith T_A, °K	Calculated line loss ratio	Calculated line loss, db
Sum	62.2 ±1.5 p.e.	291.6 ±0.2 p.e.	$5.6\ ^{+0.5}_{-0.3}$ p.e.	$1.2467\ ^{+0.0084}_{-0.0083}$ p.e.	0.958 ±0.029 p.e.
Azimuth	51.4 ±1.5 p.e.	291.6 ±0.2 p.e.	$10.5\ ^{+0.8}_{-0.6}$ p.e.	$1.1703\ ^{+0.0080}_{-0.0077}$ p.e.	$0.683\ ^{+0.030}_{-0.029}$ p.e.
Elevation	52.8 ±1.5 p.e.	291.6 ±0.2 p.e.	$11.3\ ^{+0.8}_{-0.6}$ p.e.	$1.1738\ ^{+0.0081}_{-0.0078}$ p.e.	$0.696\ ^{+0.030}_{-0.029}$ p.e.

For antenna temperature measurements, it is important to check to ensure that the antenna is picking up sky and background noise only, and not unwanted CW signals as well. Because of increased receiver sensitivity with the maser system used, it was possible to detect the presence of several CW signals between 2290 and 2300 Mc which could cause serious errors in the antenna temperature calibrations. These CW signals could be readily observed on a spectrum analyzer. The main sources of these signals were traced to signal generators and test transmitters turned on during the day at JPL. With cooperation obtained from several Laboratory personnel, the necessary equipment was turned off in the evening, enabling the antenna temperature measurements to be made without any detectable radio interference.

Because the DSIF 72 acquisition aid schedule has permitted noise temperature evaluation of only one unit to date, it is not presently known whether the noise temperature and insertion loss data presented in this reporting will be typical of both the unit tested and the second (spare) unit which is presently nearing completion.

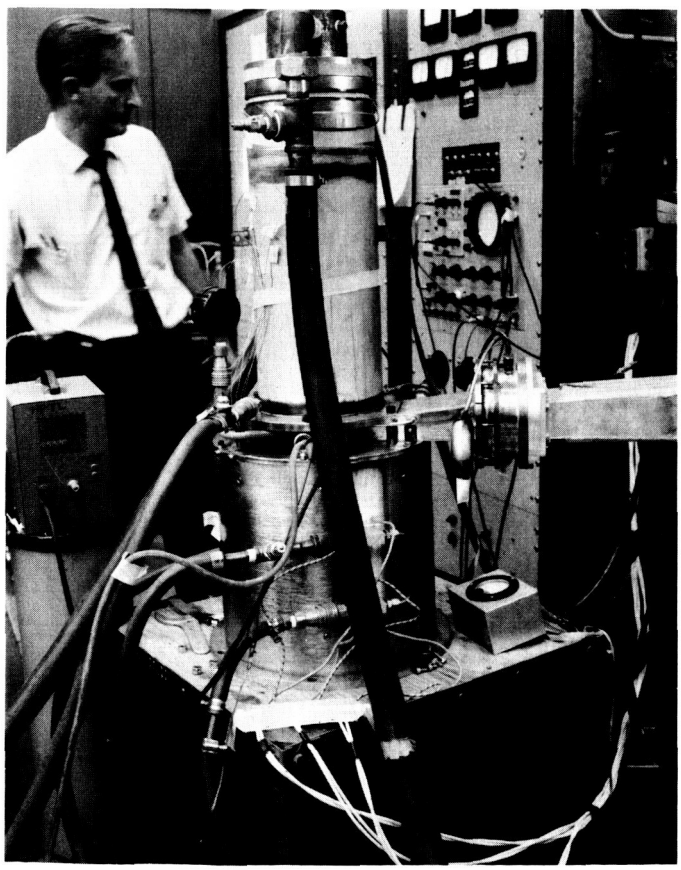

Fig. 14. Klystron test setup

B. 100-kw S-Band Final Amplifier

One of the chief elements in the program to upgrade the performance and reliability of the 100-kw S-band amplifier is the replacement of the existing klystron final amplifiers with similar but more reliable klystrons (*SPS* 37-33, Vol. III, p. 88).

The first X3060 klystron has been built and tested by the manufacturer, and partial acceptance tests were witnessed by JPL engineers. Fig. 14 shows the tube under test in the manufacturer's facility. The klystron met or exceeded specifications in all respects, except that a higher order window mode was excited near the lower end of the 2.1 to 2.4 gHz tuning range. This defect is to be eliminated before the tube is shipped to JPL. Preliminary tests results are summarized:

Frequency	2.388 gHz
Beam voltage	35 kv
Beam current	6.9 amp
Saturated output power, high-efficiency tuning	112 kw
Saturated gain	55 db
Bandwidth (3 db)	16 Mc
Efficiency	46.5%

The hardware required for mounting the klystron has been fabricated and is ready for use. Transmitter cabinet modifications required by the larger dimensions of the X3060 klystron and by plumbing changes are well under way. A focus magnet power supply for this klystron has been built and successfully tested.

C. *Mariner IV* 100-kw CW Transmitter

A new buffer amplifier for the exciter used to drive the 100-kw *Mariner IV* final amplifier was completed, tested, and installed prior to the scheduled date for sending the commands on the low-gain antenna to return the spacecraft to a cruise mode. This buffer was similar to the triode amplifier flown in *Mariner IV* and replaced a unit which exhibited excessive deterioration in output power.

Original Exciter. The equipment originally supplied to excite the 100-kw final amplifier in the *Mariner IV*

transmitter was built by JPL personnel at Goldstone, because no standard DSIF subsystem was available for this assignment.

Subsequently it developed that the output power level of the buffer amplifier deteriorated rapidly to the point where it became impossible to drive the 100-kw klystron into saturation. The final amplifier output power then dropped and the effective radiated power to the spacecraft was reduced. More significantly, the unsaturated klystron became more unstable.

New Buffer Amplifier. Life tests on the type of triode tube flown in the *Mariner IV* were encouraging, so two amplifiers (one spare) were constructed, using the *Mariner* configuration, with the cavities redesigned to operate in the 2110 to 2120 Mc band.

The amplifier is temperature-compensated and normally operated in an air-conditioned Cassegrain cone. Tests on the completed unit over the range from −5 to +125°F showed an output power variation of less than 0.1 db. The only significant temperature effect was a slight variation of the bandwidth. A few of the data points are tabulated below to illustrate this:

Temperature, °F	Frequency (3 db points)		Power Output, dbm
	Low, Mc	High, Mc	
−5	2105.1	2121.5	36.55
+25	2105.0	2121.5	36.55
+70	2105.0	2122.0	36.50
+125	2104.5	2122.0	36.55

Amplitude linearity and bandwidth of the amplifier are shown in Fig. 15. The input level was changed in 1-db steps, and the output recorded as the input frequency was swept over the passband.

The amplifier is normally operated from regulated filament and plate power supplies. However, the effect of filament voltage variations for a constant plate voltage was measured and is illustrated by Fig. 16. The normal filament voltage is 5.3 v dc. Plate voltage variations for a constant filament voltage are shown in Fig. 17. These curves were recorded with a sweep generator and *x-y* plotter. The vertical scale is nonlinear due to recorder detector characteristics. The amplifier has performed satisfactorily in service to date.

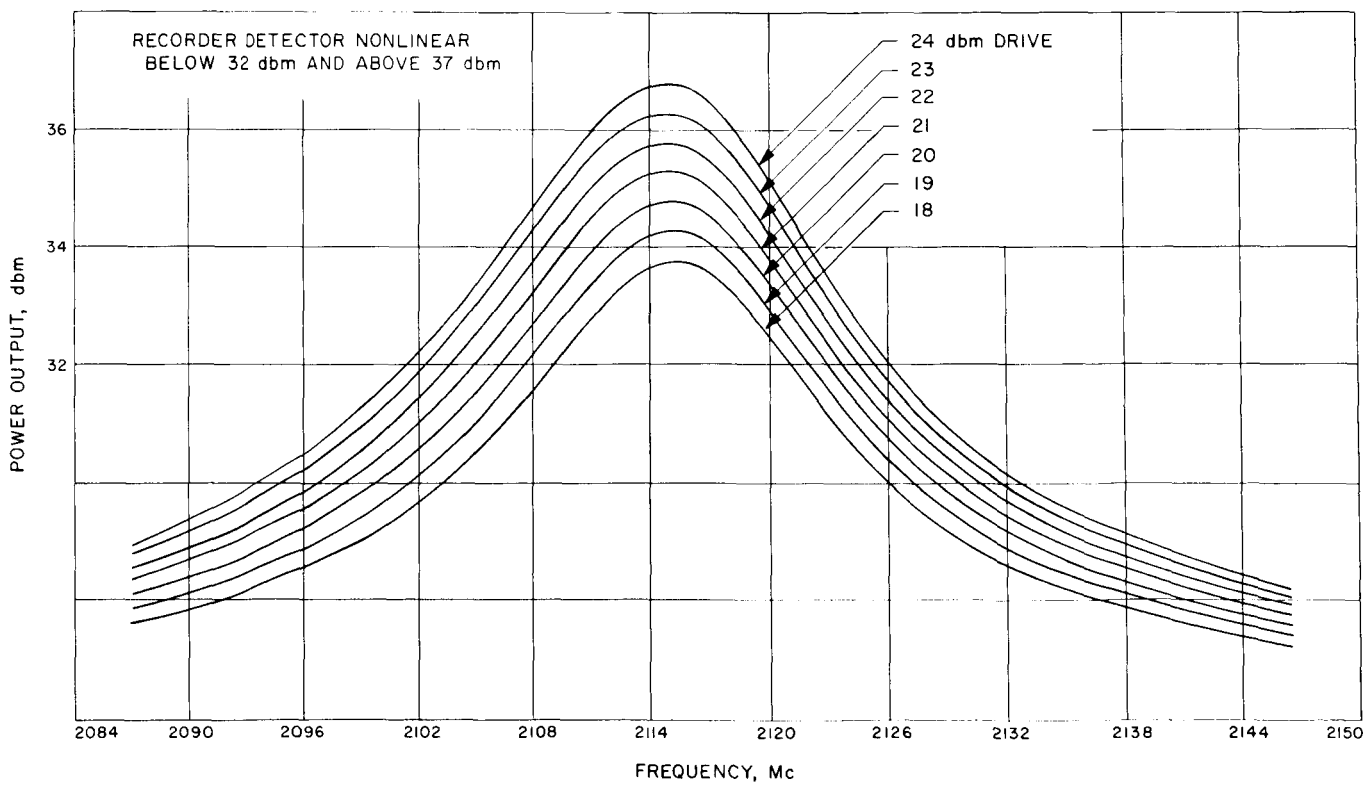

Fig. 15. Buffer amplifier gain and frequency characteristics

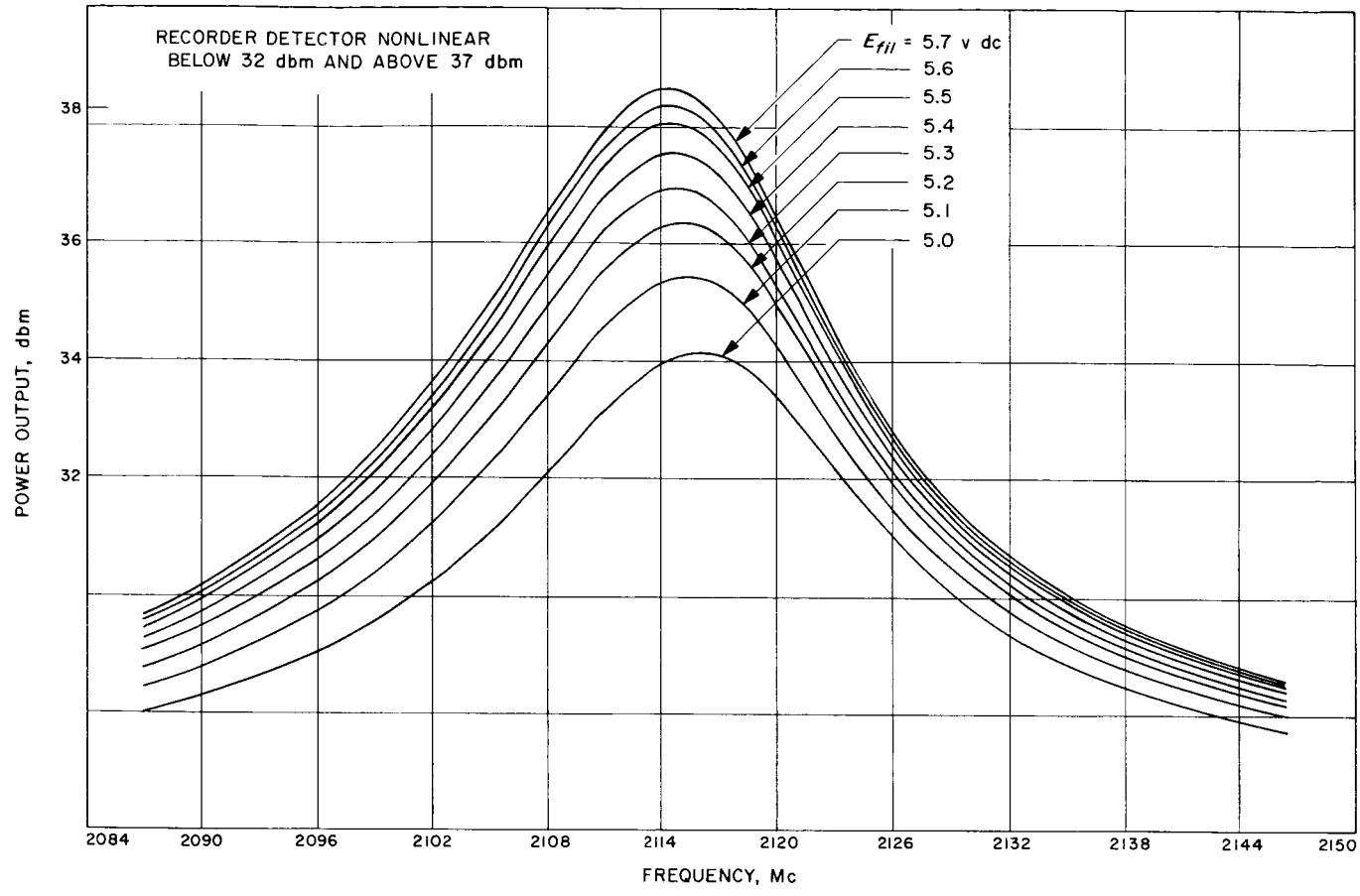

Fig. 16. Buffer amplifier sensitivity to filament voltage change, constant plate voltage E_b

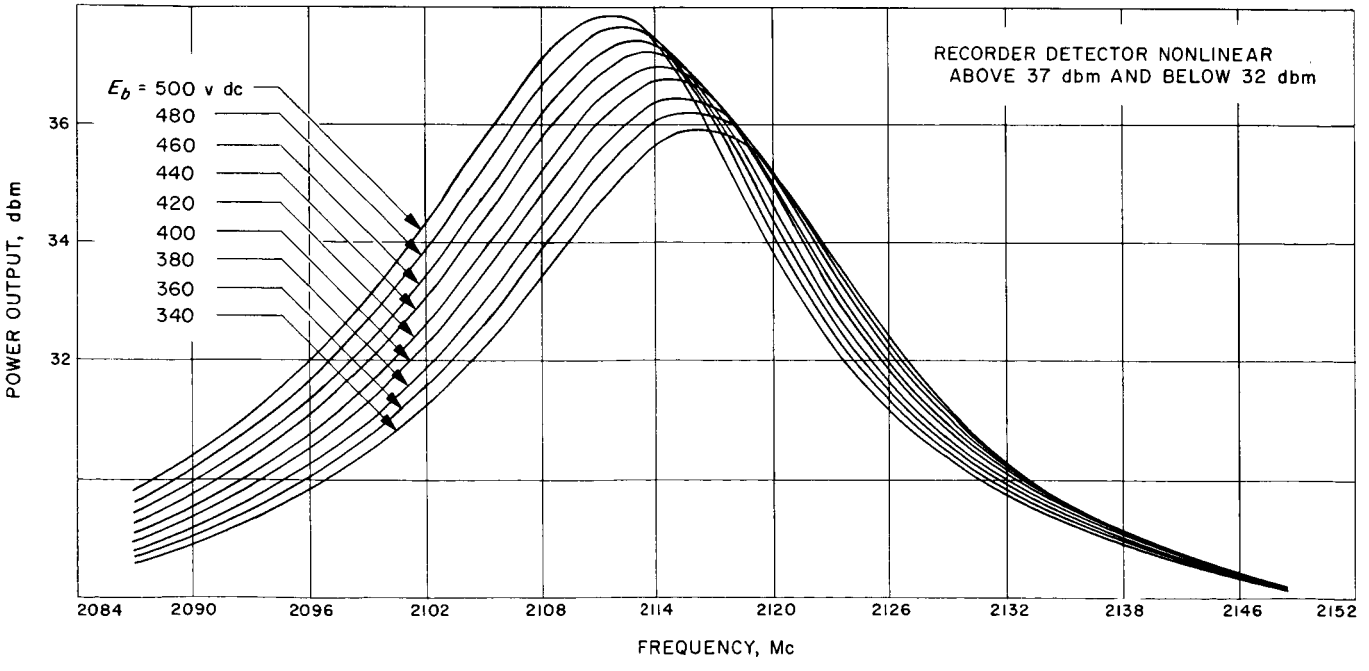

Fig. 17. Buffer amplifier sensitivity to plate voltage change, constant filament voltage E_{fil}

D. Dual Carrier Test, 100-kw Klystron

Dual carrier tests were conducted on the VA-858-A, SN 5 klystron to investigate the feasibility of amplifying two carriers simultaneously with third-order intermodulation products at least −30 db from the carriers. The tests were conducted at frequency separations from 1.5 to 8.5 Mc. Preliminary investigation shows that the intermodulation product is near the −30 db requirement, and a more refined method of measurement must be established. The VA-858-A klystron is being replaced by the new improved X3060 klystron, which is expected to reduce the intermodulation. It appears that amplifying two carriers through one klystron is possible; and, should a need arise for dual carrier operation, further testing will be conducted on the X3060 klystron.

Exciters. Suitable exciters were not available for these tests, so two signal generators driving buffer amplifiers were used as exciters. The incidental spurious noise of each exciter output was measured, and all noise was 50 db below each carrier within ±20 Mc of both carriers. The exciter outputs were combined in a coaxial 3-db hybrid with two circulators at each input to the hybrid for additional isolation (Fig. 18). The combined output of the exciters was measured for intermodulation. There was no degradation to the spectrum.

Klystron. The klystron final amplifier beam power was set to 30.5 kv at 8.05 amp as required for 100-kw output with a bandwidth of 9.7 Mc at the −1 db points (Fig. 19). The combined output from the two exciters was then used to drive the klystron to 10 kw per carrier, using the dummy load as a calorimeter for power measurements.

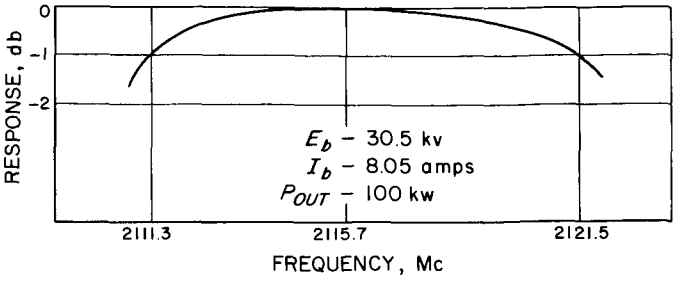

Fig. 19. VA-858-A bandwidth

The klystron outputs, as observed on a spectrum analyzer, are shown in Figs. 20 through 23. The third-order intermodulation products are approximately −30 db down from the carriers, with at least a 1-db uncertainty in the measurement. A small amount of the intermodulation products (0.5 to 1 db) is attributed to mixing in the spectrum analyzer.

The third-order intermodulation products are defined as

$$2f_{c1} - f_{c2} \quad \text{and} \quad 2f_{c2} - f_{c1}$$

where

f_{c1} = frequency of the lower carrier

f_{c2} = frequency of the upper carrier

The X3060 klystron, SN H5-30, has an efficiency of 46.5% compared to the VA-858-A, SN 5, klystron's efficiency of 36.4%. Ref. 4 (describing a 24-kw 5K70SG

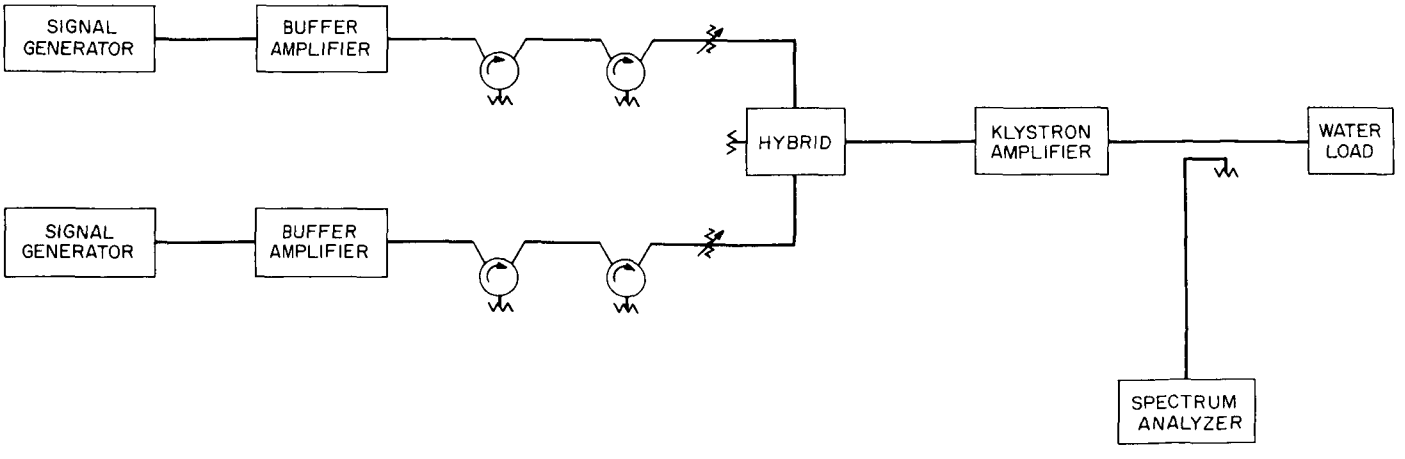

Fig. 18. Dual carrier tests

3 Mc/cm 9.8 kw EACH CARRIER
LOG SCALE 30-db INDICATION = 31 db
LOWER FREQUENCY CARRIER f_{c1} = 2115 Mc
UPPER FREQUENCY CARRIER f_{c2} = 2116 Mc

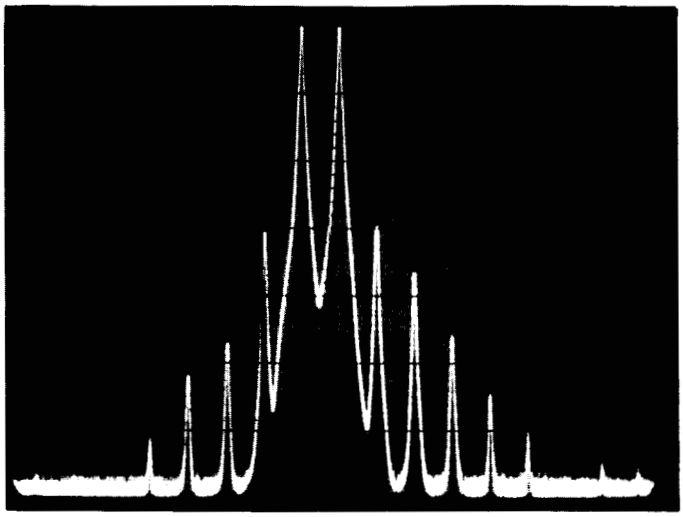

FREQUENCY INCREASE ⟶

Fig. 20. Klystron output with modulation products; carrier separation 1.5 Mc

10 Mc/cm 9.8 kw EACH CARRIER
LOG SCALE 30-db INDICATION = 31 db
f_{c1} = 2113 Mc, f_{c2} = 2119.5 Mc

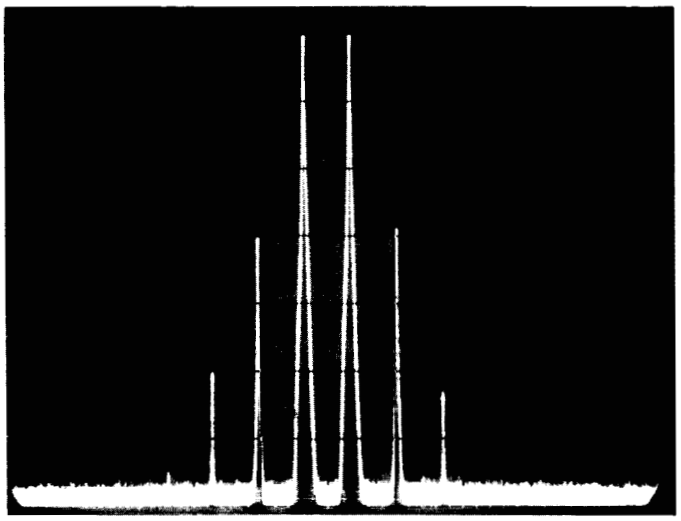

FREQUENCY INCREASE ⟶

Fig. 22. Klystron output with modulation products; 6.5-Mc separation

3 Mc/cm 9.8 kw EACH CARRIER
LOG SCALE 30- db INDICATION = 31 db
f_{c1} = 2113.5 Mc, f_{c2} = 2118.5 Mc

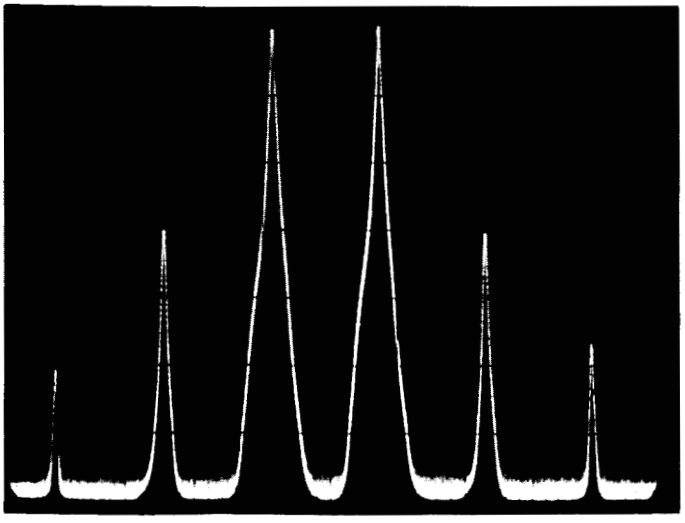

FREQUENCY INCREASE ⟶

Fig. 21. Klystron output with modulation products; 5-Mc separation

10 Mc/cm 9.5 kw EACH CARRIER
LOG SCALE 30-db INDICATION = 31 db
f_{c1} = 2112 Mc, f_{c2} = 2120.5 Mc

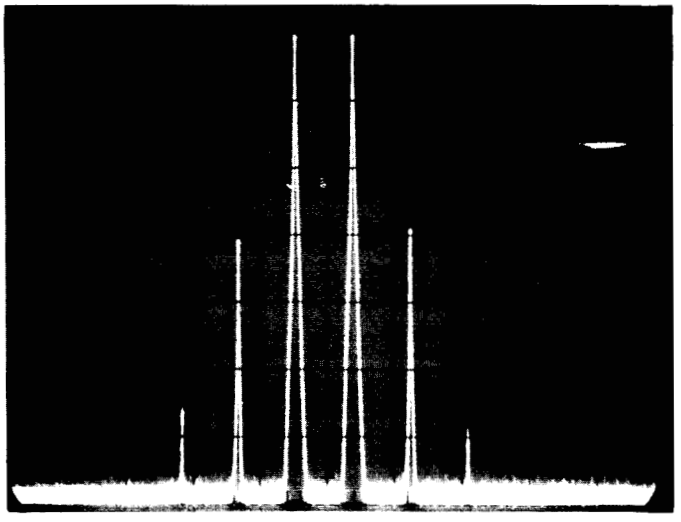

FREQUENCY INCREASE ⟶

Fig. 23. Klystron output with modulation products; 8.5-Mc separation

klystron developed specifically for dual carrier operation at 2-kw per carrier) indicates that increased efficiency gives lower intermodulation products. Based on this report, the X3060 should show a slightly improved dual carrier performance over the VA-858-A.

E. Lunar and Planetary Radar Module Development and Evaluation

30-Mc Balanced Mixer (Signal Type). During this period, the lunar and planetary radar subsystem 30-Mc balanced mixer bandwidth was increased from 20 to 100 kc to support the advanced spectrum analysis experiments. To save time and reduce cost, a spare balanced mixer was modified both mechanically and electrically. The mechanical modifications were necessary because of physical differences of the McCoy crystal filters. Electrical changes consisted of increasing the bandwidth of the input stages, and matching the filter input and output to optimize passband ripple. To reduce the effect of the mixer output on the bandwidth of the stagger-tuned 455-kc IF amplifier that follows it, the resonant circuit was removed, and a special wideband transformer installed. Physical restrictions of the module required the development of a special wide-band transformer. A ferroxcube 208F125-3C toroid core was used and a −1 db bandwidth of 71 kc to 1.3 Mc was obtained. This bandwidth was altered by the addition of RFI filtering to be 71 kc to 1.04 Mc.

Final module test results are shown in Figs. 24, 25, and Tables 2 and 3.

The 30-Mc balanced mixer has been successfully modified and installed in the spectrum receiver at the Venus site with a bandwidth of 100 kc.

Receiver Coherent Leakage Due to 30.455 Mc Balanced Mixer (Reference Type). A coherent leakage test was performed on the 30.455 Mc balanced mixer previously described in *SPS 37-27*, Vol. III, p. 92, and *SPS 37-33*, Vol. III, p. 92. The test was performed using a laboratory test system approximating the Venus site S-band planetary radar receiver (Fig. 26).

Since the design goal for the coherent leakage is a minimum of 40 db below threshold, the existing system

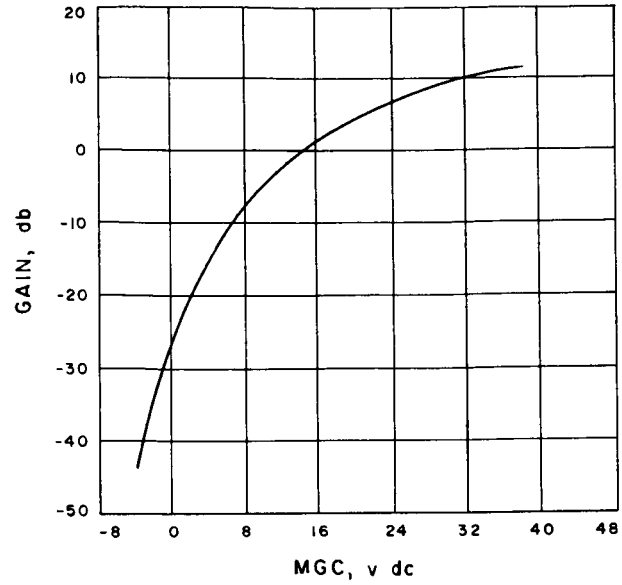

Fig. 24. Conversion gain versus MGC, signal amplifier

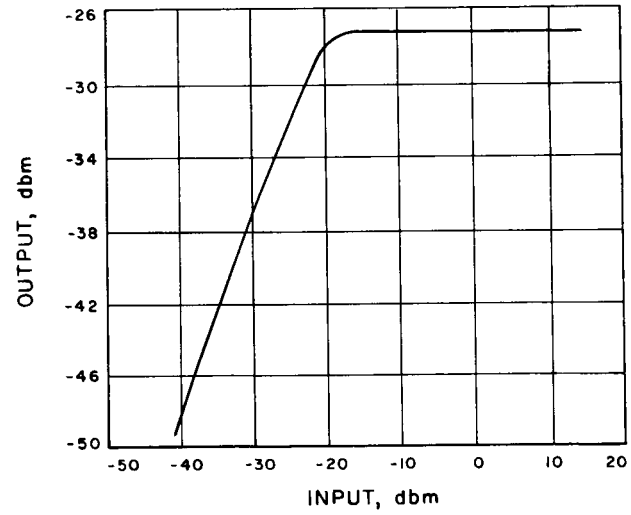

Fig. 25. Limiting curve of reference amplifier

was first tested to ascertain that the leakage of the new module could be observed. The existing test system utilized a 30.455-Mc synthesis loop similar to that described in *SPS 37-21*, Vol. III, p. 51, Fig. 48.

The carrier loop was manually controlled to produce a low-frequency beat at the amplitude detector output. Using a fast time constant in the instrumentation filter, a reference was set so that the recorder had a dynamic range of at least 40 db. The manual gain control (MGC) was set so that the input to the detector was the nominal 50 mv for the calibration.

Leakage was first checked from the input to the 455-kc IF amplifier by terminating the signal input and adjusting the MGC to the value that corresponds to threshold for the particular carrier tracking loop bandwidth (in this case, $2B_{Lo} = 5$ cps, threshold $= -157$ dbm, MGC $= +5$ v dc).

Table 2. 30-Mc balanced mixer module test results

Component	Measurement
Signal amplifier	
Input impedance	50 Ω
Bandwidth	−1 db = 98 kc −3 db = 109.4 kc (minimum goal 100 kc)
Conversion gain versus MGC	(Minimum goal + 38 v dc = +6 db) (See Fig. 24)
Mixer output impedance	49.4 Ω
Reference amplifier	
Input impedance	50 Ω
Bridge balance	60 db (minimum goal 60 db)
Bandwidth	2.05 Mc (minimum goal 1 Mc)
Limiting curve	Minimum goal limit at −10 dbm (See Fig. 25)

An approximation of the required instrumentation bandwidth can be found by observing the normal signal component of the 455 kc IF output level at threshold condition, and then the output level with noise only. This ratio approximates the signal-to-noise ratio (S/N). Since the anticipated leakage is 40 db below threshold, and to provide a S/N of 20 db for the instrumentation, the required bandwidth reduction is seen to be:

IF bandwidth/instrumentation bandwidth = S/N (at 455 kc) −40 db (anticipated leakage) − 20 db (required instrumentation S/N). In this experiment, the threshold signal $S = 50$ mv, while the noise signal $N = 8.6$ mv, or the $S/N = 7.5$ db.

From this it can be seen that $BW_{IF}/BW_{inst} = 7.5$ db -40 db -20 db $= -52.5$ db $= 1.78 \times 10^5$ or the instrumentation bandwidth $= 2$ kc$/1.78 \times 10^5 = 0.01$ cps.

An S-curve can now be obtained by adjusting the phase shifter shown in Fig. 26. A comparison of the amplitude of the calibration S-curve and the test curve indicates the amount of coherent leakage. This data is tabulated in Table 2.

Table 3. RFI leakage, 30-Mc balanced mixer

Mixer output	30.455 Mc = −66 dbm (minimum goal −44 dbm)					
	Frequency	B+	Filament 1, μv	Filament 2, μv	Plate, μv	Minimum goal, μv
Power lines and plate to plate	30.455 Mc	0.3	0.7	0.8	0.3	3
	30 Mc	1.4	0.5	0.6	0.3	3
	455 kc	0.3	0.3	0.3	0.3	3

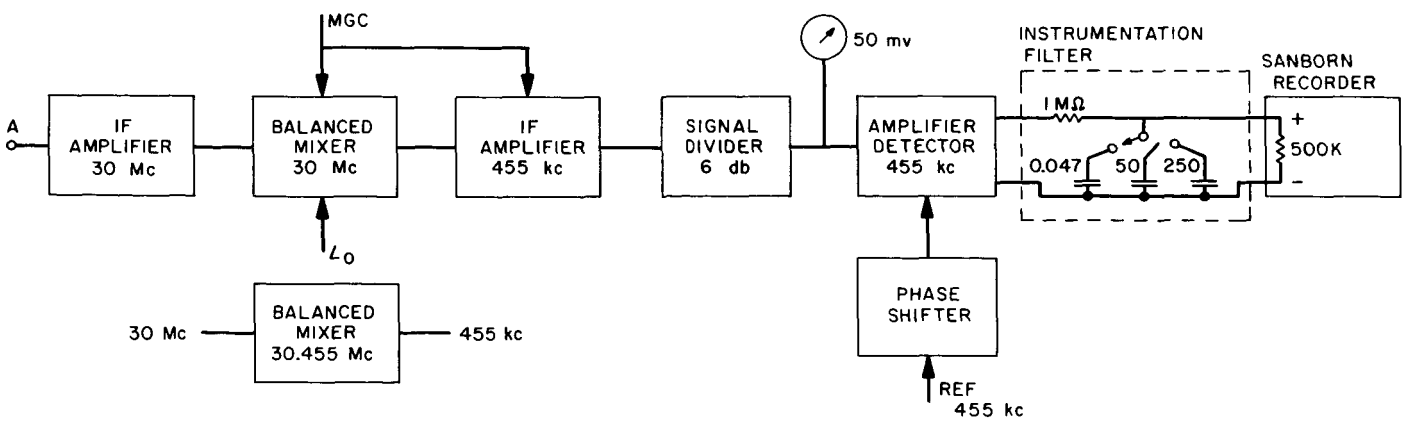

Fig. 26. Test setup to measure coherent leakage

This test was repeated by terminating the input to the 30.0-Mc IF amplifier and using the standard 30.455-Mc synthesizer loop. The test (Table 4) indicated that the laboratory system internal coherent leakage was low enough to test the new 30.455 Mc balanced mixer.

Table 4. Coherent leakage test data

Test condition	Filter time constant, sec	Sample period, min	IF gain, db	Coherent leakage, db
Terminate input to 455-kc IF amplifier	17	2	103	−47
Terminate input to 30-Mc IF amplifier (use 30.455-Mc synthesizer loop)	84	4	115	−41
Terminate input to 30-Mc IF amplifier (use 30.455-Mc balanced mixer)	84	5	115	−45

The 30.455 Mc balanced mixer was tested and found to have coherent leakage level equivalent to 45 db below threshold.

A spectral test of the output of the balanced mixer only was conducted and the results are shown in Fig. 27.

The test indicates the design goal of 40-db leakage margin below system threshold has been met satisfactorily, establishing leakage compatibility of the new central frequency synthesizer soon to be installed at the Venus Station (*SPS 37-33*, Vol. III, p. 91) with the S-band planetary radar receiver.

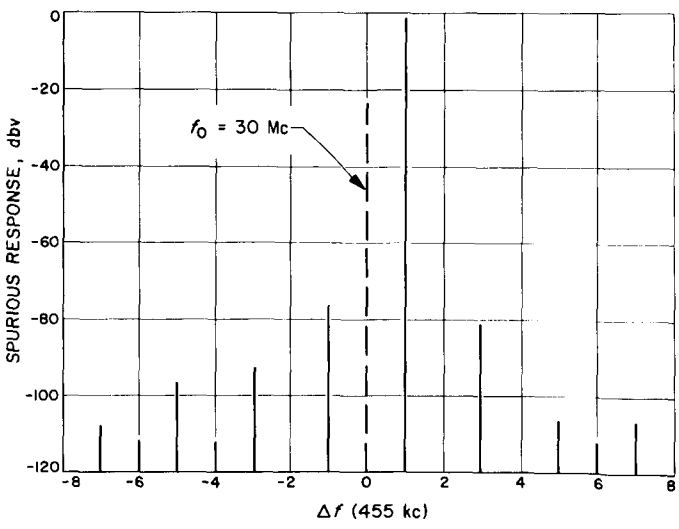

Fig. 27. Output spectrum of 30.455 Mc balanced mixer

F. An Automatic Checkout Equipment (ACE) for the Ranging Subsystem Mark I

1. Introduction. The ranging subsystem Mark I (*SPS 37-20*, Vol. III, pp. 12–15; *SPS 37-21*, Vol. III, pp. 16–18, *SPS 37-22*, pp. 5–6; *SPS 37-23*, Vol. III, pp. 11–14; *SPS 37-24*, Vol. III, pp. 9–11; and *SPS 37-27*, pp. 22–25) will permit precise determination of ranges up to 800,000 km when used in conjunction with an S-band "turnaround" transponder. It was developed for the DSIF for the purpose of tracking lunar probes and monitoring early midcourse maneuvers of planetary spacecraft. The adoption of the Mark I for use in the NASA Manned Space Flight Net (MSFN) brought about the need for fabricating these units in larger numbers and at a faster rate than had previously been planned for the DSIF alone.

The Mark I is, in a sense, a digital process-control device having many signal interfaces with other subsystems, particularly the S-band receiver/exciter. To check the operation of the Mark I completely, over an extended period of time, it appeared desirable to provide means of simulating the operational environment. Initial plans visualized such an automatic checkout means as a purchased general-purpose computer with an interface adapter designed and built by JPL. Subsequent investigation indicated that this approach was unnecessarily complex, and that appreciable savings in both money and time could be realized with special-purpose equipment, designed and built at JPL, and utilizing techniques and equipment of the kind already finding application in the Mark I.

The main application of the resulting automatic checkout equipment (ACE) has been as a tool of JPL acceptance quality assurance at the plant of the contractor supplying the Mark I ranging subsystems. The ACE has proved to be sufficiently effective and inexpensive to warrant the construction of a second unit, recently completed, for use at JPL.

2. General description. The ACE tests the reliability of ranging subsystems Mark I by repetitively exercising

their operational modes and monitoring their responses to detect erroneous operations.

The ACE (Fig. 28) is contained in a single rack, approximately 5 ft high, and mounted on casters to facilitate handling and movement.

A test cycle of the ACE with the Mark I comprises 20 sequential test states (S_0 through S_{19}). Of these, S_0 through S_{14} test the relay interlocks between the Mark I and the receiver/exciter subsystem. Test states S_{15} through S_{18} test the range-code acquisition, with simultaneous input to the Mark I of doppler information simulating both approaching and receding spacecraft. In test state S_{19} the resultant range number in the Mark I is compared with the reference range number in the ACE, which was previously calculated and stored in a toggle-switch binary register.

If an error should occur in the course of a test cycle, the operation stops, and the test engineer is informed by means of an *error* light and an audible alarm.

Fig. 28. Automatic checkout equipment (ACE)

If a test cycle is completed successfully, a *correct* light indication appears and another test cycle is automatically initiated. A cumulative count of successfully completed test cycles is maintained by means of a resettable digital counter in the ACE.

During the first portion of a test cycle, the Mark I is alternately started by command from the ACE and reset by interrupting one after another of the simulated relay signals which operationally interlock it with the radio subsystems. The range-code acquisition and doppler counting test portion is initiated automatically upon successful completion of the interlock tests. Prescribed amounts of clock doppler, representing both increasing and decreasing range, are counted into the range tally of the Mark I during the code-acquisition portion of the test cycle. After completion of code acquisition, the Mark I then being in its program state p7, prescribed amounts of RF doppler, representing both decreasing and increasing range, are counted into the range tally. The final content of the range tally is then compared with the reference range number stored in the ACE.

3. ACE functional assemblies. The ACE breaks down into four functional assemblies, all but the first of which each comprise one T-BLOC identical to the type used in the construction of the Mark I. They are the control panel assembly, the test states assembly, the time generator and counter assembly, and the ranging command assembly.

a. The control panel assembly. This assembly contains the circuitry for (1) control of the ACE and display of the test status, (2) selection of the reference range number and comparison with the Mark I range number, and (3) simulation of certain functions of the receiver/exciter and data subsystem.

ACE control and test status display. Two push buttons and a toggle switch, located on the front of the control panel (Fig. 29), control the operation of the ACE. The green *go* button is used to start a test (when the *sequencer* switch is in the *auto* position), or to step the ACE through one test state at a time (when the *sequencer* switch is in the *manual* position). The red *clear* button returns the ACE to test state S_0 in either automatic or manual sequencing mode of operation. Twenty neon light indicators, S_0 through S_{19}, indicate the progress of the ACE through the 20 corresponding test states comprising a test cycle. The result of the code-acquisition and doppler-counting test is indicated at the end of each test cycle by means of the *correct* or *error* lights. The audible alarm, associated with the *error* indication, is provided

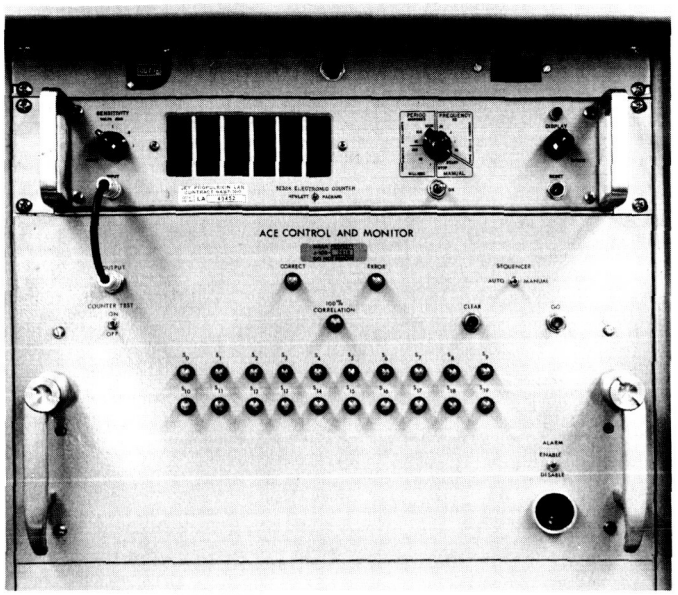

Fig. 29. ACE, showing front controls and indicators

with an *alarm enable/disable* switch. Correct acquisition of the ranging code as such is indicated by the *100% correlation* light.

Range number selection and comparison. Thirty toggle switches allow the selection in the ACE of the reference range number that will be compared at the end of each test cycle with the 30-bit Mark I range data readout. The gating circuits that perform this function are mounted under the switch panel which, in turn, is located behind the control panel.

Simulation of functions of other subdivisions. Certain signals other than relay closures are operationally received by the Mark I from the receiver/exciter and data subsystems. These signals are simulated in the ACE control panel assembly as follows: The readout command pulse is provided by a unijunction transistor oscillator operating at approximately 1 cps. The doppler counting rate is controlled by a unijunction transistor oscillator operating at approximately 6 kc. The receiver clock and exciter clock signals required to provide the basic timing for the Mark I are provided in parallel from a single source, viz., the 1-Mc time-base output of the Mark I counter-timer suitably impedance-matched in an appropriate amplifier in the ACE.

b. The test states assembly. By means of this assembly the operation of both the ACE and the Mark I are controlled. When the *sequencer* switch is in the *manual* position, operation of the *go* button steps the ACE successively through the 20 test states, regardless of the responses of the Mark I. This is a powerful tool in trouble-shooting the ACE itself. In the automatic (*auto*) mode, the ACE, in response to the *go* button operation, steps through the 20 test states automatically and sequentially, provided the responses of the Mark I are correct. The operation of the test states assembly is summarized in Table 5.

c. The time generator and counter assembly. This assembly generates the time base which synchronizes the operations within the ACE and provides and controls the doppler signals sent by it to the Mark I.

The basic operation cycle of the ACE is 29 clock periods of 1-μsec nominal duration. The specific timing pulses within a cycle are designated T_0, T_1, T_2, $\cdots$, T_{28}.

The doppler pulses from the control panel assembly drive flip-flops that serve as doppler inputs to the Mark I. By preloading the counter and terminating doppler output when it reaches zero (counting down) or capacity (counting up), a predetermined number of doppler cycles are fed to the Mark I in each appropriate test state.

The counter is a conventional binary counter which can be either incremented or decremented by a count at a time. Besides controlling the number of doppler cycles to be generated, this counter also serves to provide a *hold* following relay operation, to allow contact settling. Counter capacity is $2^{18} = 262{,}144$. A zero detector stops the counter when it reaches either zero or capacity. The *hold* (approximately ¼ sec) is implemented by loading the counter with $2^{10} + 2^9 = 1{,}536$ and decrementing at the 6-kc rate. Doppler counts are implemented by loading the counter with $2^{17} + 2^{16} = 196{,}608$, and either decrementing to zero (approximately 33 sec) or incrementing to capacity (approximately 11 sec).

Clock doppler input is thus provided to the Mark I while the ACE counter counts up once and down once, for a total of approximately 44 sec. Since this must take place while the Mark I is in the code-acquisition program states, the *integration time* switch on the Mark I must be set high enough to ensure this. A setting of 11 on this switch has been found to be the acceptable minimum.

Once the Mark I is in the tracking mode (program state p7), 196,608 counts of negative RF doppler and 65,536 counts of positive RF doppler are provided to it in a similar manner.

Table 5. ACE test states

Test state	Conditions for entry into test state	Activities in this test state
S_0	*Clear* button pushed or Correct range number received from Mark I	Reset Mark I
S_1	Go button pushed or Mark I reset and range number correct	Select Receiver 2 and Receiver 2 lock Load 1,536 into counter, count down, start Mark I
S_2	Mark I in p3	Select Receiver 1 and Receiver 2 lock
S_3	Mark I reset	Select Receiver 2 and Receiver 2 lock Load 1,536 into counter, count down, start Mark I
S_4	Mark I in p3	Select Receiver 2 and Receiver 1 lock
S_5	Mark I reset	Select Receiver 2 and Receiver 2 lock Load 1,536 into counter, count down, start Mark I
S_6	Mark I in p3	Select range mode *off*
S_7	Mark I reset	Select range mode *on* Load 1,536 into counter, count down, start Mark I
S_8	Mark I in p3	Select clock loop out of lock
S_9	Mark I reset	Select transfer loop to transmitter Select clock loop in lock Load 1,536 into counter, count down, start Mark I
S_{10}	Mark I in p1	Select transfer loop to receiver
S_{11}	Mark I in p3	Select transfer loop filter short
S_{12}	Mark I reset	Select transfer loop to receiver Select transfer loop filter open Load 1,536 into counter, count down, start Mark I
S_{13}	Mark I in p2	Select receiver mode test Reset data correct flip-flop
S_{14}	Mark I reset	Reset doppler generator flip-flops Select receiver mode operate Load 1,536 into counter, count down, start Mark I
S_{15}	Mark I in p3 through p6	Load 196,608 into counter, count up
S_{16}	Mark I in p3 through p6 Counter zero	Load 196,608 into counter, count down
S_{17}	Mark I in p7	Load 196,608 into counter, count up
S_{18}	Mark I in p7 Counter zero	Load 196,608 into counter, count down
S_{19}	Mark I in p7 Counter zero	Load 65,536 into counter, count down; when counter is zero, enable data comparison

d. The ranging command assembly. This assembly simulates the remaining radio subsystem interlocks, supplies reset and start commands to the Mark I, and determines the accuracy of the resultant range number.

The radio system interlocks are simulated by relay contact closures which are controlled by the particular test states. The accuracy of the range number is determined by sampling the output of gates in the control panel assembly at the end of the sample time delay in S_{19} and setting either the *correct* or *error* flip-flop to display the result. The delay is required to ensure that a readout command updates the contents of the Mark I readout register at least once after completion of the RF doppler input time.

Both the *start* and *reset* commands are synchronized to the clock pulses of the Mark I. The *start* command is given each time the contents of the counter register reach zero. Since the Mark I operates in its *normal program* mode in these tests, it acts upon a *start* command only when it is in the *reset* state, ignoring it at other times. The *reset* command is given whenever the ACE enters its test state S_0.

References

1. Ludwig, A., "Antenna Feed Efficiency," *SPS 37-26*, Vol. IV, pp. 200–208, Jet Propulsion Laboratory, Pasadena, California, April 30, 1964.

2. Hogg, D. C., "Effective Antenna Temperatures Due to Oxygen and Water Vapor in the Atmosphere," *Journal of Applied Physics*, Vol. 30, No. 9, September 1959, pp. 1417–1419.

3. Worthing, A. G., and Gaffner, J., "Treatment of Experimental Data," John Wiley & Sons, Inc., New York, N. Y., December 1960, p. 213.

4. "5K70SG Testing Program," Appendix, E, Eitel-McCullough, Inc., San Carlos, California.

V. Communications Research and Development

A. Experimental Closed Cycle Refrigerator for Masers

Test program. The prototype compressor system has now been run for 1500 hr and operational data continue to be accumulated. The experimental refrigerator unit which was built prior to the compressor assembly has now been tested for 3000 hr.

Remote flow rate sensor. A remote indicating flow-rate sensor was recently developed to monitor the rate of flow of gas in the Joule–Thompson expansion circuit. This all-metal unit replaces the fragile glass gauge used in the past.

The construction of the differential transducer is shown schematically in Fig. 1. The 200-μa meter indicates the difference in temperature between thermocouples A and B. The upstream thermocouple A is maintained at ambient temperature T_A, while the downstream unit is maintained at an elevated temperature T_B by means of a 1000-Ω heater. The heater power is held constant, and it is readily observed that the temperature T_B is reduced

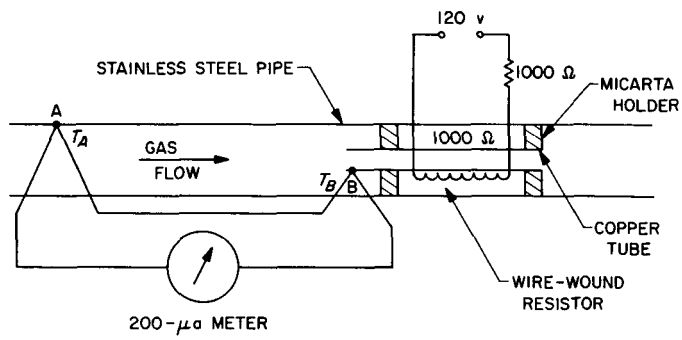

Fig. 1. Schematic diagram of flow-rate transducer

by the mass of gas flowing through the transducer. Hence, the meter indicates directly the flow rate of gas. Calibration is achieved by comparison with a standard flow meter.

It is also noted that slow changes in ambient temperature cause corresponding changes in T_A and T_B and the device is self-correcting for small temperature variations. The low impedance circuit will be particularly helpful for remote indication of this important parameter.

B. CW Signal Power Calibration With Thermal Noise Standards

1. Introduction

An attempt is being made to improve the accuracy of the calibration of the CW received signal power in the DSN. A convenient measure of a spacecraft received power level is the receiver AGC voltage which is calibrated for absolute received power, defined at the receiver input, with a calibrated test transmitter. The theory, method of data acquisition, and equipment have been discussed previously (*SPS 37-35*, Vol. III, p. 58). The *Y*-factor method used consists of accurately measuring the ratio, at the output of the receiving system, of the CW signal power P_s plus the system noise power P_n to the system noise power. The output of the detector, which is a solid state germanium diode 1N198, is affected by the signal form factor; therefore, the *Y*-factor method requires an evaluation of the diode noise versus CW power sensitivity.

2. Method and Equipment

The diode noise versus CW power sensitivity was evaluated by a comparison of CW-to-noise *Y*-factors under different conditions. The diode *Y*-factor was compared with the *Y*-factor as measured by a true RMS detector at the same SNR. In order to obtain meaningful results, the bandwidth as seen by the RMS detector must be made equal to the bandwidth as seen by the diode, or the bandwidths must be evaluated and a correction factor applied. The RMS detector used was a standard thermistor power meter which, compared with the diode, requires a relatively high input power level for an accurate readout. This high noise power requirement calls for an equalization of diode and power meter bandwidths, as well as equal shape factors, over a range of more than 70 db. Since, in practice, this is extremely difficult to achieve, the method adopted was to approximate equal bandwidths, accurately evaluate them over a sufficiently wide range of frequencies and attenuations, and apply a correction factor.

Fig. 2 shows a block diagram of the test system. A low-pass filter was required in the power meter circuit to limit the bandwidth. The input could be switched between a signal generator at the IF frequency and a matched termination. G_1 is the gain supplied by a chain of wide-band transistor amplifiers centered at the IF frequency, A is the attenuation provided by a precision attenuator, and the narrow-band filter (NBF) is a crystal filter with a bandwidth of about 8 kc (*SPS 37-35*, Vol. III, p. 58). Some gain, G_2, supplied by a wide-band transistor amplifier similar to an element of G_1, was required after the NBF to raise the noise level. First, a *Y*-factor was measured with the diode as the detector; the same *Y*-factor was then measured with the power meter as the detector.

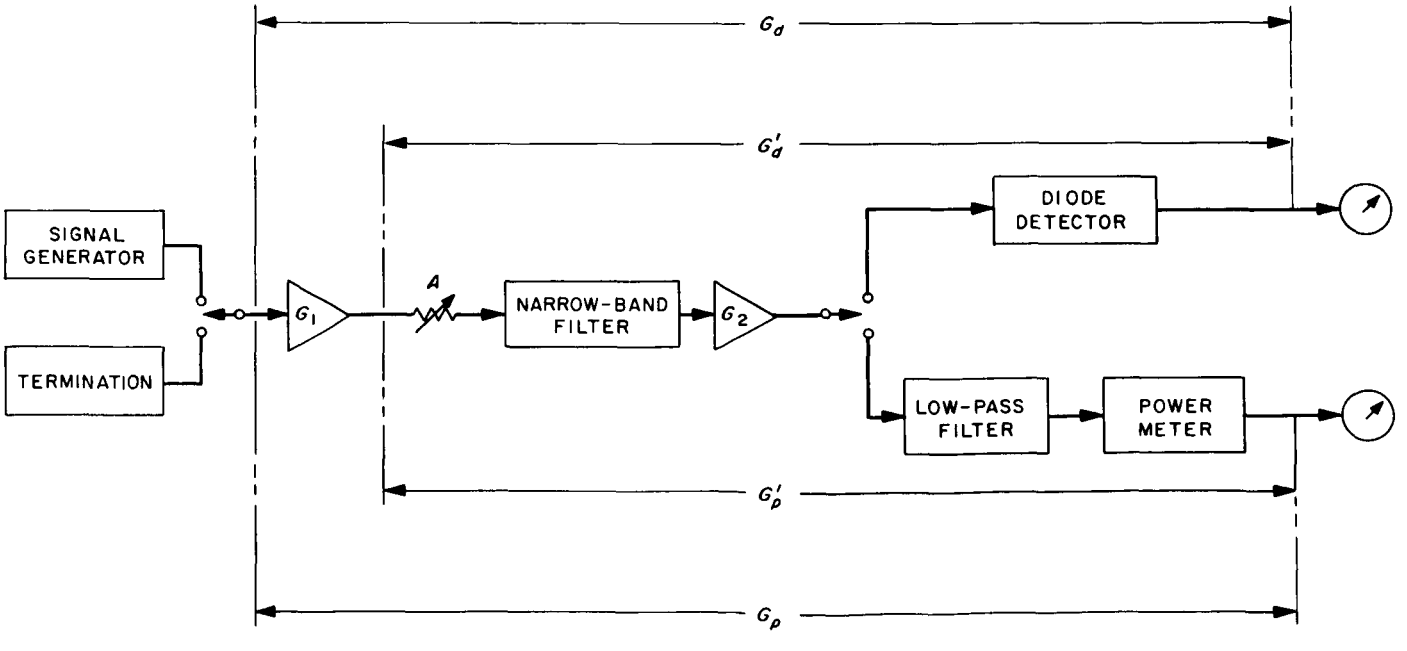

Fig. 2. Block diagram for diode sensitivity evaluation

The source of CW power was a commercial signal generator. The amplifier chain, resistively terminated on the input, provided the noise power. A large number of Y-factors were measured with SNRs in the range of 1 to 30 db. The results were repeated for different diode bias levels.

3. Theory

With the gain notation as shown in Fig. 2, the power meter and diode Y-factors described in *SPS 37-35*, Vol. III, p. 58 can be defined as

$$Y_p = 1 + \frac{P_{si}G_p(f_s)}{kT_s\int_0^\infty G_p(f)df} \tag{1}$$

$$Y_d = 1 + \frac{P_{si}G_d(f_s)}{\alpha kT_s\int_0^\infty G_d(f)df} \tag{2}$$

where α is an unknown correction factor to be applied to the Y-factor measured by the diode to make

$$Y_d = Y_p$$

and where

P_{si} = the input power
f_s = signal frequency
T_s = system temperature
k = Boltzmann constant
Y_p = Y-factor measured by the power meter (ratio)
Y_d = Y-factor measured by the diode (ratio)

Solving Eqs. (1) and (2) for α,

$$\alpha = \frac{Y_p - 1}{Y_d - 1}\cdot\frac{G_d(f_s)}{G_p(f_s)}\cdot\frac{\int_0^\infty G_p(f)df}{\int_0^\infty G_d(f)df} \tag{3}$$

Eq. (3) may be normalized thus:

$$\left.\begin{aligned}\frac{G_d(f_s)}{G_{do}} &= g_d(f_s)\\ \frac{G_p(f_s)}{G_{po}} &= g_p(f_s)\end{aligned}\right\} \tag{4}$$

where the subscript o refers to the point of maximum gain.

Also,

$$\left.\begin{aligned}\frac{G_d(f)}{G_{do}} &= g_d(f)\\ \frac{G_p(f)}{G_{po}} &= g_p(f)\end{aligned}\right\} \tag{5}$$

Substituting Eqs. (4) and (5) in Eq. (3):

$$\alpha = \frac{Y_p - 1}{Y_d - 1}\cdot\frac{g_d(f_s)}{g_p(f_s)}\cdot\frac{\int_0^\infty g_p df}{\int_0^\infty g_d df} \tag{6}$$

However,

$\int_0^\infty g_p df = B_p$ is the bandwidth seen by the power meter, and

$\int_0^\infty g_d df = B_d$ is the bandwidth seen by the diode

Hence,

$$\alpha = \frac{Y_p - 1}{Y_d - 1}\cdot\frac{g_d(f_s)}{g_p(f_s)}\cdot\frac{B_p}{B_d} \tag{7}$$

The ratios $b = B_p/B_d$ and $g = g_d(f_s)/g_p(f_s)$ were evaluated by measuring B_p and B_d over a sufficiently wide range of frequencies and attenuations. Eq. (7) is then written

$$\alpha(db) = 10\log_{10}\left\{\frac{Y_p - 1}{Y_d - 1}\cdot g\cdot b\right\} \tag{8}$$

4. Error Analysis

$$[PE_{\alpha(db)}]^2 = \left[\frac{\partial\alpha(db)}{\partial Y_p}\right]^2(PE_{Y_p})^2 + \left[\frac{\partial\alpha(db)}{\partial Y_d}\right]^2(PE_{Y_d})^2 + \left[\frac{\partial\alpha(db)}{\partial g}\right]^2(PE_g)^2 + \left[\frac{\partial\alpha(db)}{\partial b}\right]^2(PE_b)^2 \tag{9}$$

$$= \left[\frac{10\log_{10}e}{Y_p - 1}\right]^2(PE_{Y_p})^2 + \left[\frac{10\log_{10}e}{Y_d - 1}\right]^2(PE_{Y_d})^2 + \left[\frac{10\log_{10}e}{g}\right]^2(PE_g)^2 + \left[\frac{10\log_{10}e}{b}\right]^2(PE_b)^2 \tag{10}$$

But, since $Y_{p(db)} = 10\log_{10}Y_p$, and

$$PE_{Y_p} = \left[\frac{\partial Y_p}{\partial Y_{p(db)}}\right](PE_{Y_{p(db)}}),$$

Eq. (10) may be written:

$$[PE_{\alpha(db)}]^2 = \left[\frac{Y_p}{Y_p - 1}\right]^2 (PE_{Y_{p(db)}})^2 + \left[\frac{Y_d}{Y_d - 1}\right]^2 \times (PE_{Y_{d(db)}})^2 + \left[\frac{10\log_{10}e}{g}\right]^2 (PE_g)^2 + \left[\frac{10\log_{10}e}{b}\right]^2 (PE_b)^2 \quad (11)$$

Eqs. (8) and (11) have been programmed in Fortran and the data reduced by computer.

5. Results

The diode in the Venus Station system has been evaluated. Measurements of bandwidths have yielded the results

$$b = 1.0334$$

$$g = 1.00$$

The diode correction factor $\alpha(db)$ was evaluated for SNRs from 1 to 30 db, and for diode bias levels of 2, 4, and 7 mv. Within the accuracy of the experiment, α does not vary for SNRs from 10 to 30 db, nor for diode bias levels between 2 and 7 mv. Within these ranges, the average resulting α was 0.39 db, with a probable error of 0.03 db.

Work on the evaluation of the detectors used at the Pioneer and Echo Stations is in progress. The correction factors thus derived will modify the CW signal power calibrations that have been reported previously and have been underway for some time.

C. Simultaneous Lobing Radiometric Tracking System

The S-band system for the 210-ft-diameter antenna will use a simultaneous lobing angle tracking feed system. A radiometer used in conjunction with the tracking feed would be a useful device for angle pointing and gain calibrations of the antenna system using radio star sources. This technique is especially important for the 210-ft-diameter antenna, as this antenna does not have a collimation tower.

Testing of the simultaneous lobing radiometric tracking system, which was reported in earlier issues of the *SPS*,[1] is now being resumed. On September 1, 1965, the system was installed and used at the Echo Station of the Goldstone Tracking Station in conjunction with the 85-ft-diameter antenna and the S-band receiver system. On this and subsequent nights, various radio sources were tracked and tracking data were taken. Fig. 3 shows a sample of the hour-angle (HA) residuals obtained by tracking Omega Nebula on the nights of September 22 and 24.

On October 5 and 6, the system was operated in an experiment designed to eliminate the necessity of a collimation tower when phasing the receiver for automatic tracking of a spacecraft. In this experiment, the simultaneous lobing radiometer and the radio source Crab Nebula were used, together with a signal generator to

[1] *SPS 37-27*, Vol. III, pp. 57–61; *SPS 37-28*, Vol. III, pp. 48–51; *SPS 37-30*, Vol. III, pp. 38–44; *SPS 37-31*, Vol. III, p. 36; *SPS 37-26*, Vol. IV, pp. 216–220; *SPS 37-35*, Vol. IV, p. 13.

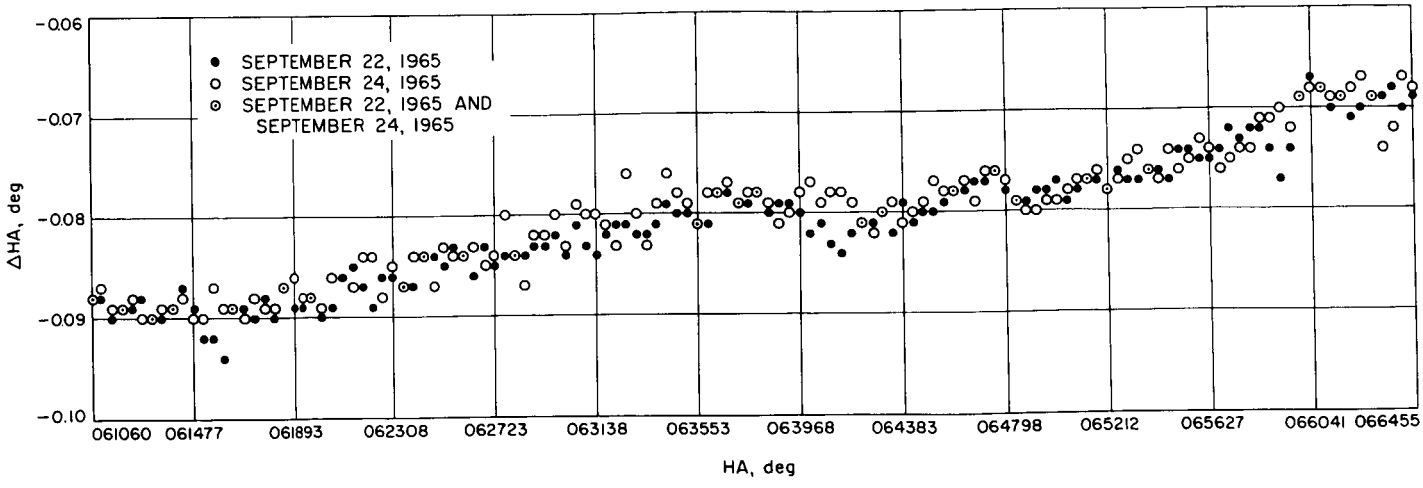

Fig. 3. Auto track on Omega Nebula

phase the receiver, and the boresight and phasing were checked against the collimation tower. The experiment was performed on the HA axis of the Echo Station 85-ft-diameter antenna. The results of this experiment are shown in Table 1. The phasing and the HA coordinate obtained in the conventional manner are shown in Table 2.

Table 1. Phasing of HA channel of the receiver using a radio source

Date	Radio source	
	Phase shifter setting	Collimation tower boresight HA coordinate
October 5, 1965	341 deg	272.062
October 6, 1965	17.5 deg	272.050

Table 2. Phasing of HA channel of the receiver using the collimation tower

Date	Collimation tower	
	Phase shifter setting	Collimation tower boresight HA coordinate
October 5, 1965	310 deg	272.058
October 6, 1965	358 deg	272.054

The average difference between the phase shifter settings obtained from the collimation tower and those obtained from the radio source is approximately 25 deg.

The results obtained clearly demonstrate the feasibility of the system; however, before the system can be pronounced operational, the technique must be further refined.

D. Two-Way RF Carrier Acquisition

A preliminary laboratory investigation has been made of two-way RF carrier acquisition using a Block II S-band receiver–exciter and a test transponder modified to simulate a Block II *Apollo* transponder. The investigation covered experimental verification of the frequency rate capability of the transponder and the receiver (widest MSFN bandwidth) as a function of signal level for a 20-deg peak phase error. In addition, the amount by which the acquisition sweep frequency must exceed the receive frequency in order to achieve RF phase lock was investigated for both the up-link and down-link (simulated). This preliminary investigation is described and the results obtained are presented here.

Fig. 4 is a simplified block diagram of the laboratory test setup which shows how the acquisition sweep voltage was applied to the exciter voltage controlled oscillator (VCO). Since the available receiver–exciter and the test transponder operated at the 2295/2113.3 Mc DSIF frequencies, and the available transponder predetection filter was designed for operation at the MSFN frequency (2287.5/2106.4 Mc), the test transponder was modified (as shown in Fig. 5) to operate with an external fixed frequency reference supplied to the phase and automatic gain control (AGC) detectors. This frequency was set to provide the second IF frequency at the center of the predetection filter passband. The AGC time constant in the transponder was 0.5 sec for these tests, and the ground receiver was operated with a 4-sec AGC time constant (widest bandwidth position for MSFN).

The test transponder was modified to have the following characteristics within the tracking range shown, which represent the Block II transponder parameters.

RF loop threshold noise bandwidth	700 cps
RF loop predetection filter noise bandwidth	15,000 cps
Strong signal open loop gain	3.3×10^6 (1/sec)
Tracking range	± 90 kc ($\pm 4.3/10^5$)

Fig. 6 shows the frequency rate capability of the modified test transponder calculated for the parameters listed above as a function of signal level for a frequency displacement of 4.3 parts in 10^5 and a total phase error (due to frequency displacement plus frequency rate) of 20 deg. Also plotted in Fig. 6 are the experimentally measured data obtained by sweeping the exciter VCO about nominal frequency ± 4.3 parts in 10^5 at varying rates with a triangular sweep waveform. Experimental and calculated data are in good agreement. Fig. 7 shows a similar frequency rate plot for the ground receiver which was modified to have the following parameters, which represent the MSFN receiver parameters (widest RF loop bandwidth).

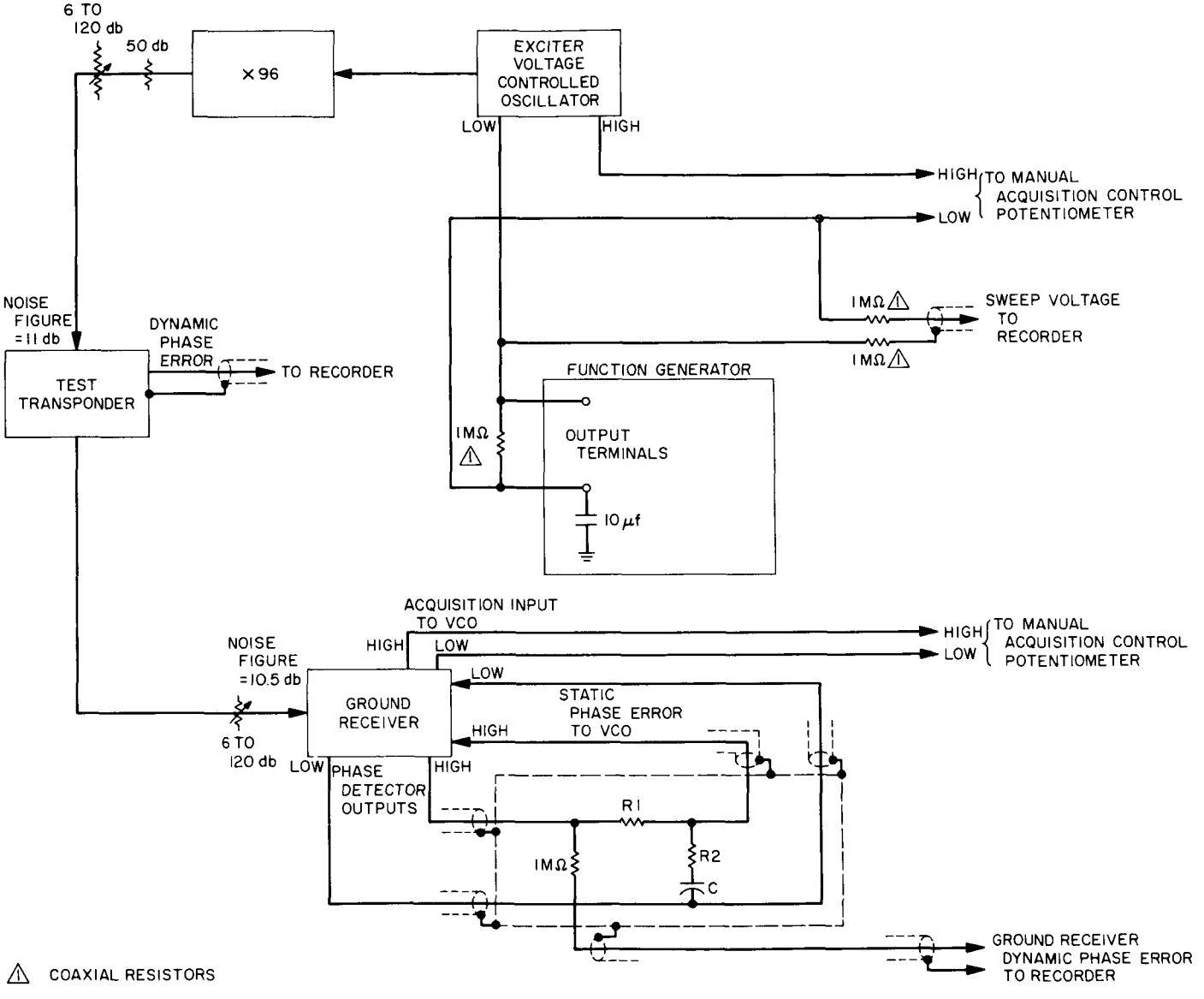

Fig. 4. RF acquisition test setup

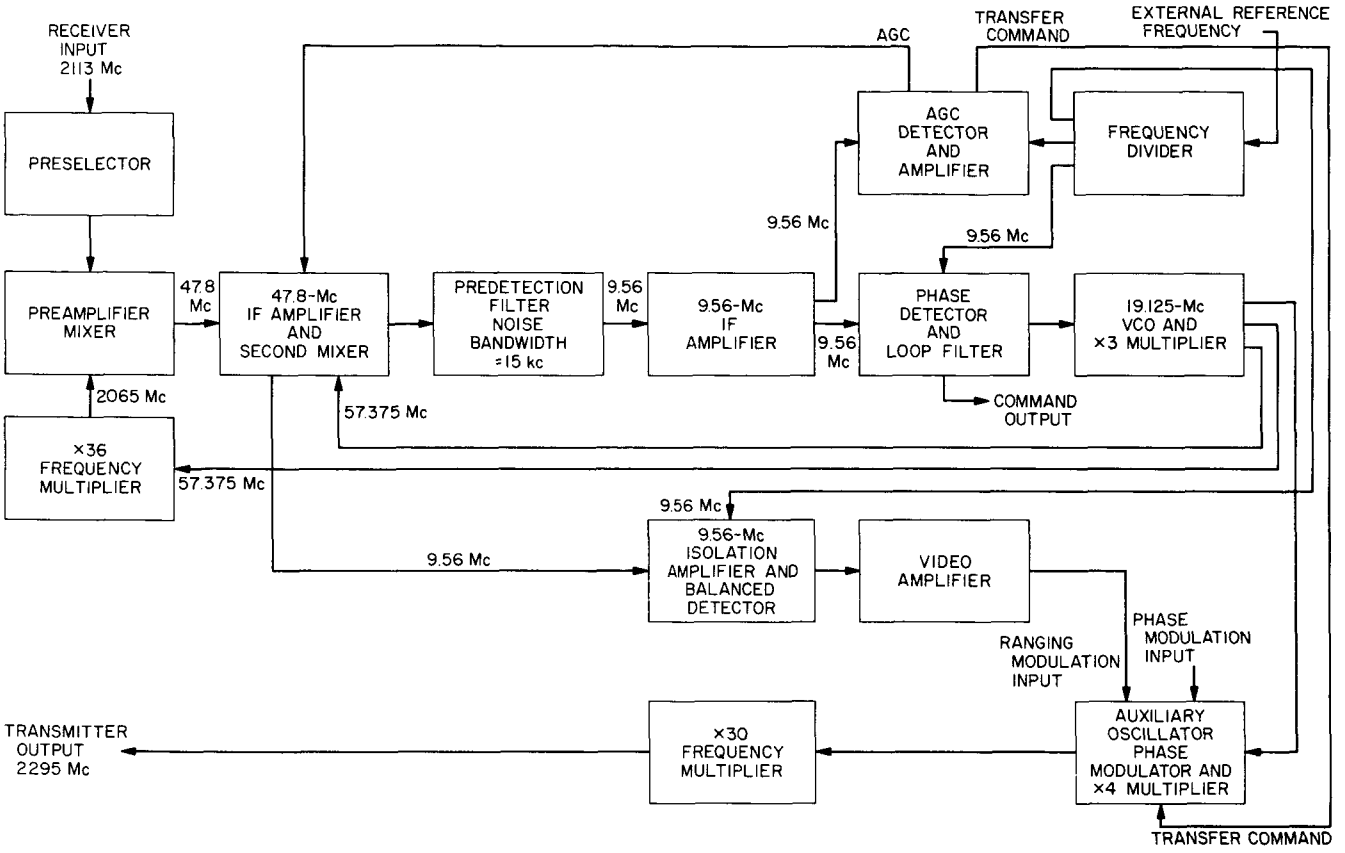

Fig. 5. Modified S-band test transponder

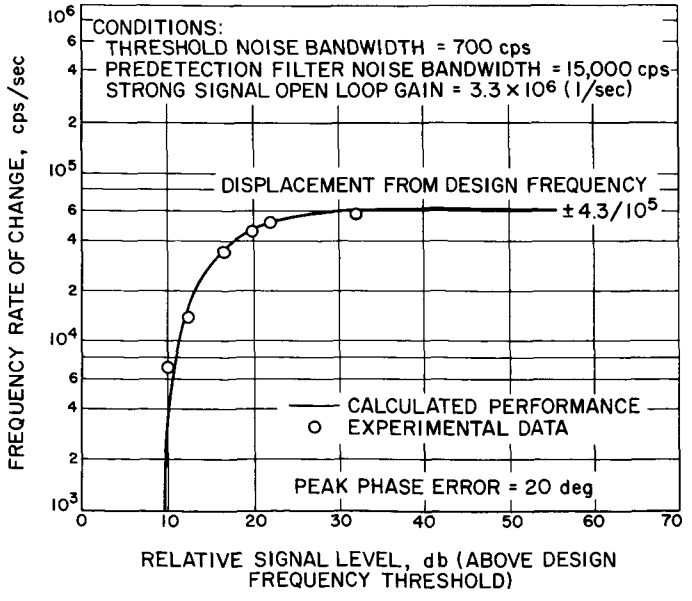

Fig. 6. Block II transponder—carrier frequency rate capability versus signal level

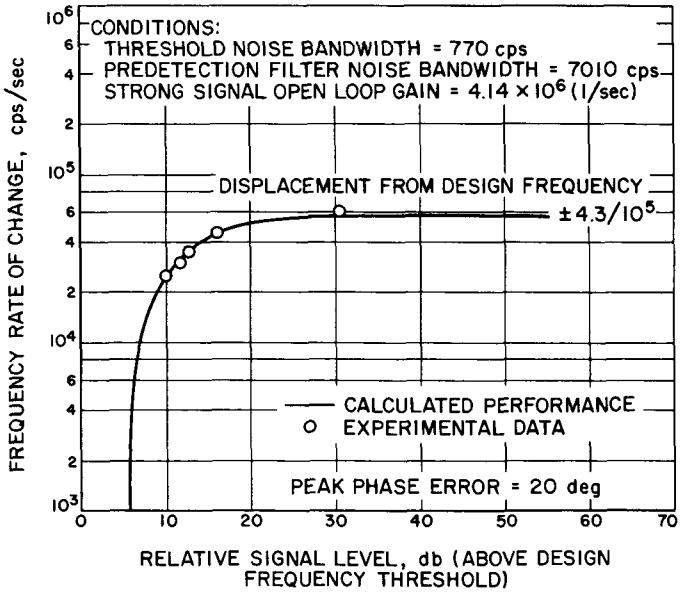

Fig. 7. MSFN receiver—carrier frequency rate capability versus signal level

RF loop threshold noise bandwidth	770 cps
RF loop predetection filter noise bandwidth	7000 cps
Strong signal open loop gain	4.14×10^6 (1/sec)
Tracking range	$\pm 9/10^5$

Again, experimental and calculated data are in good agreement. Fig. 8 shows a typical recording of phase error in the transponder and in the receiver which was obtained while sweeping the exciter VCO about nominal frequency.

Measurement was made of the amount by which the acquisition sweep frequency must exceed the receive frequency in order to achieve RF phase lock. The sweep generator was set to produce a ± 2.3 parts in 10^5 sweep amplitude with a 35,000 cps/sec sweep rate at S-band (triangular sweep waveform). For the simulated up-link measurements, the exciter VCO frequency bias was changed from nominal, by means of the manual acquisition control, until RF lock in the transponder could be achieved only a portion of the time. The frequency difference between the sweep amplitude ($2.3/10^5$) and the exciter frequency change from nominal introduced manually provides the amount by which the simulated up-link acquisition sweep frequency must exceed the transponder receive frequency to achieve RF phase lock. This measurement was made as a function of signal level into the test transponder to provide the experimental data plotted in Fig. 9. For the simulated down-link measurements, the exciter was swept 4.3 parts in 10^5 about nominal frequency (to insure phase lock in the test transponder), and the receiver VCO frequency bias was changed from nominal, by means of receiver manual acquisition control, until RF lock in the receiver was achieved only a portion of the time. In this case, the difference between down-link sweep amplitude and the receiver frequency change from nominal introduced manually provides the amount by which the simulated down-link acquisition sweep frequency must exceed the receiver frequency to achieve RF phase lock. The simulated down-link measurement was made as a function of

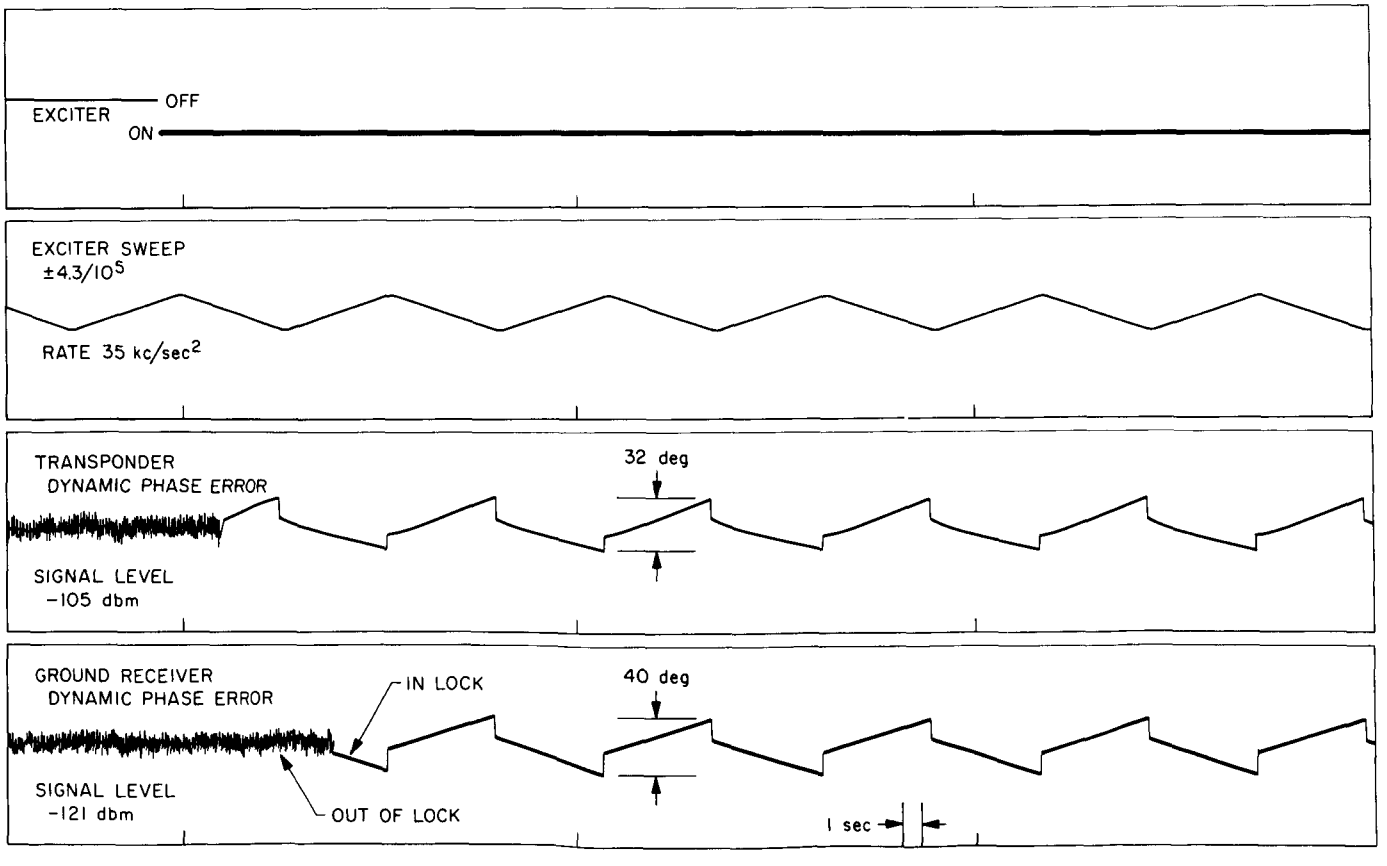

Fig. 8. Typical recording—two-way RF acquisition

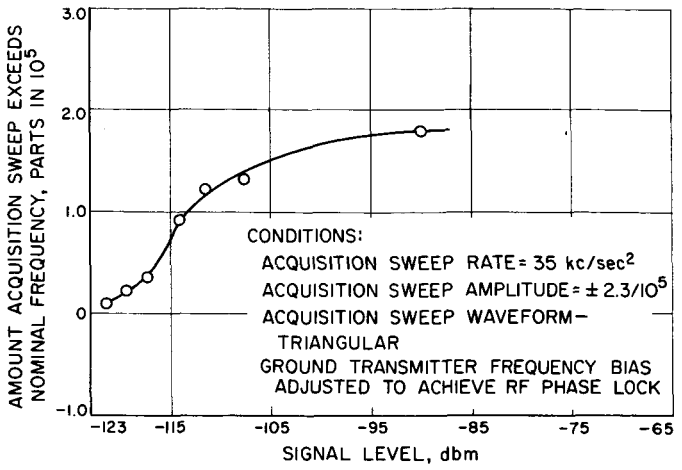

Fig. 9. Simulated Block II transponder RF acquisition

signal level into the receiver to provide the experimental data shown in Fig. 10. These data were obtained with a slight modification (in the form of a low-pass filter) to the RF loop tracking filter.

The following general comments relate to the experimental data plotted in Figs. 9 and 10. The effect is quite marked, since a small change in frequency bias (about $1/10^6$) results in a change from RF phase lock to an out-of-lock condition and vice versa when RF acquisition is attempted. It appears that the excess sweep is required to overcome an apparent frequency pushing effect caused in the out-of-lock condition when the out-of-lock beat frequency appearing at the phase detector output modulates the receiver local oscillator, and one sideband of this beat frequency (modulated on the local oscillator) is heterodyned through the receiver mixers and IF amplifiers. This appears at 10 Mc in the RF loop predetection bandwidth and is predominate relative to the other sideband. An S-band spectrum analyzer was used to observe the out-of-lock beat frequency sidebands which appear on the local oscillator signal at strong input signal levels. As the input signal level is reduced, the out-of-lock beat frequency sidebands are replaced by noise modulation on the local oscillator. Investigations made on both a laboratory S-band receiver–exciter and SN 23 receiver–exciter indicate that a minor modification in the form of a low-pass filter is required in the RF loop tracking filter to maintain a characteristic similar to Fig. 10 for the MSFN receivers.

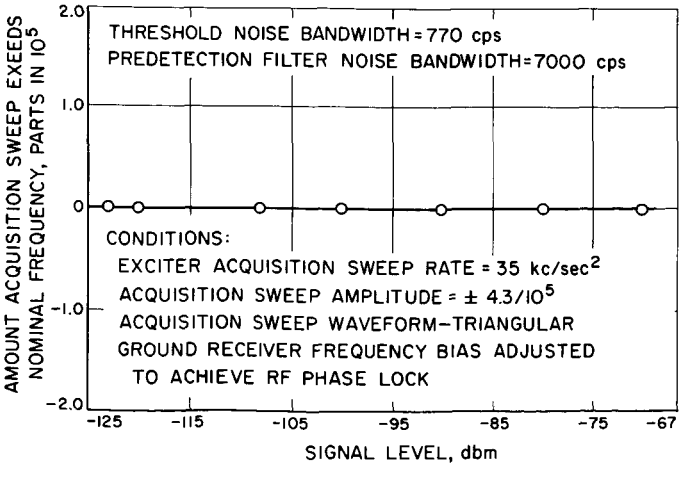

Fig. 10. Ground-based receiver RF acquisition

The preliminary investigation of a simulated Block II transponder presented here does *not*, in all probability, represent the performance of the Block II (or Block I) transponders relative to the excess RF acquisition sweep (through nominal) required to achieve RF phase lock. This experimental information is presented to point out that, in order to develop detailed RF acquisition procedures, this characteristic must be known and investigated for both the Block I and Block II transponders.

E. Venus Station Operations

1. Experimental Activities

The major station activities during the past two-month period were *Mariner* 1964 spacecraft support, X-band lunar radar, S-band planetary radar, and radio star tracking. Table 3 summarizes the activities at the Venus Station during this period.

Table 3. Summary of Venus Station experimental activity (August 11–October 13, 1965)

Activity	Hours	Percent
Primary experiments		
X-band lunar radar	401	26.1
S-band planetary radar	33	2.1
Radio star tracks	32	2.1
Mariner support		
Transmission, reception, and testing	477	31.1
Testing, calibration, construction, and scheduled maintenance	561	36.5
Holidays and scheduled nonoperation time	32	2.1
Total	1536	100.0

The X-band experiments on the Moon were the most sophisticated attempted to date and included total spectrum, mapping, and open-loop ranging, using 1-μsec steps. This lunar experiment was also the longest in duration, extending over a three-month period of activity, and was not entirely free from difficulty. A bar graph (Fig. 11) is presented listing those equipment failures which caused a greater than 15-min time loss, as well as the number of such occurrences for each item.

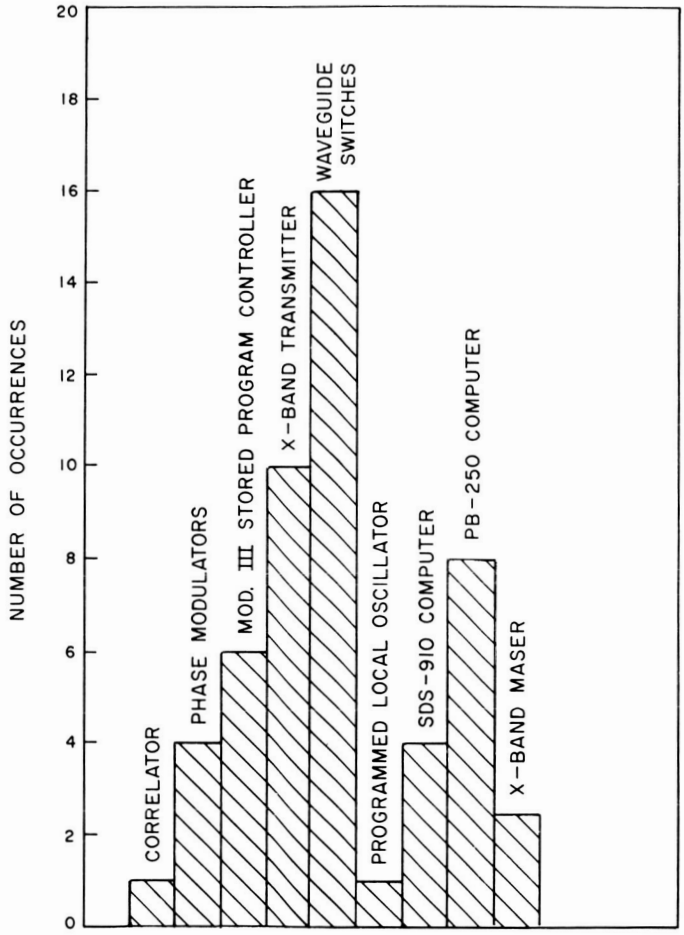

Fig. 11. Equipment failures causing greater than 15-min time loss during lunar radar experiment

A preliminary measurement of the apparent radio temperature of the Sun at 2295 MHz was made using the 85-ft antenna and a DSIF traveling wave maser. The antenna was bore-sighted on the Sun, and a comparison was then made between the noise output from the receiver when terminated in an ambient temperature load and the noise output from the receiver when terminated in the antenna and looking at the Sun. Table 4 summarizes the results, indicating an apparent solar brightness temperature of 16,400°K at 2295 MHz. No corrections have yet been made for possible limiting in the maser at the high signal levels represented by this temperature.

Table 4. Apparent radio brightness temperature of Sun at 2295 MHz

Measurement	Ambient load	Sun	Quiet sky
Noise output ratio, db	0	17.30	−8.92
Approximate system temperature, °K	305	16,400	39

2. Subsystem Performance

a. 100-kw transmitter (operation). For this reporting period, the R&D transmitter was used with a *Mariner* klystron (SN 6) to test the 10-kw diplexer operation at 100 kw. These tests were run in the cone test area (Fig. 12), using the water load to terminate the output of the diplexer. A total of 180.3 filament hours and 18.7 beam hours was accumulated during these tests.

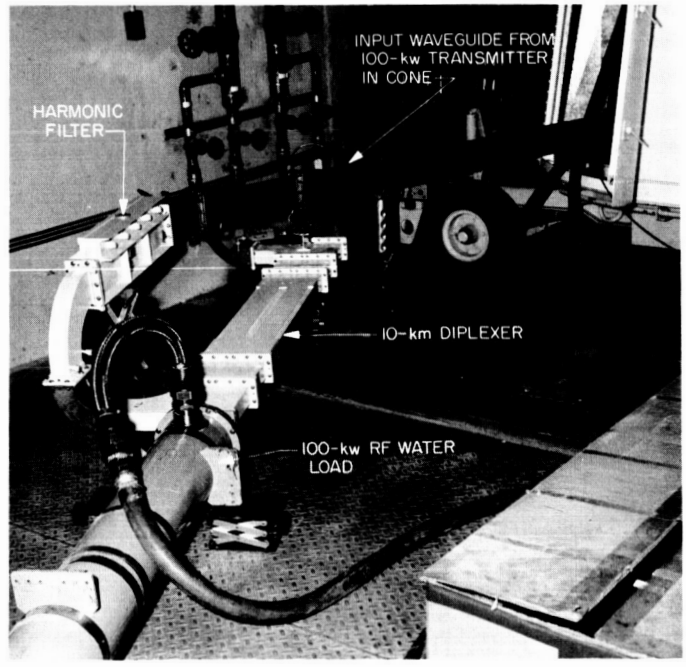

Fig. 12. Diplexer test

On October 5, 1965, the R&D cone was installed on the antenna, with the *Mariner* amplifier replacing the R&D amplifier which had been removed to be modified for use with the new Eimac 100-kw klystron and magnet.

b. Mariner 100-kw transmitters. During this reporting period the *Mariner* transmitters have operated on the spacecraft or in the water load for a total of 298.9 filament hours and 193.9 beam hours on Amplifier 1 and 454.2 filament hours and 256.1 beam hours on Amplifier 2. The transmitters and the associated power equipment experienced several failures during testing and tracking, the most significant of which are:

(1) Failure of bearings in eddy-current coupling.

(2) Breakdown of silicon-controlled rectifiers (SCR) in reflected power amplifiers.

(3) High voltage cable breakdown and shorting.

(4) Failure of starter pump relays.

(5) Failure of resistor in limit amp control circuit.

These failures have all been corrected, and modifications and improvements have been made or are in progress to reduce these problems in future operations.

c. System improvements and modifications. The eddy-current coupling bearings were modified so that better lubrication could be obtained. The performance and reliability of this unit are under investigation for possible replacement or redesign.

The reflected power amplifier SCRs were replaced with higher voltage breakdown units, and added filtering was installed to reduce transients. New and redesigned high voltage cable is on order to replace existing cable.

d. Mod. IV receiver. Throughout most of this period, the Mod. IV receiver was maintained in its X-band–S-band configuration. Lunar radar experiments were conducted at X-band frequencies, and *Mariner* post-encounter backup status was maintained at S-band frequencies. On several occasions the Mod. IV receiver was used as the prime *Mariner* receiver, and in all cases the performance was normal. After October 1, some of the components in the Mod. IV receiver *Mariner* subsystem cabinet were returned to JPL for modification and use in other systems. The only equipment failure in the *Mariner* receiver involved a voltage controlled oscillator (VCO) selection relay, and this was repaired during a *Mariner* non-view period.

X-band portion. Operation of the X-band portion of the Mod. IV receiver was normal during this period. The waveguide installation from the X-band signal generator to the receiver converter was finished, radio frequency leakage measurements were completed, and the data were forwarded to the JPL project engineer.

R&D portion. Modification of the Mod. IV receiver for operation at 2388 Mc is in process. At present, the open-loop portion is operational and is being used in a Venus total spectrum and ranging experiment. Work is continuing on the closed-loop portion. When the work is completed, both open- and closed-loop operation will be possible. Until this time, no receiver sensitivity measurements can be made. Two equipment failures — one involving coldplate power supply and the other a VHF keyer module — have occurred thus far. Both faults have been corrected and receiver operation has been restored. The Resdel signal generator is undergoing repair at JPL.

e. Programmed local oscillator (PLO). Although operation of the digital portion was good throughout this period, several failures did occur. Continued difficulty was encountered with the tape reader section, resulting in erratic operation. A more serious problem was the failure of the VCO control potentiometer. This is the second potentiometer to fail in the last six months. These failures have since been corrected, and the system is now operating normally.

The main VCO bias power supply has been reinstalled in the PLO, and will be used in conjunction with the closed-loop portion of the Mod. IV receiver.

f. Central frequency synthesizer (CFS). The divide-by-100 module was reinstalled in the CFS and checked for proper operation. The new standby batteries for the rubidium frequency standard are on site, and their installation is being planned. These batteries will replace the present nickel cadmium standby batteries in an effort to improve system reliability.

3. Mariner 1964 Spacecraft Support

The post-encounter support of the *Mariner* 1964 spacecraft from the Venus Station consisted of transmission periods designed to prevent unwanted spacecraft-to-ground antenna transfer, command transmission, and telemetry reception, as required.

Command activity included the transmission, on August 2, 1965, of the commands necessary to instruct the spacecraft to cease transmitting picture video and return to normal cruise mode (in which science and engineering telemetry only is transmitted). However, the highlight of the command activity was the transmission, on October 1, 1965, of the command which effectively terminated Phase 1 of the *Mariner* 1964 mission. This command, DC 12, caused the spacecraft, which was 191×10^6 mi away at the time, to switch to the omnidirectional antenna on the spacecraft-to-ground link.

F. Frequency Generation and Control

1. Programmed Exciter

a. Introduction. The programmed exciter (PE) is in the final stage of construction. Much development work has been done in the RF, digital, and construction areas prior to assembling this system.

The basic theory of operation of the PE appears in *SPS* 37-32, Vol. III, pp. 36–44. For ease of reference, a block diagram of the system showing both the RF and digital sections of the system is repeated here (Fig. 13).

b. RF section.

Development. Development work has been done on each RF module in the PE system. A wide-band distribution amplifier (WBDA) with a bandwidth from 10 kc to 50 Mc was developed to maximize the versatility of the system. The PE can serve as a local oscillator centered at any frequency in the bandwidth of the amplifier. The doppler distribution amplifier is a modified version of the WBDA operating from 3 to 4 Mc. The WBDA is now in the final stages of construction.

A 24-Mc voltage controlled oscillator (VCO) to be used in conjunction with the PE was also developed. The results of this work and the operation and performance of the WBDA will be discussed in a future publication.

A schematic of the integrator module is presented in Fig. 14, and photographs of the layout are shown in Figs. 15 and 16. The integrator has met or exceeded each of the following requirements:

Input: ± 30 v max., min. step = 5 mv, max. step = 5 v

Output: -1 to -11 v dc, 3-ma max. current

Time constant: RC = 100-sec normal operation
RC = 10-sec fast acquire mode

Output noise: $< 5\ \mu$v p-p

Stability: $< 5\ \mu$v/sec drift

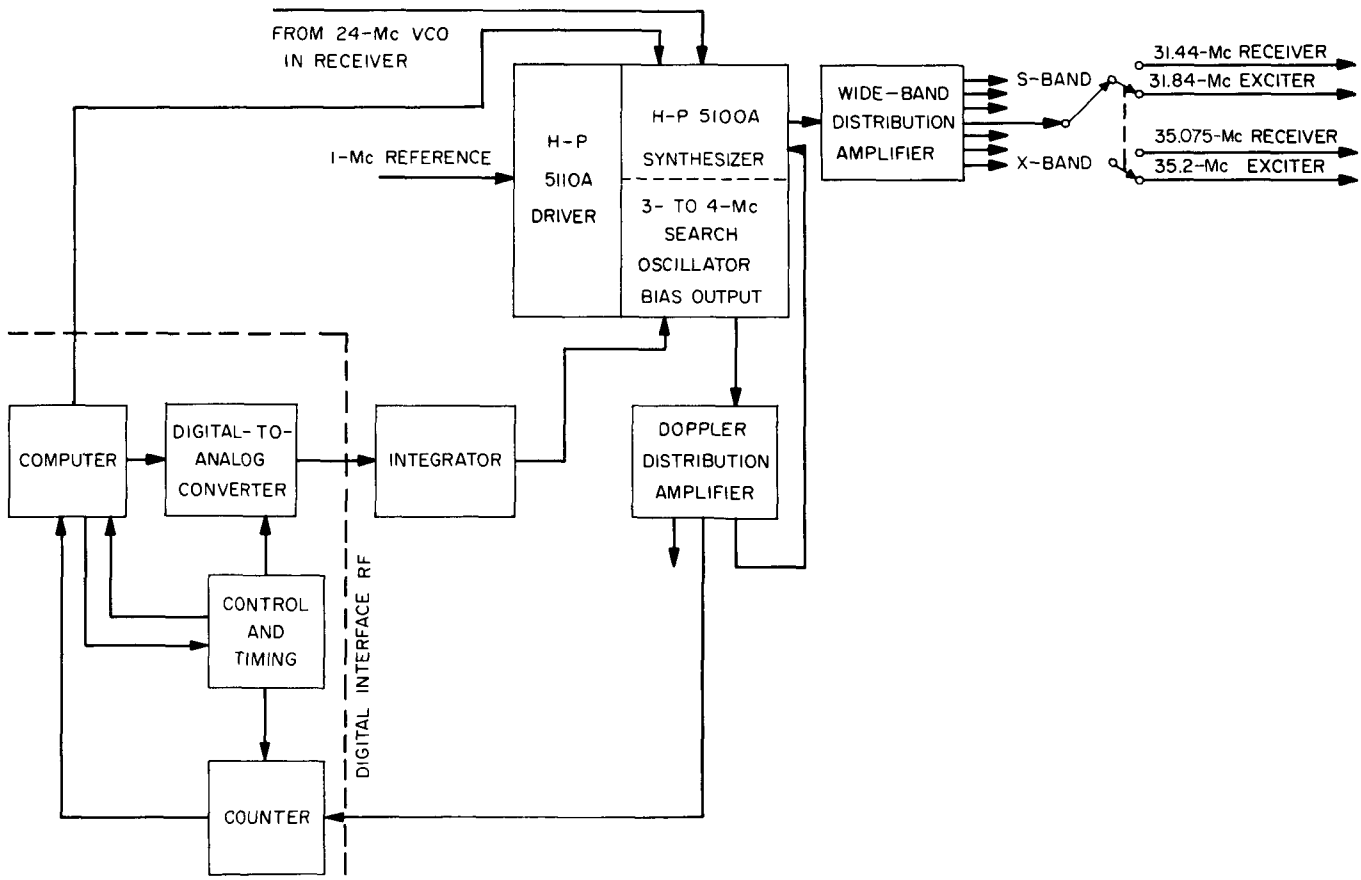

Fig. 13. Programmed exciter block diagram

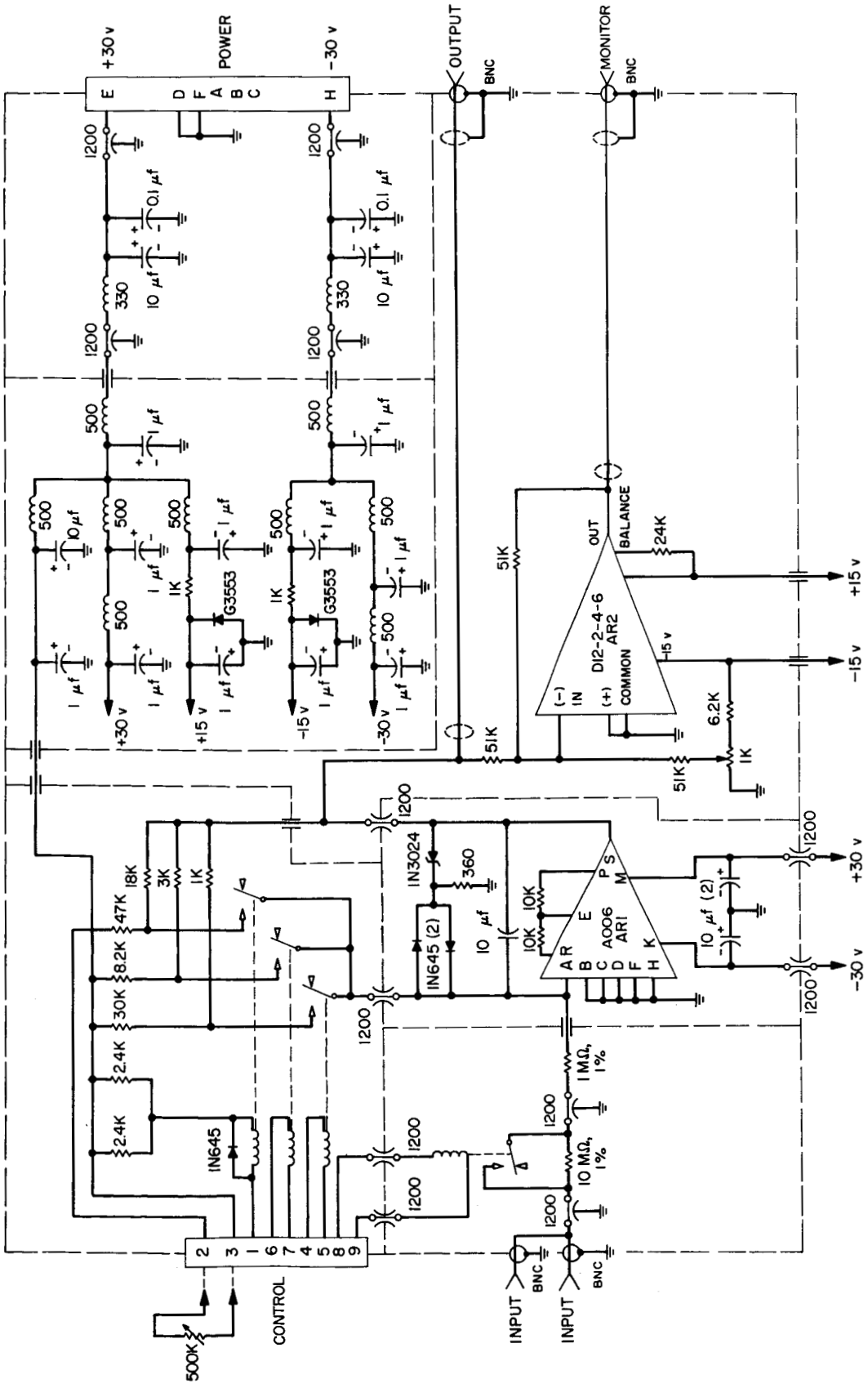

UNLESS OTHERWISE SPECIFIED, ALL RESISTANCES ARE IN OHMS, ALL CAPACITANCES IN PICOFARADS, AND ALL INDUCTANCES IN MICROHENRYS

AR1, 2 = OPERATIONAL AMPLIFIERS

= STAND-OFF CAPACITOR

= FEEDTHROUGH CAPACITOR

= MECHANICAL FEEDTHROUGH, NO CAPACITANCE

RELAYS ARE 6 v dc, 288-Ω COIL

Fig. 14. Integrator schematic

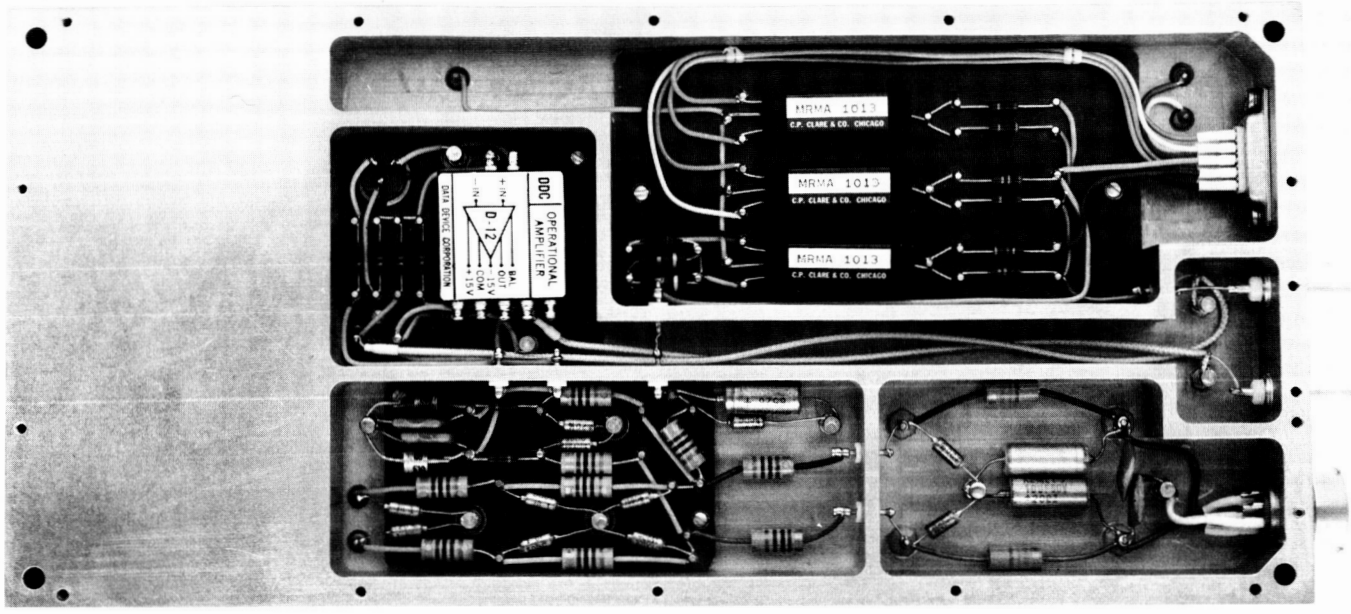

Fig. 15. Integrator layout, front

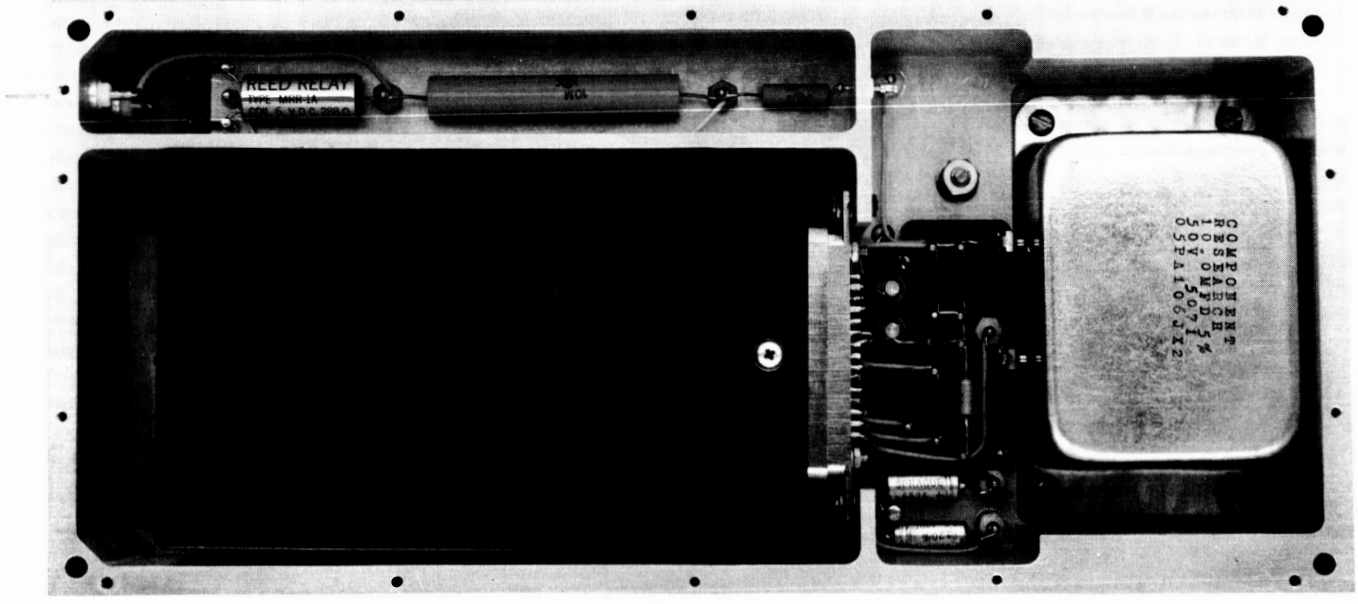

Fig. 16. Integrator layout, back

In addition, the integrator has computer-controlled relays to set the output voltage to −1 or −11 v dc, the extremes of the output range. The output voltage is clamped at +1 and −15 v dc by a diode circuit across the 10-μf integrating capacitor; the search oscillator which follows is thus protected from excessive bias voltage. A monitor amplifier meters the output voltage without disturbing the stability of the integrator. The highly stable performance of the integrator is enhanced by the use of low temperature coefficient and low aging metal film resistors and a polystyrene 10-μf integrating capacitor.

The integrator was tested in operation with the search oscillator of the Hewlett-Packard (H-P) synthesizer (Fig. 17). A typical result of the test is shown in Fig. 18. The short-term drift (1 sec) of the integrator is within specification. The long-term drift (>1 sec) can readily be corrected when operating in the closed-loop configuration

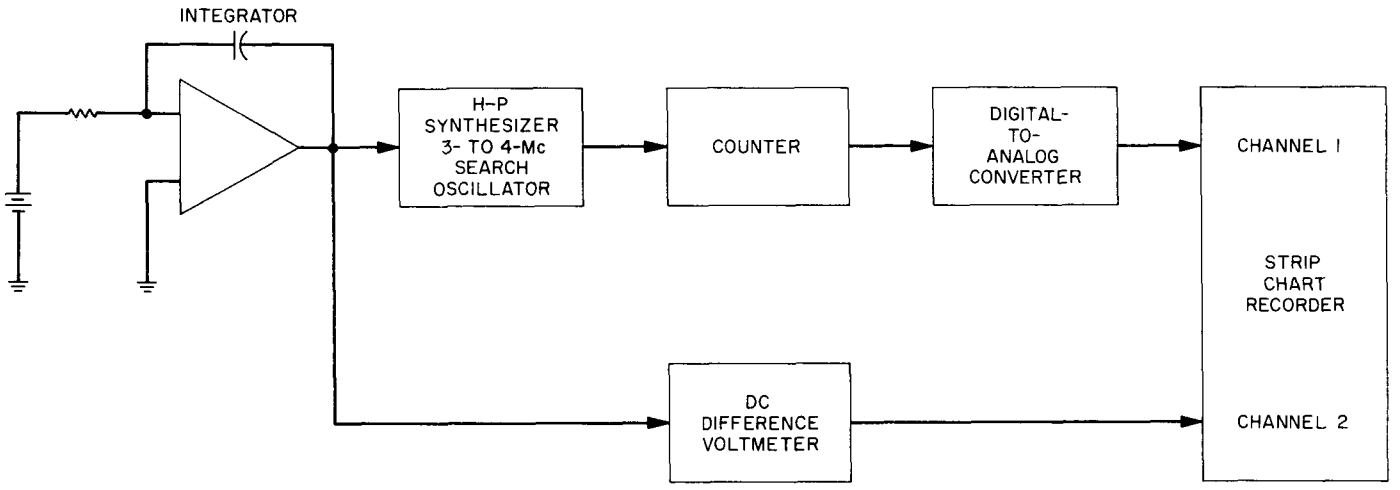

Fig. 17. Stability test configuration

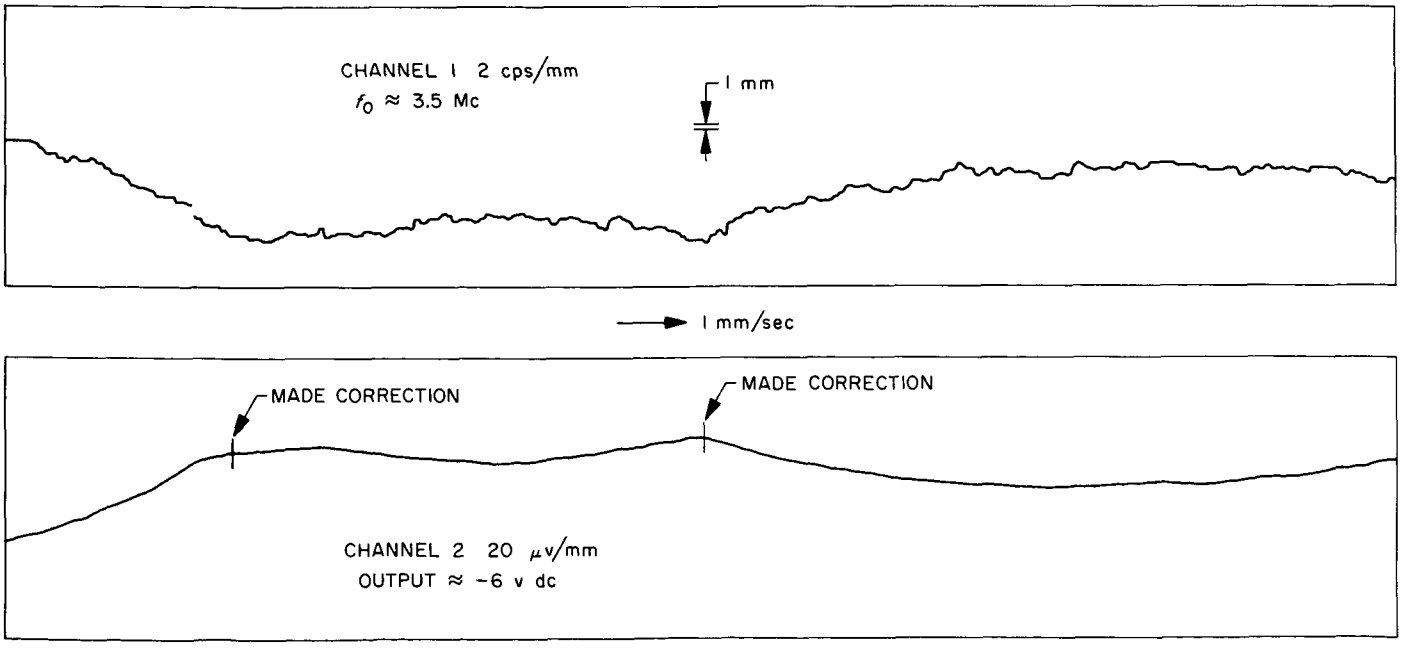

Fig. 18. Stability test results

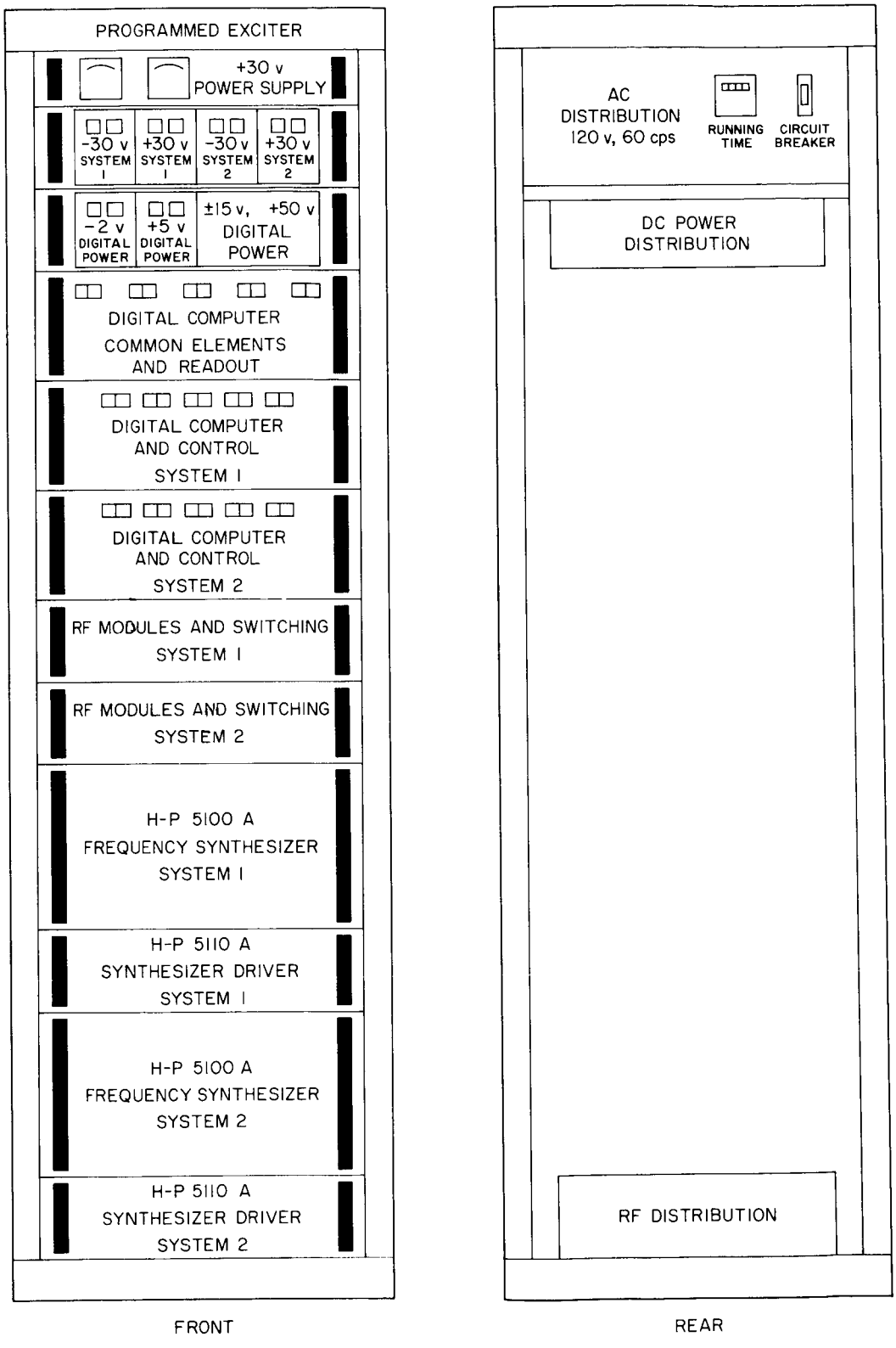

RACK SHOWN WITH DOORS REMOVED

Fig. 19. Cabinet configuration

of the PE (Fig. 13). The short-term deviation of the search oscillator-integrator combination is equal to or better than the 5-cps peak-to-peak deviation required by the PE system (*SPS 37-32*, Vol. III, p. 38).

System construction. As reported in *SPS 37-33*, Vol. III, p. 91, two complete PE systems (as shown in Fig. 13) will be housed in one standard JPL cabinet. The cabinet configuration is shown in Fig. 19. The power supplies are air-cooled, 60-cps supplies mounted at the top of the cabinet for best heat dissipation.

The indicators and switches are in functional groupings mounted at eye level. The digital microcircuits are mounted on vertical cards in sliding drawers, and the RF equipment and relays are on a horizontal aluminum plate behind blank panels. All RF and digital cables for communication with other systems feed from the bottom of the cabinet. All equipment is mounted on slides for ease of maintenance and repair.

c. Digital section. A block diagram of the PE digital section is shown in Fig. 20. Coarse frequency control of the synthesizer is accomplished by the decade switching control, which selects, under computer control, the various decade numbers of the desired frequency in the same manner as do the pushbuttons on the front panel. Pushbutton control is operative only when the synthesizer is switched to the local mode; conversely, the decade control is operative only in the remote mode.

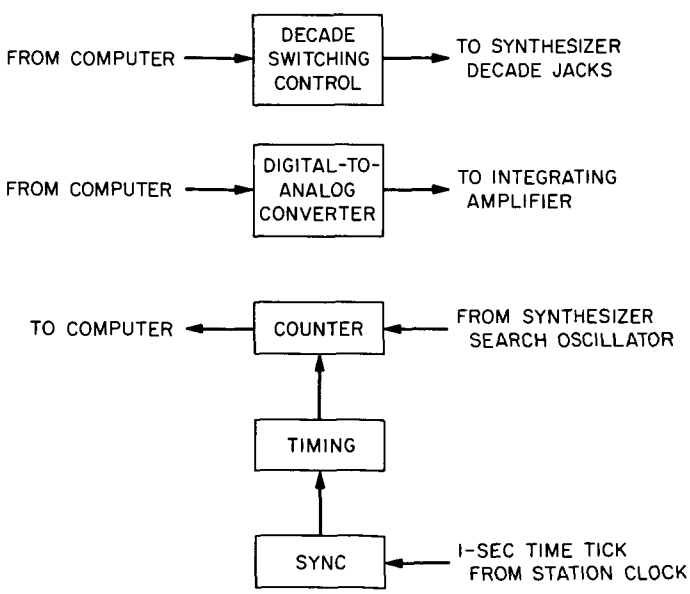

Fig. 20. Programmed exciter — digital section

Fine frequency control of the synthesizer is accomplished by remotely controling the synthesizer search oscillator. This is done by the digital-to-analog (D/A) converter followed by an integrating amplifier. The output of the integrating amplifier is sufficiently noise-free to obtain a search oscillator resolution of one part in 200,000. Binary numbers into the D/A converter represent a rate at which the search oscillator is to change. The range of the D/A converter is ± 1000 increments, where each increment causes a frequency sweep of 5 Hz/sec in the search oscillator range of 3 to 4 MHz. At an S-band frequency of 2388 MHz, this represents a rate capability of up to 38 Hz/sec in increments of 0.038 Hz/sec.

The exact frequency of the search oscillator is determined by the counter. A register in the counter continuously counts the frequency of the search oscillator. At periodic intervals of either 1 or 0.1 sec, the computer can read the instantaneous count of this register. Frequency is then computed by taking the difference between the present and past counter reading. The computer arithmetic is such that even when the counter recycles through zero, a correct difference can be obtained.

The sync permits the computer to synchronize the timing logic to within 2 μsec of the leading edge of the 1-sec station time tick.

Counter. The requirement for continuously counting with periodic readout of the instantaneous counter value implies the use of two counter registers: One register performs the continuous counting function, and the second register stores the desired instantaneous value of the first register for interrogation by the computer. If the direct design approach to this problem is taken, i.e., having the first register a continuous counter which transfers its count on command to a second static register, serious difficulties arise. Ripple counter design of the first register is precluded because the carry information might be in the midst of rippling down the counter when the transfer command comes. Furthermore, the ripple time may be as much as 5 or 6 times the period of the frequency being counted. Alternatively, a synchronous counter must be designed in which all carry information can be completely propagated in the time interval between successive input cycles. For a 24-bit register counting 4 MHz, an inordinate amount of gating logic and circuit speed is required.

To circumvent the above problems, the system shown in Fig. 21 has been devised. Two 24-bit ripple counters are used, one a master and the second a slave. Both

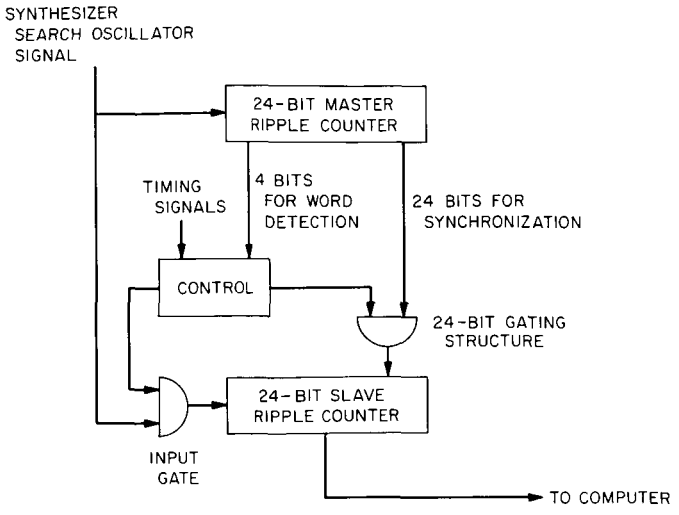

Fig. 21. Counter system

counters count the input frequency, but, in addition, the slave counter may be synchronized to the master counter or disconnected from the input signal by the control logic.

Operation of the system is as follows: Some time before the count value is desired, both the input and the synchronizing signals are connected to the slave counter. The synchronizing signals are fed directly into the DC inputs of the slave counter flip-flops. When a carry ripple is propagating down the master counter, the slave counter is in an indeterminate state due to possible interference between the synchronizing signals and the slave internal ripple signals. When no ripple is present in the master counter, the state of the slave counter is exactly that of the master counter. The control disconnects the synchronizing signals from the slave counter at a time when no ripple is in the master counter.

The condition of no ripple exists when the first four least significant bit positions of the master counter are equal to one. This indicates that 15 counts of the input frequency have occurred after the previous major carry bit has been propagated. Sufficient time has thus been allowed for all carries to have been completely propagated.

At this time both counters are counting the same signal and contain the same count, but otherwise are completely independent of each other. When the instantaneous count value is desired, the input signal is disconnected from the slave counter. After any carry ripples have finished propagating in the slave counter, the individual slave counter flip-flops may be read by the computer.

D/A converter. The D/A converter has been specially designed to operate directly from integrated circuit flip-flops which have a supply voltage of +5 v. These flip-flops form an 11-bit static register which holds the computer-derived rate number. The D/A converter produces a DC voltage with a value proportional to the count in the static register.

A simplified schematic of the D/A converter is shown in Fig. 22. The converter contains 11 binary scaled current sources which may be selectively summed by an operational amplifier. Each current source has two steering diodes, one to the operational amplifier and the other to the driving flip-flop. If the flip-flop voltage is less positive than +2.5 v, the current is steered away from the operational amplifier and into the driving flip-flop. If the flip-flop voltage is more positive than +2.5 v, the current is steered into the operational amplifier, where its binary value contributes to the output DC voltage. The input to the operational amplifier remains constant at +2.5 v, regardless of the amount of current switched into it. The gain and bias current are adjusted to produce a DC output voltage from −5 to +5 v over the complete range of code inputs.

A major portion of drift and voltage uncertainty versus temperature variation is due to the variable voltage drop across the steering diodes leading to the operational amplifier. For example, in the most significant bit posi-

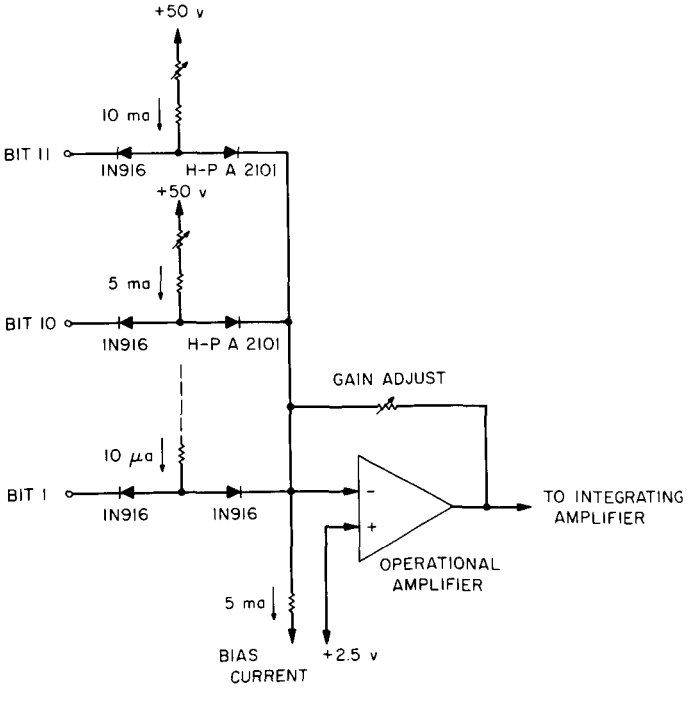

Fig. 22. Digital-to-analog converter

tion, a 50-mv voltage change is equivalent to one whole code increment change. This effect diminishes by a factor of two for each successive lower-order bit position. To minimize this condition, the operational amplifier steering diodes in the four most significant bit positions are metal-silicon hot carrier diodes with a low barrier potential. The voltage drop temperature coefficient of these diodes approaches zero for currents in the vicinity of 10 ma. At low currents the temperature coefficient is much less than that of the silicon junction diodes used in the other steering positions.

Construction. Most of the circuitry in the digital section of the PE consists of integrated circuits. These circuits are mounted on specially designed circuit boards containing a power distribution system, a ground plane, terminal pads, and connectors, as shown in Fig. 23. Sixty-six microcircuits as well as a variety of discrete components may be mounted on one board. Wire-wrap pins extending through the board permit interconnection by means of the wire-wrapping technique; in addition, these pins provide an anchor for the mounting of the discrete components. Fig. 24 shows the wiring side of the circuit

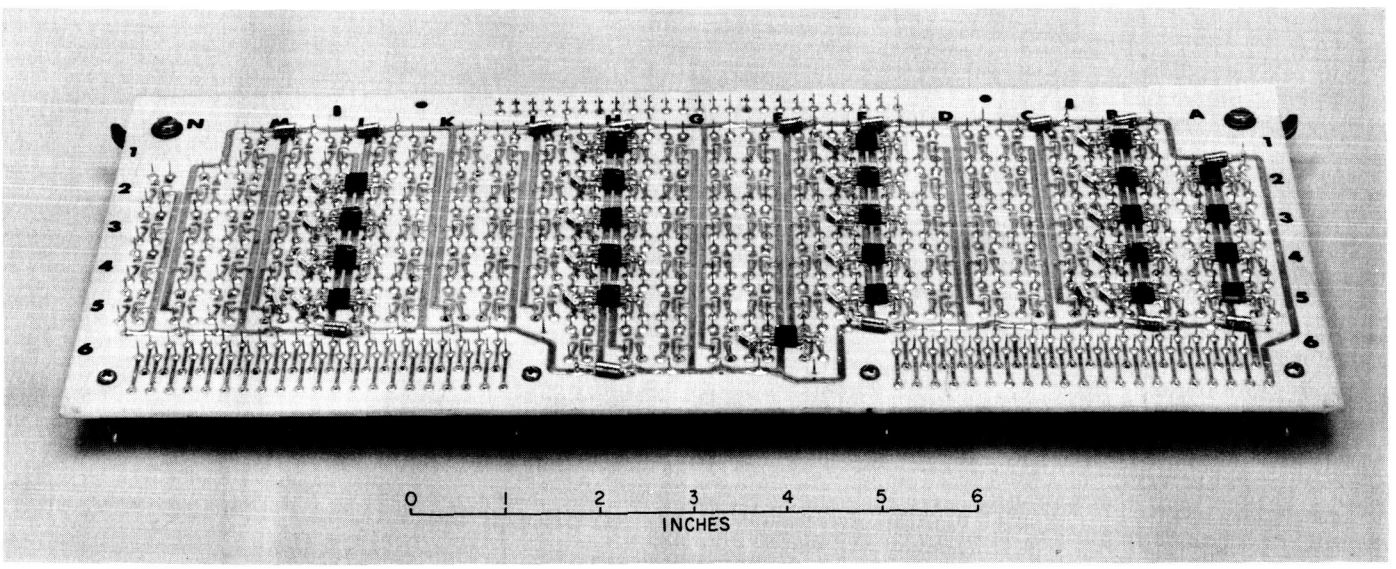

Fig. 23. Microcircuit board — component side

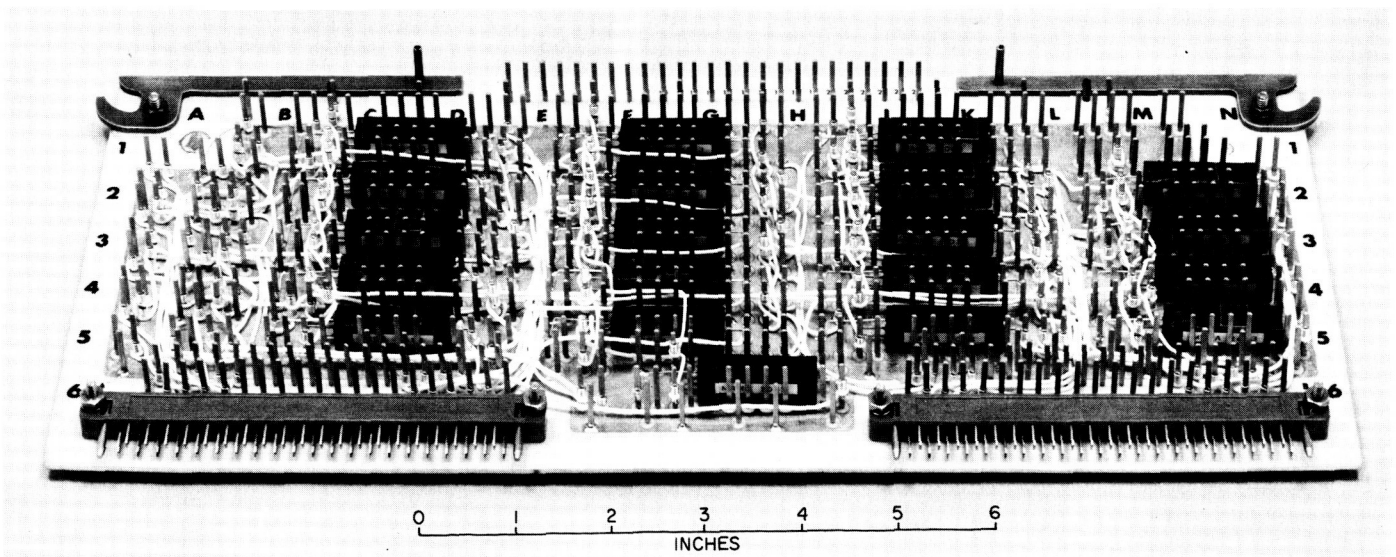

Fig. 24. Microcircuit board — wiring side

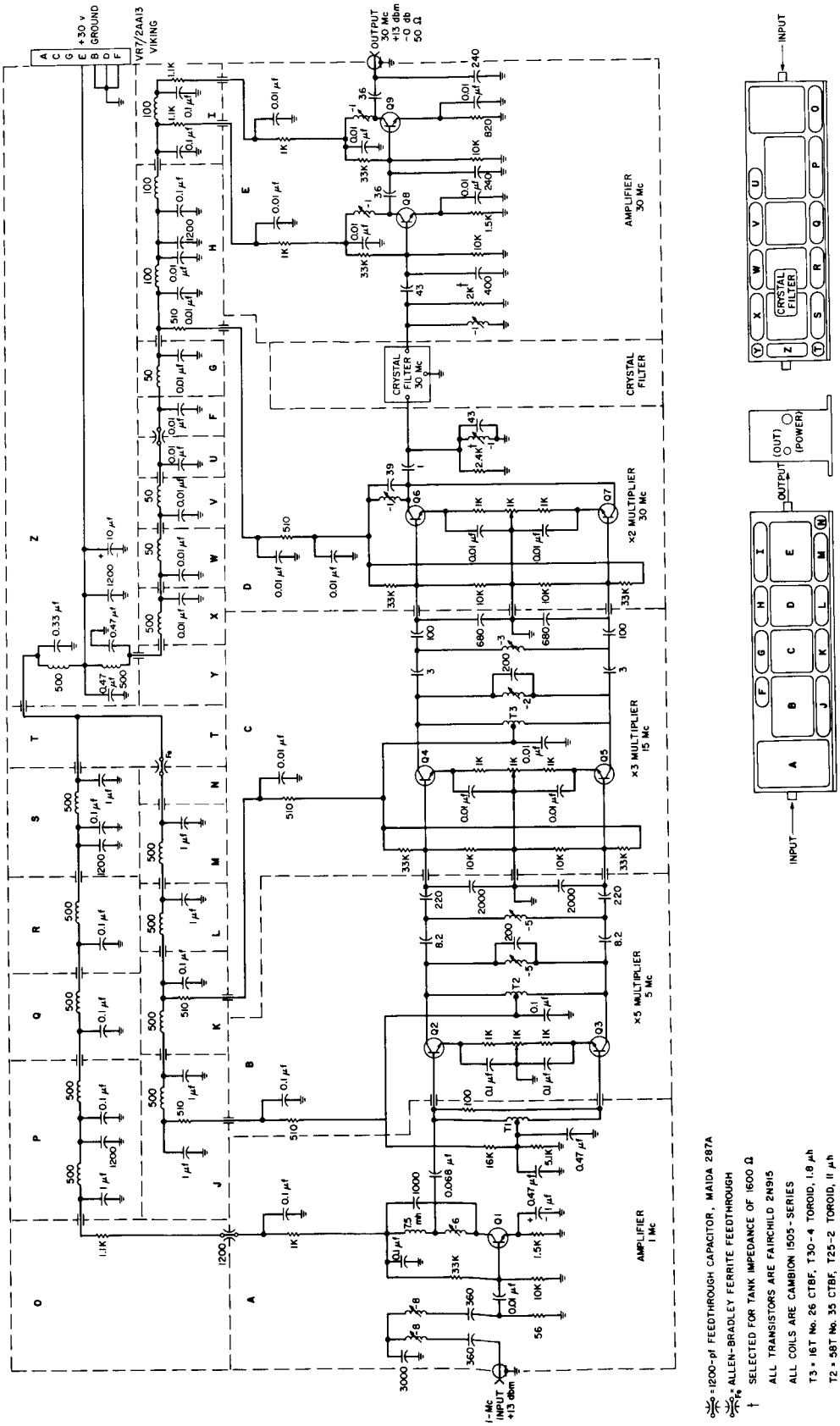

= 1200-pf FEEDTHROUGH CAPACITOR, MAIDA 287A

= ALLEN-BRADLEY FERRITE FEEDTHROUGH

† SELECTED FOR TANK IMPEDANCE OF 1600 Ω

ALL TRANSISTORS ARE FAIRCHILD 2N915

ALL COILS ARE CAMBION 1505-SERIES

T3 = 16T No. 26 CTBF, T30-4 TOROID, 1.8 μh

T2 = 58T No. 35 CTBF, T25-2 TOROID, 11 μh

T1 = 30T No. 32 CTBF, T25-15 TOROID, 8 μh

UNLESS OTHERWISE NOTED ALL RESISTANCES ARE IN OHMS, ALL CONDUCTANCES ARE IN MICROHENRY'S, AND ALL CAPACITANCES ARE IN PICOFARADS

Fig. 25. Schematic diagram of × 30 frequency multiplier

board as well as the mounting of the read relays used in the decade control block.

Two connectors allow 76 signal leads to connect to the board, in addition to the power system of +5 v, −2 v, and ground. The lever arms attached to the board serve the three-fold function of extraction tool, insertion tool, and locking mechanism. The entire logic of the PE digital section is contained on ten cards which fit in a 7-in. relay rack drawer.

2. S- and X-Band Central Frequency Synthesizer

a. Introduction. A ×30 frequency multiplier has been developed to supply the 30 Mc required for system and station reference signals (*SPS 37-33*, Vol. III, p. 92). A module status report is given here.

b. Frequency multiplier. The frequency multiplier consists of solid-state circuitry on terminal boards housed in a gold-plated cavity-type chassis. A combined series of multipliers, amplifiers, and crystal filter raised the input frequency from 1.0 to 30.0 Mc (Fig. 25). This module was developed at JPL, and the final model was fabricated by a local vendor. Performance features are: output level of +13 dbm (−0 db, +3 db) into 51Ω; a power drain of 0.75 w from a +30-v dc supply; input impedance of 51Ω ±10% for ±3 db at the +10-dbm input level; and isolation from output to input > 60 db at any frequency.

The total bandwidth of the frequency multiplier, which is determined by the crystal filter, is 1870 cps. The bandpass ripple is < 0.5 db over this range. The output spectrum contains no measureable internally generated spurious signals. Second harmonic distortion of the 30.0-Mc signal is 0.457%.

The RF leakage of 1.0, 5.0, 15.0, and 30.0 Mc was checked at the power line, the input and output terminals (TNC connector), and all external mechanical junctions. All leakage signals are ≤ 1.0 μv. With the input terminal open or terminated, 12 μv of 30 Mc appear on the output connector.

The limiting characteristics are seen in Fig. 26. An input signal loss of 39 db can still provide the required +13-dbm level.

Power supply variations versus the 30-Mc output level are presented in Fig. 27. A DC supply loss of 30% can still maintain the +13-dbm output.

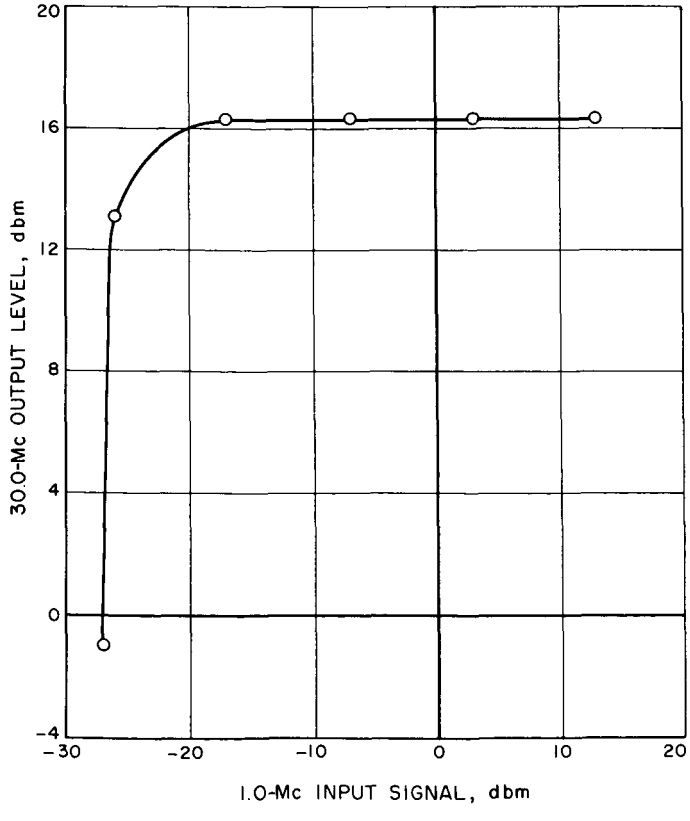

Fig. 26. Limiting characteristics of ×30 frequency multiplier

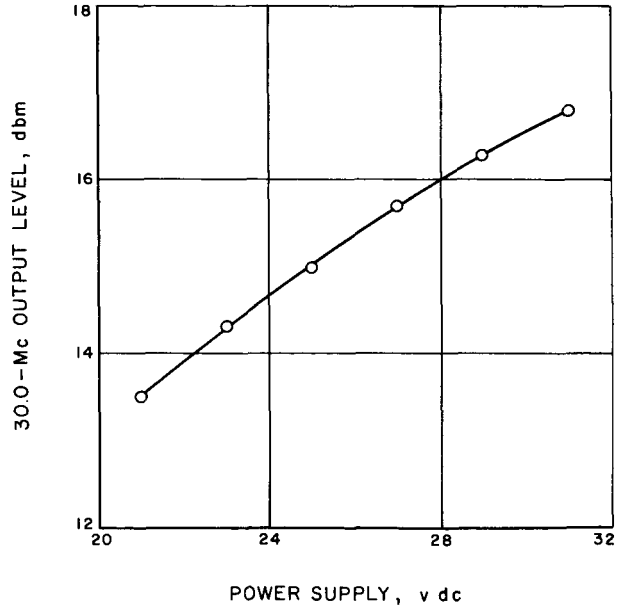

Fig. 27. Power supply variations versus 30-Mc output

The frequency multiplier was subjected to a temperature environment from 0 to 50°C for 3 hr at each temperature point. The usable output suffers a 0.4-db degradation, as shown in Fig. 28.

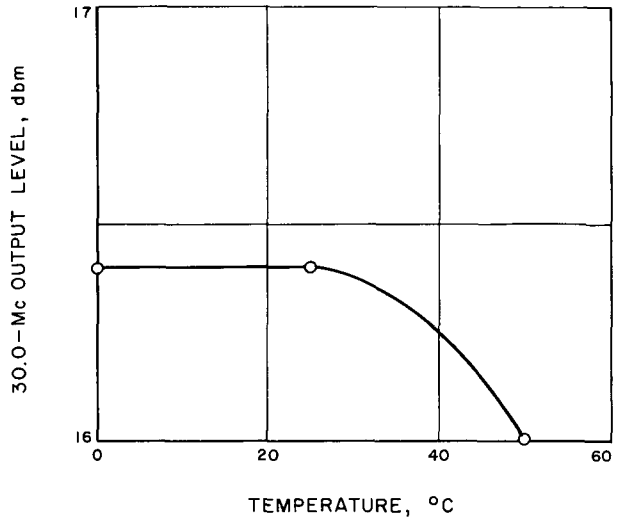

Fig. 28. Temperature versus output

c. Balanced mixers. Two balanced mixers and four VCOs have been modified by an external vendor. Performance data appear on Table 5. (See also *SPS 37-27*, Vol. III, p. 92, and *SPS 37-33*, Vol. III, p. 93.)

d. Module status. At this time, 73% of all the required modules are completed and installed. Of the remaining modules, 18.5% are awaiting test, with 6.8% in testing and 1.7% in development. The rubidium vapor frequency standard has been installed and has been operating continuously for 1865 hr.

3. S- and X-Band Interim Frequency Synthesizer

a. Introduction. In September 1965, the S- and X-band interim central frequency synthesizer (ICFS) completed its first full year of operation. Reports on system performance have been included regularly in Volume III of the *SPS* under the "Venus Station Operations" section. In this report, the year's activity on the ICFS is summarized; modifications and system problems are explained, and the current status of the system is described.

b. Modifications. The original system diagram appears as Fig. 34 in *SPS 37-30*, Vol. III, p. 65. In this same volume (pp. 63–66), it was noted that the 1-Mc crystal filter appeared to be causing excessive phase noise in the system. The filter was removed and development of a new filter was initiated. This development is nearing completion and will be reported at a later date.

The ICFS was further modified by the addition of a ×4 multiplier from 1 to 4 Mc (*SPS 37-34*, Vol. III, p. 62). The 4-Mc signal was used in the programmed local oscillator (PLO) to offset the PLO nominal output frequency from 31.44 to 35.44 Mc (Fig. 29). This change was necessary in order to accommodate the Venus Station *Mariner IV* encounter receiver (*SPS 37-33*, Vol. III, pp. 58–62). This work was completed on June 9, 1965.

Table 5. Performance data on balanced mixers and VCOs

Short-term stability, parts/10^9	Module	Spurious signals, μv	RF leakage (all frequencies), μv	Dynamic range, both inputs for constant output, db	Input impedance, VSWR	Harmonic distortion, %	Variation of output with power supply variation of 30%, %
—	3.635-Mc balanced mixer	290	≤ 1.0	40	≤ 1.10	0.89	21.5
—	35.075-Mc balanced mixer	15	≤ 1.0	20	≤ 1.10	0.73	20
1.0	31.44-Mc VCO	0.0	≤ 1.0	—	—	0.28	4.72
1.0	31.84-Mc VCO	0.0	≤ 1.0	—	—	1.01	7.44
3.0	35.075-Mc VCO	0.0	≤ 1.0	—	—	1.20	12.7
1.0	35.2-Mc VCO	0.0	≤ 1.0	—	—	1.0	6.83

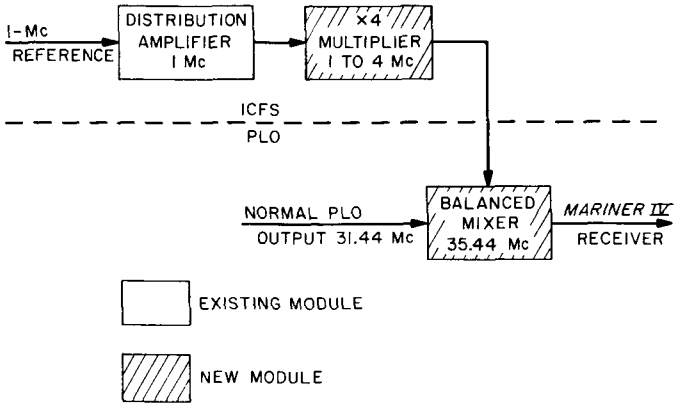

Fig. 29. ICFS-PLO *Mariner IV* modification

The rubidium frequency standard in the ICFS uses its own DC power supply during normal operation. In addition, standby batteries float across the DC line to provide full load current in the event of an AC power failure. The standby batteries should be capable of providing a 2-amp current at 24 to 28 v dc for 72 hr. The present nickel-cadmium batteries were evaluated (*SPS 37-34*, Vol. III, p. 62) to determine their capability. These batteries were able to operate the rubidium standard for only 6 to 8 hr. A high voltage charge did not improve the situation.

As a result of this evaluation, lead-acid standard cells were purchased to replace the nickel-cadmium cells. These new standby batteries are now being installed, and will be located in a separate enclosure outside of the Venus Station control room. Tests will be performed to determine their operating capability.

c. System problems. The rubidium frequency standard in the ICFS exhibited excessive phase noise (*SPS 37-32*, Vol. III, p. 66). A new standard with 100% solid-state electronics was introduced which improved performance; after an initial failure, this new unit has been operating satisfactorily. The original rubidium standard has also been modified to 100% solid-state electronics and is now operating satisfactorily at JPL as a system spare.

In July 1965, phase noise variations occurring at 90-sec intervals were a problem of concern. This trouble was traced to the oven cycling of a 31.44-Mc VCO which was modulating the DC power line. Further investigation disclosed that the remote sensing of the 30-v dc power supply was inoperative. These two problems were corrected, and the 90-sec phase noise variations disappeared.

Two distribution amplifiers and the ÷100 module exhibited excessive phase jitter. Shielded coils with loose tuning slugs and aging tantalum capacitors proved to be a source of this problem. The coil slugs were potted with silicon rubber or eliminated where possible, and the tantalum capacitors were replaced with ceramic capacitors. Correction of the system problems has eliminated the spurious and intermittent phase jitter conditions.

d. Current system status. System performance tests were made in August 1965. The VCOs were all readjusted to center frequency to correct for crystal aging. The phase noise was measured for each phase-locked loop, and no unusual spurious noise was evident.

Compared with that of one year ago, present phase noise shows some degradation in measured performance (Table 6). This degradation is not serious since it represents only a 10 to 20% change in just two of the loops. The improvement in the 31.84-Mc loop is probably a result of the modification of the above-mentioned ÷100 module.

Table 6. Bandwidth and phase noise of system phase-locked loops

Phase-locked loop VCO frequency, Mc	Bandwidth $2B_L$, cps	Phase noise September 1964 deg, rms[a]	Phase noise September 1965 deg, rms[a]
30.455	5	0.15	0.14
31.44	3	0.17	0.15
31.84	3	0.15	0.09
35.075	1	0.20	0.24
35.2	1	0.30	0.32

[a]Due to oscillators and synthesizers

The synthesizer can now provide 55 output signals at 16 different frequencies; at present, 37 signals are being used.

e. Conclusion. The system appears to be free from spurious and intermittent problems. The installation of new standby batteries should greatly improve the reliability of the system in the event of a power failure. Work is continuing on the 1-Mc crystal filter and the synthesizer itself to improve the measured phase noise of the system.

G. Information Systems

1. Teletype Coding Scheme Resulting From One-Way Teletype Error-Rate Experiments

Before an encoding and decoding scheme for ultra-reliable inter-DSN teletype usage (described in *SPS 37-33*, Vol. III, pp. 109, 110; *SPS 37-34*, Vol. III, pp. 64–68; and *SPS 37-35*, Vol. III, pp. 71–76) could be adopted, the error characteristics of the inter-DSN teletype channels had to be determined. This was recently accomplished, and a coding scheme has now been formulated. The encoding program has been written, and efforts on the decoding program are under way.

a. One-way teletype error-rate experiments. These experiments consisted of sending two test messages (pseudorandom message tapes) daily to the overseas DSIF stations. Each message consisted of 3184 teletype characters, each having an odd parity to compensate for the character deleted by the communications processor at the Goddard Space Flight Center (*SPS 37-35*). After their return by mail, the tapes were compared with the original message on an SDS (Scientific Data System) 930 digital computer at the Goldstone Venus Station. The results of this comparison are given in Table 7. Since previous experiments had determined that, for the code length in question (15 teletype characters), the channels used do not exhibit any "burst" error characteristics, no burst data were included in the experiments.

The overall character error rate was found to be 3×10^{-4} (129/413,920). The 10^{-2} worst-case error rate found was in agreement with that of previous experiments. This worst-case error rate is that which is assumed in a theoretical analysis of code performance. A 10^{-4} synchronization error rate with no burst characteristics was also found and, hence, had to be considered in the formulation of the coding scheme.

As may be seen in Table 7, the bit error rates of the five teletype channels are essentially equal. The greater number of errors in Channels 4 and 5 noted previously (*SPS 37-34*) was not noted in these experiments. There was approximately the same number of bit errors in the $1 \rightarrow 0$ and $0 \rightarrow 1$ classes (110 and 118, respectively); however, as expected, on many tapes one or the other type of error predominated. This imbalance was not of sufficient magnitude to be considered in the coding scheme formulation.

b. Coding scheme formulation. The code chosen was the (15,9) Solomon-Mattson code over the 16-element field, consisting of information and check characters. However, one of the information characters is a synchronization symbol. Only the first four teletype levels are used for information, and the fifth is used as parity on the first four (as is done when using the present telemetry teletype system, which, however, does not use the Goddard processor). This code has a minimum distance of 7 and is thus capable of correcting three character errors in one word of length 15. However, due to equipment complexity and for reliability purposes, it was decided to correct single errors only and to repeat the operation if more than one error is found. The code can then detect all quintuple errors, eliminating the possibility of these or smaller errors being confused with single errors. Since the possible presence of mis-synchronization must be considered, it is planned to correct single synchronization errors in the absence of a character error and to correct single character errors in the absence of a synchronization error. All other types of errors which are present will be detected in the process, and repeat transmission will then be requested.

Due to the mathematical properties of the (15,9) code, a quintuple error–synchronization error combination which would cause incorrect decoding of a word (i.e., confusion with a single error) would be rare. In fact, the worst-case output-word error probability using this code is less than 10^{-10}.

For the teletype link from the DSIF to JPL, a higher error rate is believed tolerable; therefore, a similar code, but one with less redundancy, has been chosen for this mode of operation. This, a (15,11) code, yields a worst-case error probability of 10^{-8}.

The decoding scheme for the (15,9) code takes a 0.5-sec worst-case running time and a 10-msec average running time on an SDS 930 computer. Since the length-15 coded teletype word requires 2.5 sec at a 30-bit/sec rate, real-time operation can be realized even in the worst case.

The probability that a repeat transmission will be required is equivalent to the probability of a detected but uncorrected error and equals .01 in the worst case.

Table 7. Results of one-way teletype error-rate experiments

DSIF Station	Number of tapes	Synchronization errors	1→0 Errors for indicated channel					0→1 Errors for indicated channel					Total errors for indicated channel					Pattern errors				
			1	2	3	4	5	1	2	3	4	5	1	2	3	4	5	Single	Double	Triple	Quadruple	Quintuple
Woomera	45	11	8	7	5	7	4	19	5	9	4	4	27	12	14	11	8	27	7	2	0	0
Tidbinbilla	40	10	6	7	2	9	9	6	5	8	3	4	12	12	10	12	13	37	7	3	3	0
Johannesburg	42	14	6	14	7	12	6	14	7	16	4	10	20	21	23	16	16	21	12	5	4	0
Madrid	3	2	0	0	0	1	0	0	0	0	0	0	0	0	0	1	0	1	0	0	0	0
Total	130	37	20	28	14	29	19	39	17	33	11	18	59	45	47	40	37	86	26	10	7	0

Erratum

The following figure is a corrected version of Fig. 27, p. 92, of SPS 37-33, Vol. III, May 30, 1965.

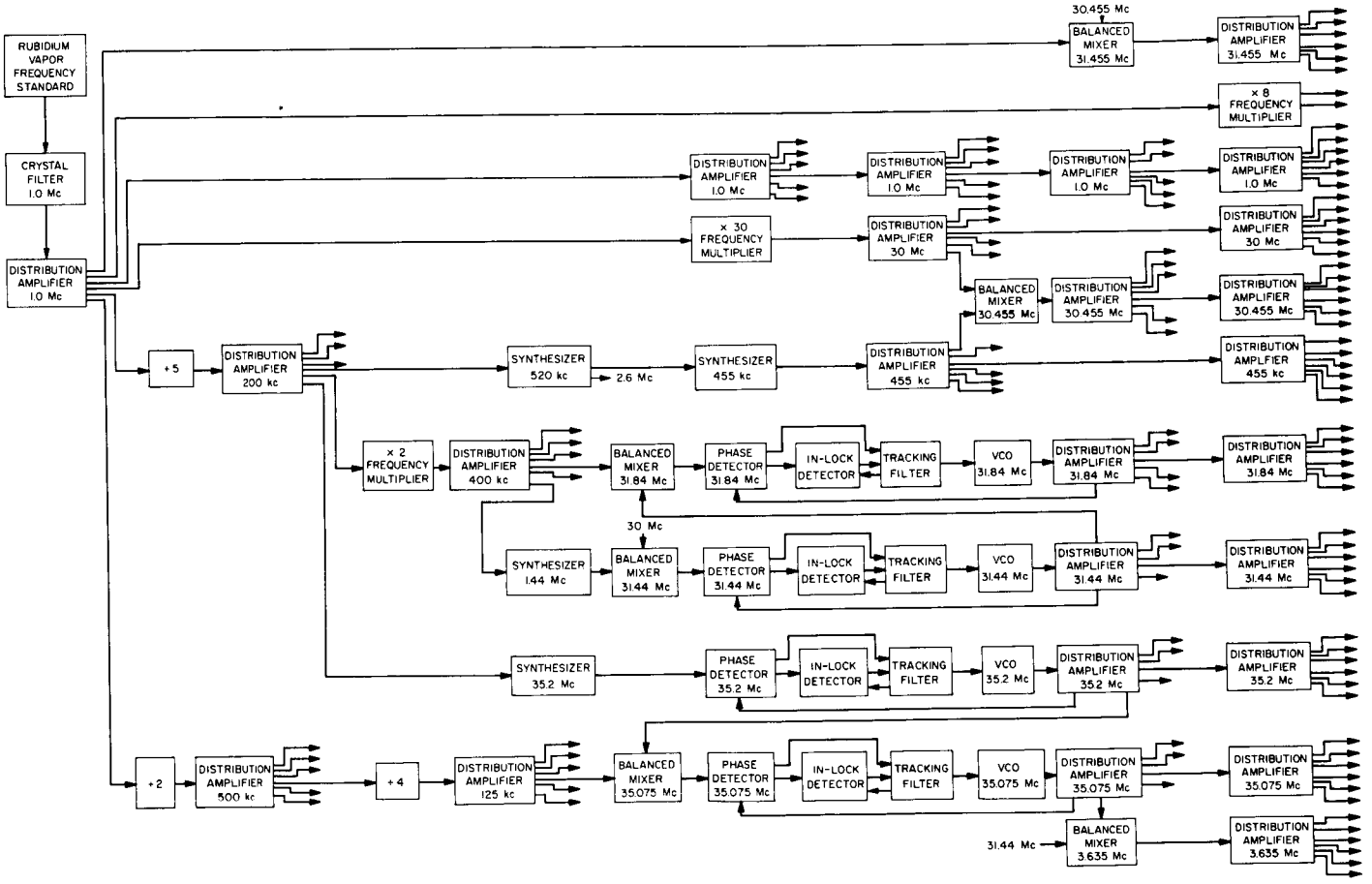

Central frequency synthesizer